Prepared for:
Elena McDonald-Buller
Project Manager
Texas Air Quality Research Program

Prepared by:
Chris Emery, Uarporn Nopmongcol, Pradeepa Vennam, Tejas Shah, Lynsey Parker, Yuge Shi and Greg Yarwood
Ramboll US Consulting, Inc.

August 2021

Improving Estimates of Wind-Blown Dust from Natural and Agricultural Sources Final Report

AQRP Project No. 20-011

QA Requirements: Audits of Data Quality: 10% Required

RAMBOLL

Improving Estimates of Wind-Blown Dust from Natural and Agricultural Sources

Ramboll
7250 Redwood Boulevard
Suite 105
Novato, CA 94945
USA

T +1 415 899 0700
https://ramboll.com

Contents

Table of Figures

Table of Tables

ACKNOWLEDGEMENT

The preparation of this report (Project No. 20-011) was funded by a grant from the Texas Air Quality Research Program (AQRP) at The University of Texas at Austin through the Texas Emission Reduction Program (TERP) and the Texas Commission on Environmental Quality (TCEQ). The findings, opinions and conclusions are the work of the author(s) and do not necessarily represent findings, opinions, or conclusions of the AQRP or the TCEQ.

LIST OF ACRONYMS AND ABBREVIATIONS

2-D	Two-dimensional
3-D	Three-dimensional
A12	Astitha et al. (2012)
ACM2	Asymmetric Convective Model, version 2
AFWA	Air Force Weather Agency
Al	Aluminum
AQRP	Air Quality Research Program
BAND	Bandelier, New Mexico
BELD	Biogenic Emission Landuse Database
BIBE	Big Bend, Texas
Ca	Calcium
CACR	Caney Creek, Arkansas
CAMx	Comprehensive Air quality Model with extensions
CB6r5	Carbon Bond version 6, revision 5
CCRS	Coarse crustal particulate matter
CDL	Cropland Data Layer
CF	Coarse/fine mode aerosol chemistry
CGS	Centimeter/gram/second units convention
CM	Coarse aerosol mass (also PMC)
cm	centimeter
CMAQ	Community Multiscale Air Quality model
CSN	Chemical Speciation Network
CST	Central Standard Time
EC	Elemental carbon
EMAC/MESSy	European Centre for Medium-Range Weather Forecasts/Hamburg climate model with the Modular Earth Submodel System
EPA	Environmental Protection Agency
FCRS	Fine crustal particulate matter
Fe	Iron
FPAR	Fraction of photosynthetically active radiation
g	gram
GRSA	Great Sand Dunes, Colorado
GUMO	Guadalupe Mountains, New Mexico
IMPROVE	Interagency Monitoring of Protected Visual Environments
I/O	Input/output
in/hour	inch per hour
K	Potassium
K18	Klingmueller et al. (2018)
kg	kilogram
km	kilometer
LAI	Leaf area index
LULC	Land use/land cover
m	meter
Mg	Magnesium
MKS	Meter/kilogram/second units convention
Mn	Manganese

MODIS	Moderate Resolution Imaging Spectroradiometer
MP	Modeling platform
MSA	Metropolitan Statistical Area
Na	Sodium
NASS	National Agricultural Statistical Service
NCAR	National Center for Atmospheric Research
NEI	National Emission Inventory
NEIC	National Emissions Inventory Collaborative
NLCD	National Land Cover Database
NMB	Normalized mean bias
NME	Normalized mean error
NO_3	Nitrate
NOAA	National Oceanic and Atmospheric Administration
NOx	Nitrogen oxides
OA	Organic aerosol
PiG	Plume-in-Grid
PM	Particulate matter
$PM_{2.5}$	Fine particulate matter with aerodynamic diameter less than 2.5 microns
PMC	Coarse aerosol mass (also CM)
QA/QC	Quality assurance/quality control
RHR	Regional Haze Rule
SACR	Salt Creek, New Mexico
s	second
Si	Silicon
SIP	State Implementation Plan
SO_4	Sulfate
SOAP	Secondary Organic Aerosol Partitioning chemistry
TCEQ	Texas Commission on Environmental Quality
TERP	Texas Emission Reduction Program
Ti	Titanium
UoC	University of Cologne
US	United States
USDA	United States Department of Agriculture
USGS	United States Geological Survey
WBD	Windblown dust
WBDUST	Windblown dust model
WESTAR	Western States Air Resources Council
WIMO	Wichita Mountains, Oklahoma
WRAP	Western Regional Air Partnership
WRF	Weather Research and Forecasting meteorological model
WRF-Chem	Weather Research and Forecasting meteorological model with chemistry
µg	microgram
µm	micrometer or micron

EXECUTIVE SUMMARY

Under AQRP Project 20-011, Ramboll improved the windblown dust emission model (WBDUST) with updated parameterizations and more locally specific and temporally resolved vegetation data. The project started with a detailed evaluation of windblown dust (WBD) models employed in several widely used photochemical modeling systems, and a comparison of their features, formulations, and input datasets against the WBDUST modeling framework. From this review, we identified and implemented specific improvements to the WBDUST formulation. The second phase involved identifying, reviewing, and adapting alternative landcover and year/season-specific cropland activity datasets specific to the US to further improve the characterization of WBD from agricultural lands. Finally, we used the Comprehensive Air quality Model with extensions (CAMx) to assess the effects of all WBDUST updates on simulated particulate matter (PM) concentrations. Modeling results were compared against measurements from monitoring sites in federally protected Class I Areas throughout the south-central US. Emission estimates were speciated for key crustal (soil-derived) elements such as calcium, iron and others that influence atmospheric chemistry and enable more refined model evaluation because they are explicitly monitored.

CAMx test runs revealed that key parameters controlling dust emissions are wind drag partitioning and, to a lesser extent, the amount of vegetative dust suppression. Specifically, we found that it is very important for both processes to specify vegetation cover for each individual emissive landuse/landcover (LULC) type within each grid cell rather than relying on grid-composite values. This additional refinement greatly improved simulated crustal PM concentrations throughout the western US. The WBDUST formulation updates alone resulted in improved model performance separate from the introduction of refined cropland cover and activity datasets.

Model-observation agreement for fine and coarse WBD concentrations has improved substantially with the updated WBDUST model over the original version. The new model is capable of generating sufficient dust on par with measured concentrations in all seasons. Across the entirety of 2016, the model reproduced dust component concentration within a factor of two of measurements. Model performance varied substantially across months and sites. Generally, the model systematically over predicted fine dust components and total coarse mass in the spring and autumn, but under predicted during the summer when measured levels increase. Model performance for coarse mass tended to be better than for individual fine dust elemental components or their sums. There were no clear performance tendencies for fine elemental concentrations across the sites analyzed here, but overall, the relative elemental compositions were appropriately characterized with the majority of mass contained in silicon, aluminum, and iron. This suggests that the various sources of dust speciation applied within WBDUST generally characterize US regional soil composition adequately.

Crustal elements (e.g., calcium and iron) in WBD impact the chemistry of secondary inorganic (sulfate, nitrate, ammonium) and potentially organic compounds. Improved WBD emissions result in both increases and decreases in all of the secondary inorganic particulate species. For sulfate, impacts are generally small with perhaps some tendency toward concentration

increases more than decreases, especially in the eastern US with higher sulfur emissions. Nitrate concentrations tend to be higher in all months, especially in the western US, due to increased abundance of neutralizing cations that convert gaseous nitric acid to particulate nitrate. Effects on ammonium are opposite and smaller, with generally more concentration decreases than increases in the western US for all months. WBD cations tend to displace ammonia as neutralizing agents for sulfate and nitrate.

We offer the following recommendations for future consideration:

- Land use characterization is critically important to WBD from both natural and crop landscapes, and so we encourage the use of the most detailed land type coverages available.
- Temporal variations in vegetative patterns are equally important as their spatial distribution. Overstated springtime dust emissions from expansive cropland areas indicate continued over-simplification of how they are treated in the WBDUST model, e.g., what fraction is cultivated at any given time during the planting seasons, and what fraction is consistently irrigated or not (the latter being implicitly assumed). Improved information on tilling activity and irrigation is needed.
- Certain elemental species exhibit consistent high bias relative to routine ambient measurements, particularly iron, which is an important catalyst for aqueous sulfate production from SO_2. Speciation profiles should be reviewed and updated as new information becomes available.
- Related to the point above, proper modeling of surface conditions is essential to the WBD process. Updates to WBDUST may be necessary as WRF performance in simulating several surface variables improves, particularly soil moisture.
- An inter-model comparison among WBDUST and the other models and schemes reviewed herein should be conducted in the most consistent manner possible.

1.0 INTRODUCTION

1.1 Background

The Texas Commission on Environmental Quality (TCEQ) conducts photochemical modeling to support regulatory air quality programs, including State Implementation Plans (SIPs) addressing Texas ozone nonattainment areas and the federal Regional Haze Rule (RHR; EPA, 2021a). TCEQ applies the Comprehensive Air quality Model with extensions (CAMx; Ramboll, 2021) for these purposes.

For the RHR SIP, TCEQ simulated visibility degradation caused by particulate matter (PM) within federally protected "Class I Areas" (national parks and wilderness areas) throughout the south-central US. That modeling under predicted soil-derived PM relative to speciated PM monitoring (Ramboll, 2020a), especially in the coarse mode (larger than 2.5 microns). TCEQ used the CAMx preprocessor "WBDUST" to estimate emission of windblown dust (WBD). Ramboll also noted insufficient emission estimates from WBDUST in several past modeling applications. Therefore, we have attributed the cause of TCEQ's dust under predictions to WBDUST. Separately, Ramboll's initial attempt to implement minor updates to WBDUST that relax certain restrictions on the numerous criteria that must align to emit dust had negligible to minimal effects. A subsequent update to remove an imposed cap on wind stress, which directly determines dust emission rates, resulted in large PM over predictions.

Whereas fine PM (less than 2.5 microns) commonly includes a multitude of primary and secondary inorganic and organic compounds from a variety of sources, including crustal (soil-derived) components, the majority of coarse PM derives from direct emissions of crustal material. Crustal emissions are especially difficult to estimate given the variety of source mechanisms, both natural and anthropogenic, and environmental conditions that lead to high spatial and temporal variability. Understandably, WBD represents an appreciable fraction of the total uncertainty in crustal emissions, while dust impacts at monitoring sites can be highly influenced by local emissions that may not be sufficiently resolved by grid models.

Under AQRP Project 20-011, Ramboll improved the WBDUST emission model with updated parameterizations and more locally specific and temporally resolved data to define vegetative cover. The project started with a detailed evaluation of WBD models employed in several widely used photochemical modeling systems, and a comparison of their features, formulations, and input datasets against the WBDUST modeling framework. From this review, we identified and implemented specific improvements to the WBDUST formulation. The second phase involved identifying, reviewing, and adapting alternative landcover and year/season-specific cropland activity datasets specific to the US to further improve the characterization of WBD from agricultural lands. Finally, we used CAMx to assess the effects of all WBDUST updates on simulated PM concentrations. Modeling results were compared against measurements from monitoring sites in Class I Areas throughout the south-central US. Emission estimates were speciated for key crustal (soil-derived) elements such as calcium, iron and others that influence atmospheric chemistry and enable more refined model evaluation because they are explicitly monitored.

The remainder of this Section reviews PM results obtained in past modeling applications using the WBDUST emission model. Section 2 describes the WBDUST algorithm, input datasets and assumptions, and then compares those to WBD schemes employed in other widely used models, noting key differences in methodologies. Section 2 closes with a list of specific updates selected for the WBDUST parameterization based on our review and from initial process-level testing. Section 3 presents our review and selection of available US vegetative and agricultural datasets that can support the updated WBDUST model. It then describes the preparation of these datasets and process by which they are used in WBDUST to improve the spatial and temporal characterization of emissive lands. Section 4 presents CAMx PM simulation results comparing the original and updated WBDUST versions against measurement data. Section 5 provides our conclusions and recommendations for future work.

1.2 Review of Past CAMx WBDUST Estimates

1.2.1 Ramboll and TCEQ 2016 Modeling Platforms

In 2018-19, the US Environmental Protection Agency (EPA) developed a national Modeling Platform (MP) spanning the year 2016 (EPA, 2019). The 2016 MP employs a North American domain with 36 km grid resolution, and a nested US domain with 12 km grid resolution (Figure 1-1). EPA developed meteorological fields using the Weather Research and Forecasting (WRF; NCAR, 2021) model based on EPA's standard configuration. EPA and multi-jurisdictional planning organizations compiled anthropogenic emissions data in a joint Inventory collaborative study (NEIC, 2021). Annual, county-level fugitive dust emission rates from anthropogenic sources (i.e., agricultural and construction activities, roads, etc.) were included in the nonpoint sector according to the 2014 V2 National Emission Inventory (NEI; EPA, 2021b). During processing to model input files, EPA reduced fugitive dust emissions where and when at least 0.01 inches of precipitation occurred or there was snow cover; wind conditions were not considered for these sectors. This methodology is consistent with anthropogenic fugitive dust estimates developed in other regulatory MPs. However, WBD was not included in EPA's 2016 emissions because the MP primarily supports the Community Multiscale Air Quality (CMAQ; EPA, 2021c) model, which possesses an in-line WBD algorithm. Separately, Ramboll developed 2016 hourly WBD emissions for CAMx using the first release of the WBDUST emission model (v1.0) in combination with the 2016 MP meteorology (hereafter referred to as the Ramboll 2016 MP).

TCEQ also developed a CAMx-based 2016 MP to assess visibility progress in Texas and across the south-central US (Ramboll, 2020a). The TCEQ MP is largely based on the EPA MP described above, however, TCEQ separately derived meteorological fields using WRF and developed emission estimates for certain natural sectors (biogenic, fires, oceanic, and lightning NOx). This included applying WBDUST v1.0 in combination with TCEQ's MP meteorology.

We evaluated the performance of both Ramboll and TCEQ MPs in replicating total PM mass and species component concentrations at numerous Class I Area monitoring sites within and near Texas (Figure 1-2). These sites are operated by the Interagency Monitoring of Protected Visual Environments network (IMPROVE, 2021).

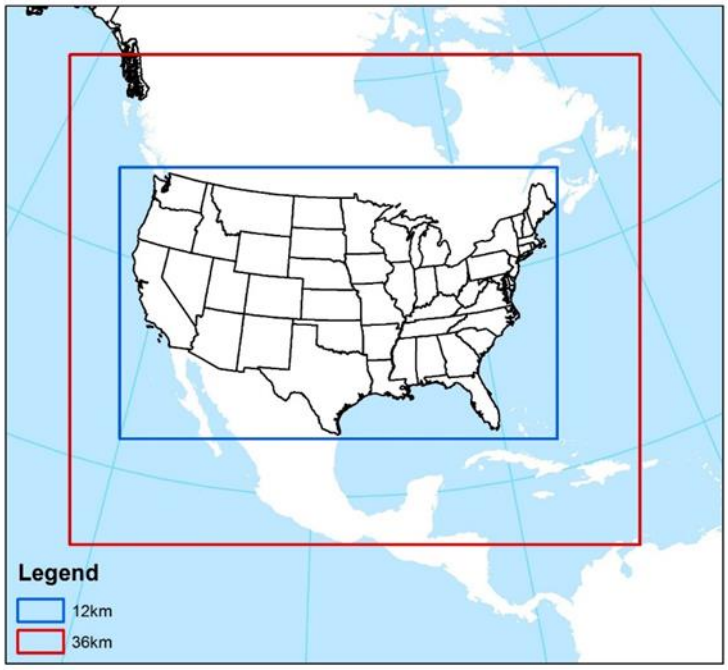

Figure 1-1. Modeling grids employed in the EPA, Ramboll and TCEQ 2016 Modeling Platforms.

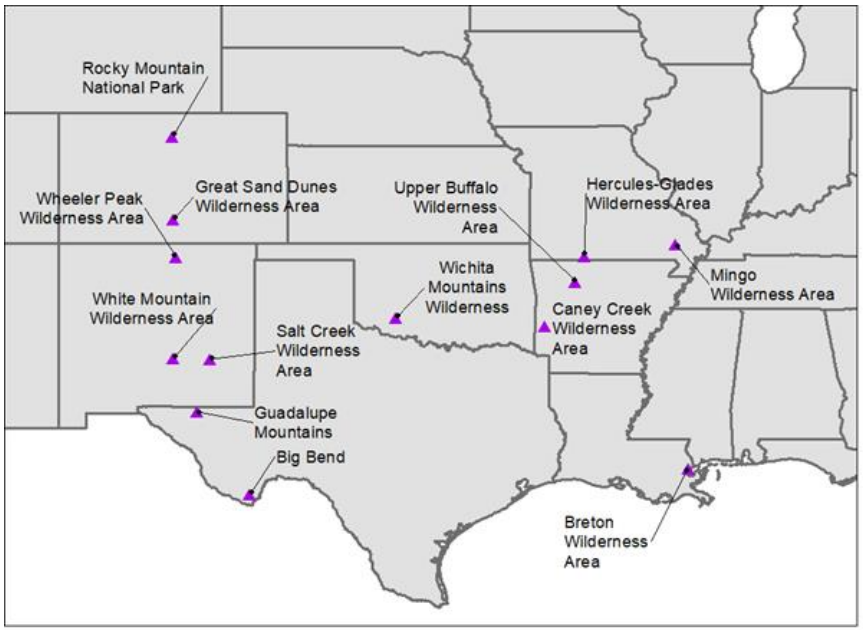

Figure 1-2. Federal Class I Areas with PM monitoring sites operated by the IMPROVE network in Texas and nearby states.

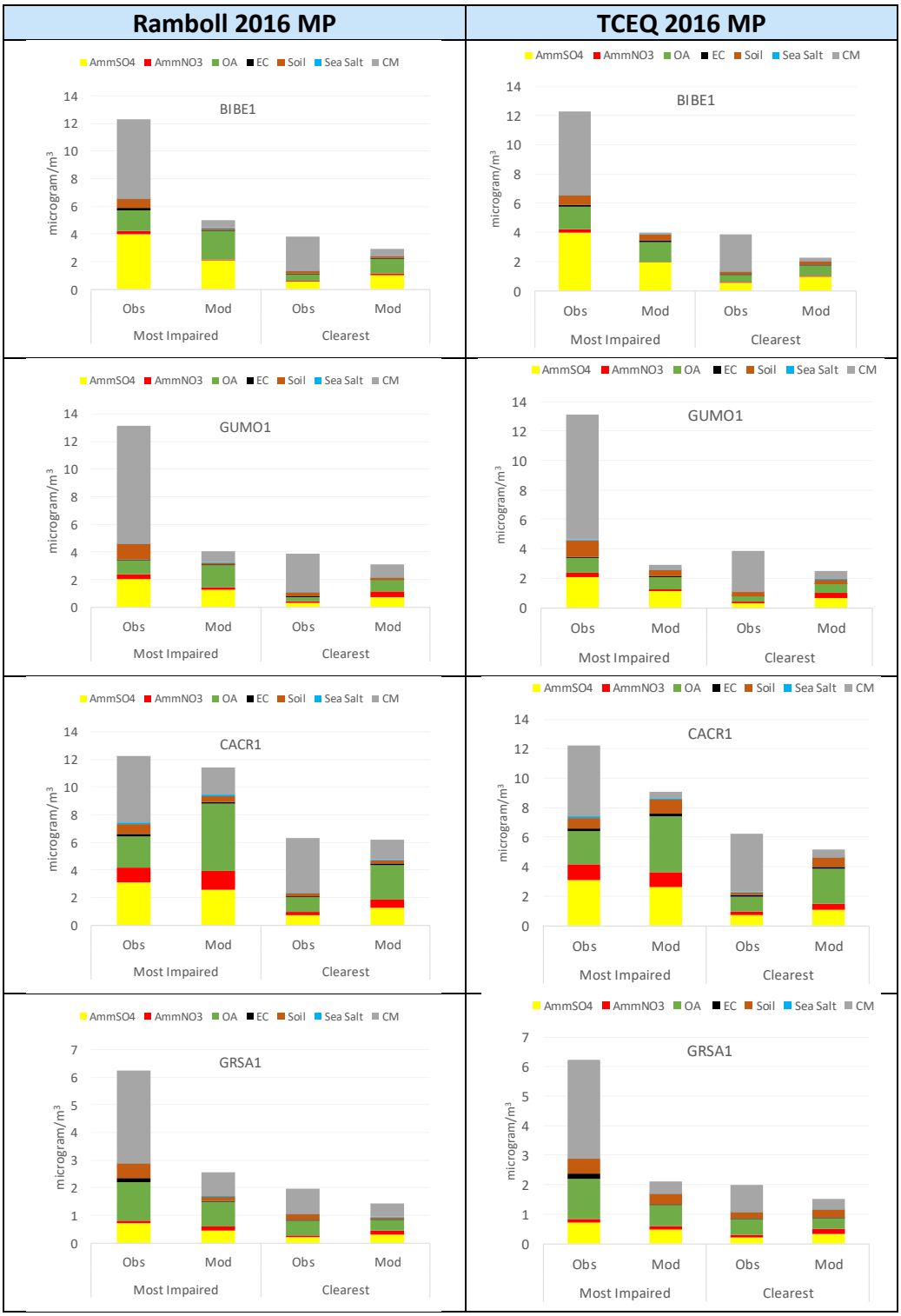

Figure 1-3. Comparison of observed (Obs) and modeled (Mod) PM components in the Ramboll MP (left) and the TCEQ MP (right) at four IMPROVE sites: Big Bend (BIBE), Guadalupe Mountains (GUMO), Caney Creek (CACR) and Great Sand Dunes (GRSA). Results are shown for the most impaired and clearest visibility days in 2016.

Figure 1-3 shows examples of these comparisons at four Class I sites that reported large PM fractions of crustal material. Both MPs exhibited very similar performance results, especially large underestimates of coarse mass (CM; grey bars) on both the clearest and most impaired days, and under predictions of fine soil (brown bars) on the most impaired days. Poor performance in replicating CM may be due, in part, to highly localized emissions that the model cannot resolve.

Figure 1-4 presents a time series of observed and predicted (Ramboll MP) PM components on the most impaired visibility days through 2016 at the Big Bend IMPROVE site. Results from other dust laden IMPROVE sites in the western US were very similar, although they were associated with much less sulfate (presumably from the nearby Carbon power plant). Modeled CM and fine soil were consistently under predicted on all poor visibility days.

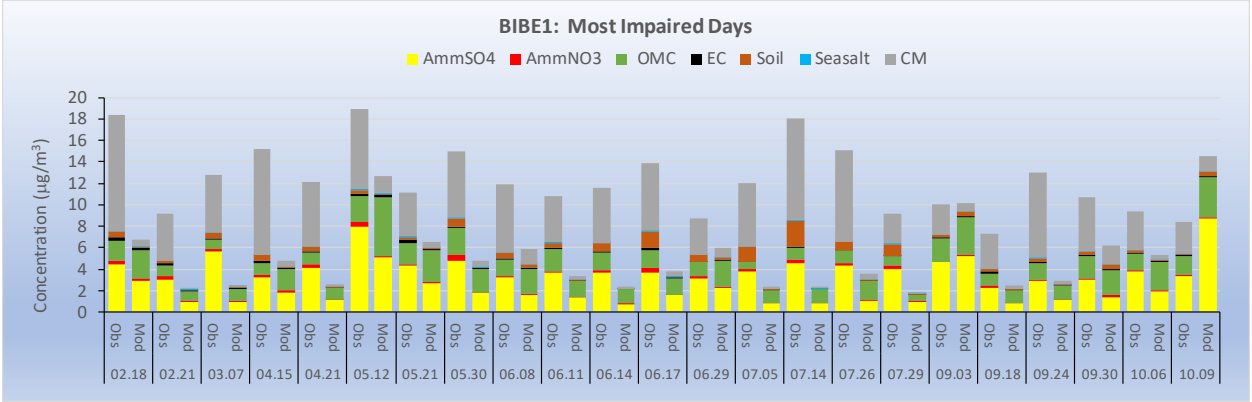

Figure 1-4. Comparison of observed (Obs) and modeled (Mod) PM components in the Ramboll MP at the Big Bend IMROVE site on the most impaired days of 2016.

Figure 1-5 shows seasonal normalized mean bias (NMB; signed error) and normalized mean error (NME; absolute error) for the fine PM soil component at individual IMPROVE sites throughout the 12 km 2016 MP domain. A similar plot is shown in Figure 1-6 for the CM component. In all seasons, both fine soil and CM were largely under predicted throughout the western US and within the southwest in particular. The largest errors tended to occur during the spring and summer seasons, while the smallest errors tended to occur in autumn. Sites in the eastern US exhibited large over predictions in fine soil, but this is more likely related to emission estimates for other fugitive sources rather than WBD.

1.2.2 WRAP 2014 Modeling Platform

The Western Regional Air Partnership (WRAP), through the Western States Air Resources (WESTAR) Council, developed a CAMx-based 2014 MP to assess visibility progress throughout the western US (Ramboll, 2019). The WRAP grid system also employed a North American grid at 36 km resolution, and all meteorological and emission inputs on that grid were developed by EPA. However, WRAP included a smaller western US grid at 12 km resolution for which WRAP developed all meteorological and emission inputs. WRAP applied WBDUST v1.0 in combination with their 12-km MP meteorology.

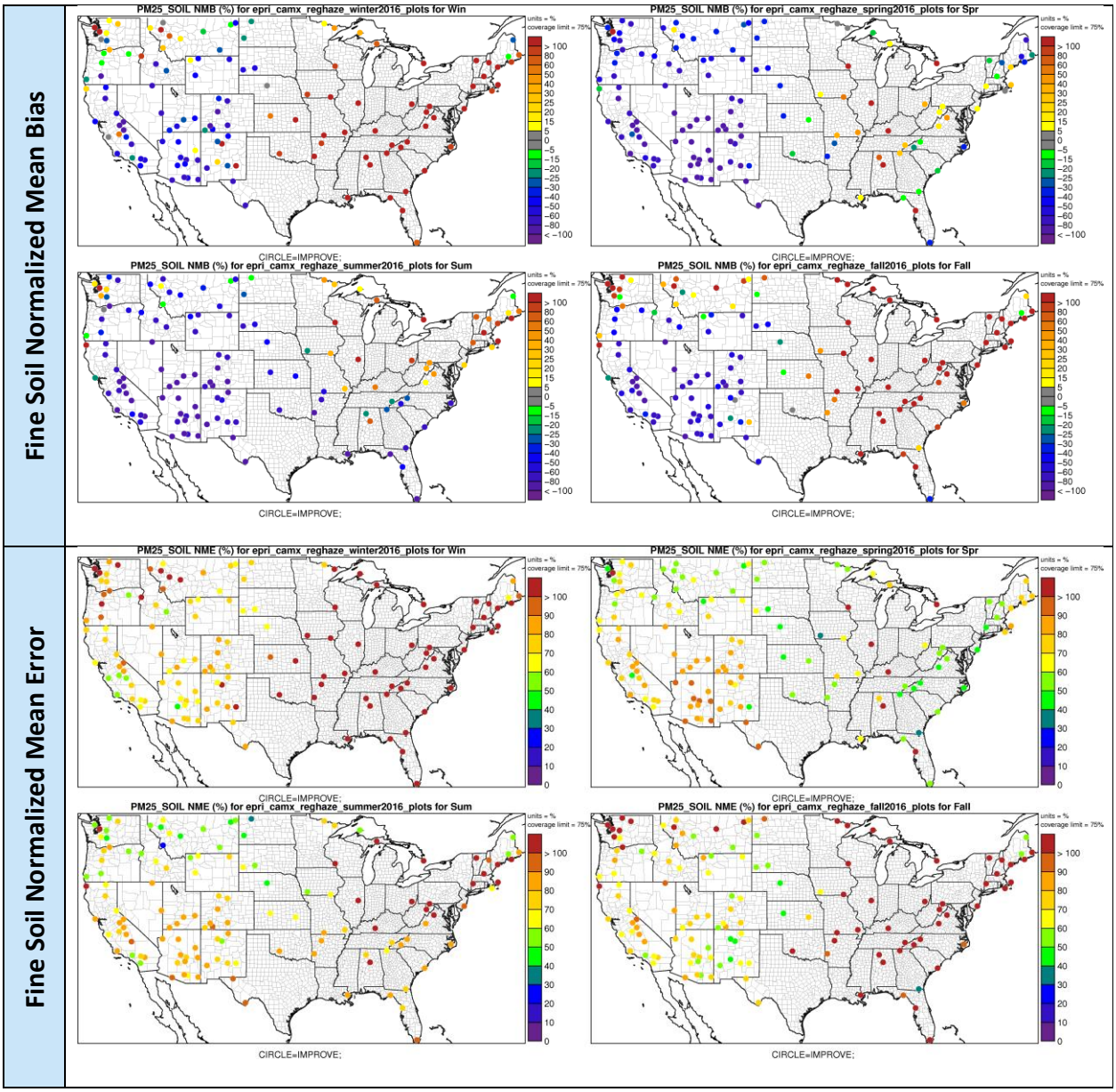

Figure 1-5. Seasonal normalized mean bias (signed error, %) and normalized mean error (absolute error, %) for the fine PM soil component at individual rural IMPROVE sites throughout the 12 km 2016 MP domain. Winter (top left), spring (top right), summer (bottom left), autumn (bottom right).

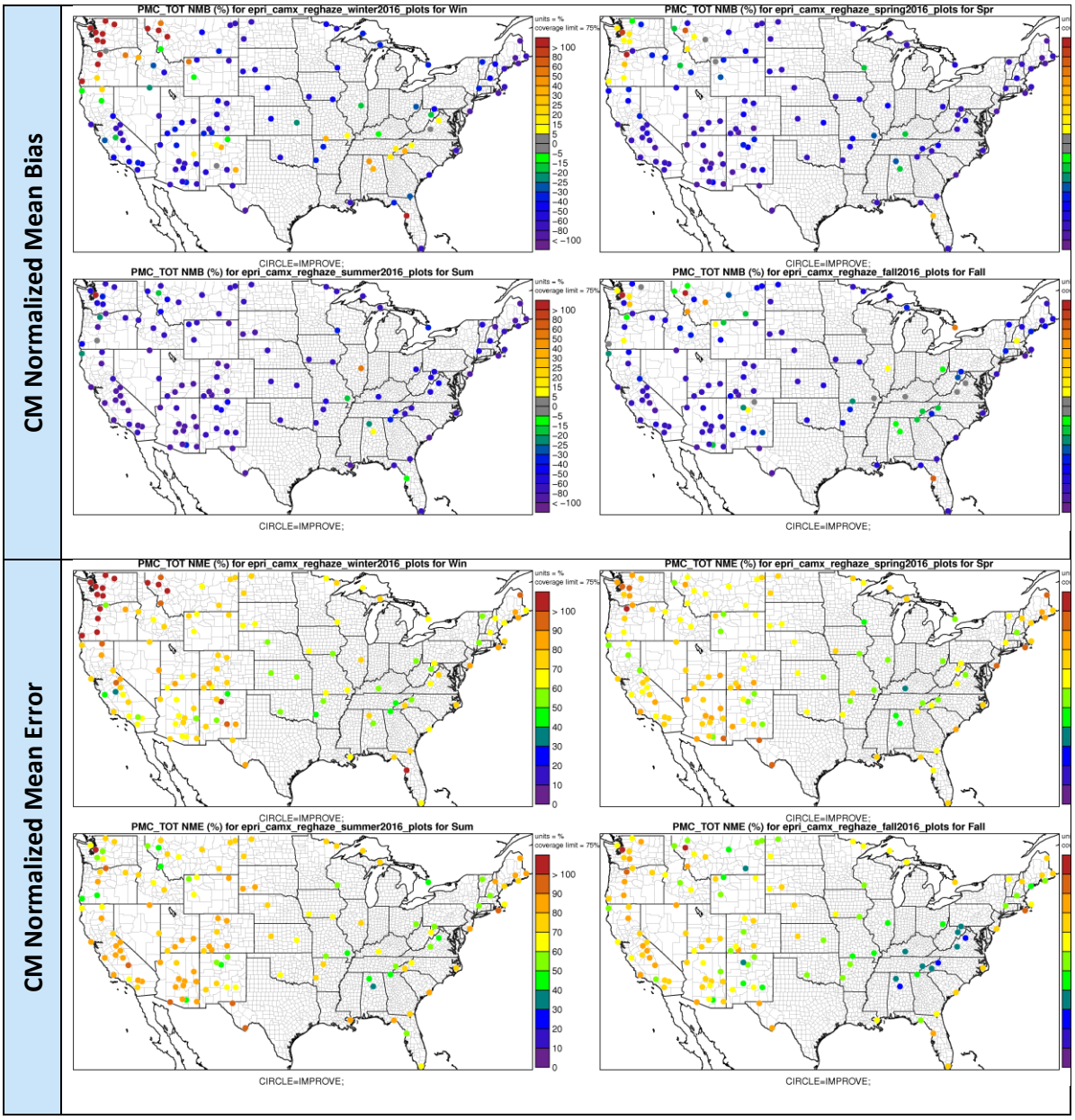

Figure 1-6. Seasonal normalized mean bias (signed error, %) and normalized mean error (absolute error, %) for CM at individual rural IMPROVE sites throughout the 12 km 2016 MP domain. Winter (top left), spring (top right), summer (bottom left), autumn (bottom right).

Figures 1-7 and 1-8 show similar seasonal NMB plots as Figures 1-5 and 1-6 for PM fine soil and CM, respectively, at IMPROVE sites within the 12 km modeling grid. WRAP results exhibited nearly identical patterns to the Ramboll 2016 MP results, with the largest under predictions occurring throughout the southwest US in spring and summer, and the least under predictions in winter and autumn.

Figures 1-9 and 1-10 present seasonal scatter plots of fine soil and CM at sites throughout the 12-km WRAP modeling grid. Sites measuring fine soil include the IMPROVE network at rural sites and the Chemical Speciation Network (CSN; EPA, 2021d) at more urban sites. Only the IMPROVE network reports CM. Fine soil at IMPROVE sites were consistently under predicted every season with average NMB ranging -30% in winter and autumn to -80% in spring. Biases at CSN sites, however, ranged from large over predictions in winter and autumn to slight under predictions in spring and summer. Performance at CSN sites was likely not related to WBD but rather local urban-oriented anthropogenic fugitive sources such as road dust. CM under predictions at IMPROVE sites were consistent with fine soil, with seasonal NMB ranging -50% to -70%.

The modeling results reviewed here clearly demonstrated a lack of crustal material throughout the western US, over all seasons, and across all three applications. This performance issue was consistent regardless of source of meteorology, choice of year or domain. The use of WBDUST was the one consistent feature among all three applications.

1.3 Minor Modifications to Increase Dust Emissions

In late 2019, Ramboll identified two specific issues in WBDUST that mostly likely contributed to underestimated emissions:

1. The capping of friction velocity (U*) in the Klingmueller et al. (2018) algorithm upon which WBDUST is based: with this cap, U* rarely exceeded the threshold friction velocity for raising dust, and when it did, it was often too low to emit a sufficient amount. The cap also limited dust emissive areas to only the driest and non-vegetated areas, which in the US are concentrated in relatively small areas in southeast California, western Utah, and Northern Mexico.
2. Excessive leaf area index (LAI), which is the key parameter for defining the amount of vegetation cover: particularly for croplands, LAI can seasonally approach zero, yet input LAI fields or defaults assigned by landcover classification are often far too high in the western US throughout the year. This effectively restricted crop, shrub, and grasslands from being able to emit dust, despite well-documented historical and contemporary dust events in west Texas and Oklahoma where these three landcover types are dominant.

Subsequently, Ramboll released WBDUST v1.1, which included two simple modifications:

1. Removal of the U* cap.
2. Averaging of global clay and LAI input data at 0.1-degree resolution (~10 km) to the CAMx grid if CAMx resolution exceeds 20 km;

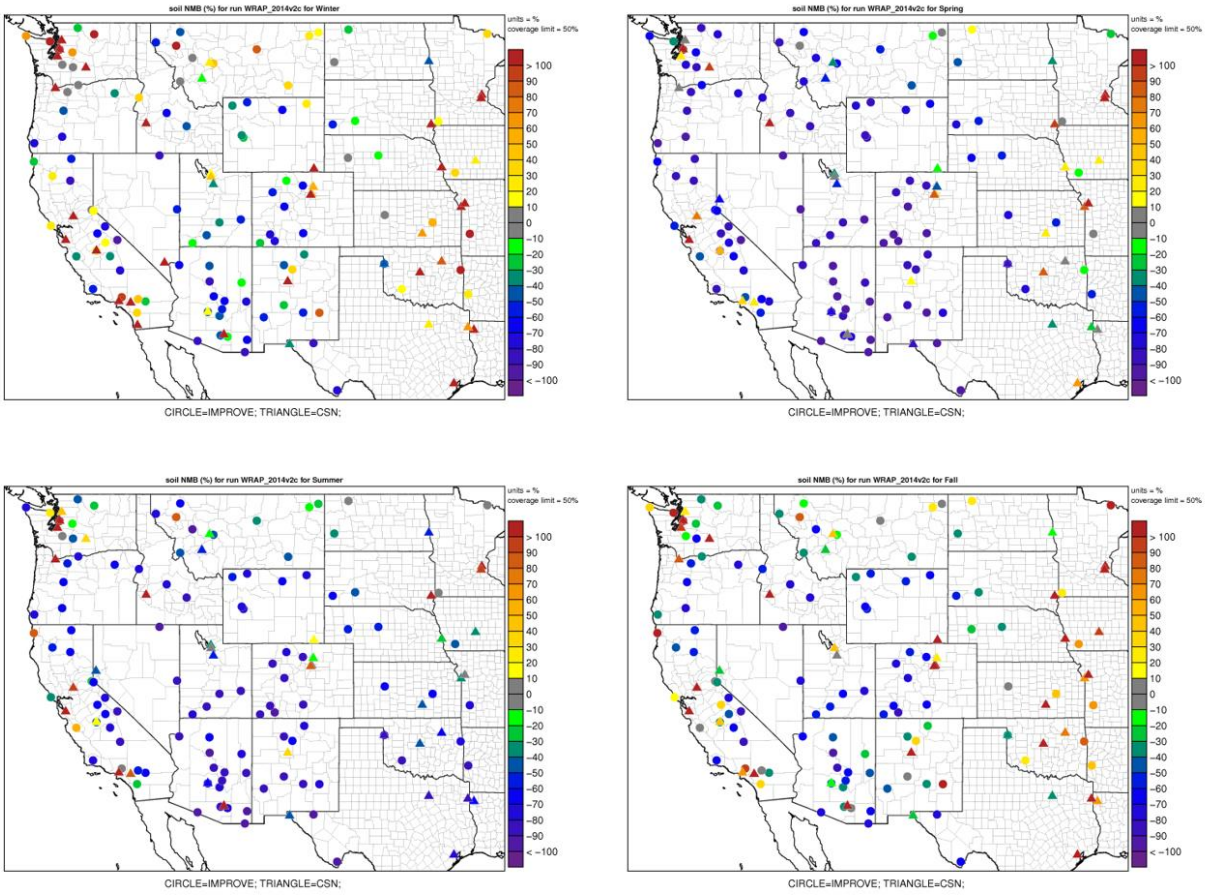

Figure 1-7. Seasonal normalized mean bias (signed error, %) for the fine PM soil component at individual rural IMPROVE and urban CSN sites throughout the 12 km WRAP 2014 MP domain. Winter (top left), spring (top right), summer (bottom left), autumn (bottom right).

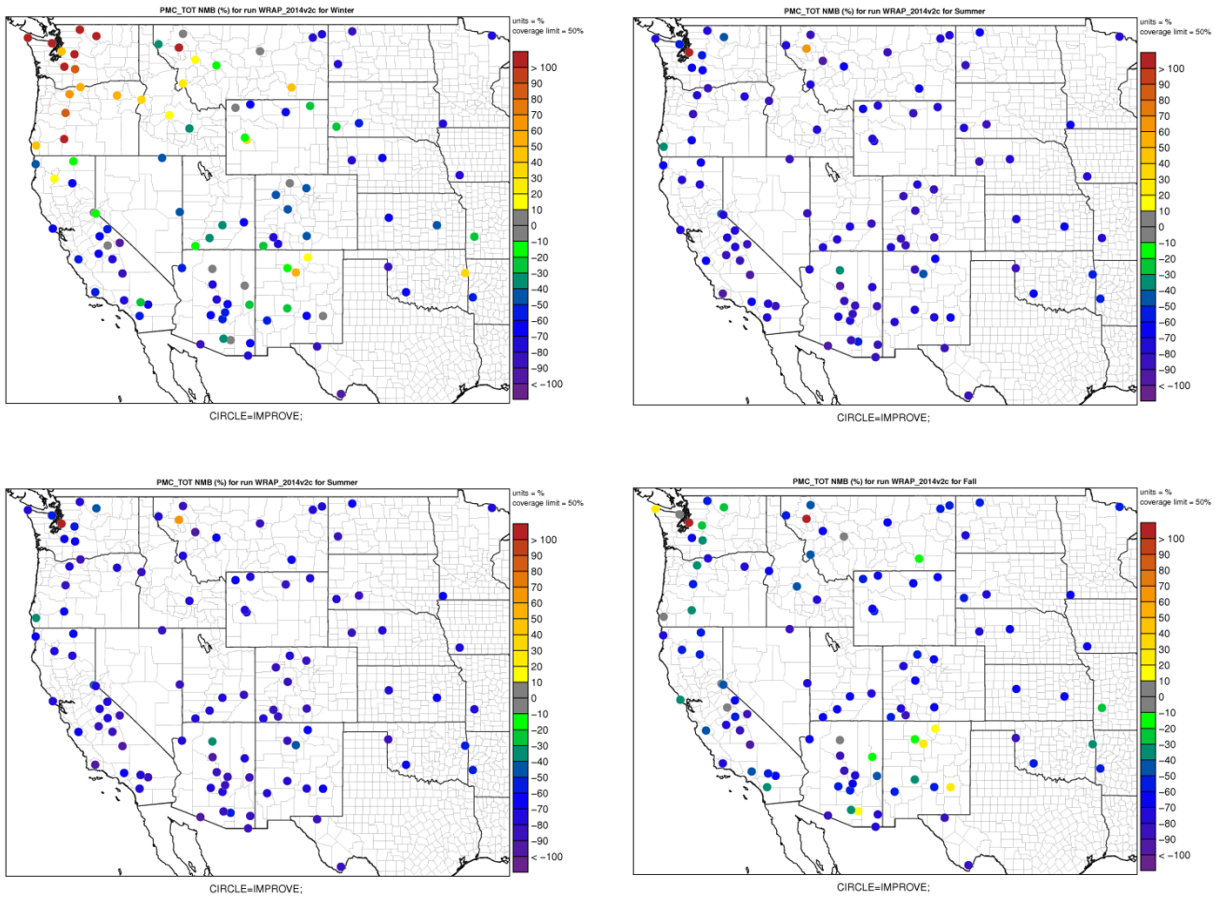

Figure 1-8. Seasonal normalized mean bias (signed error, %) for CM at individual rural IMPROVE sites throughout the 12 km WRAP 2014 MP domain. Winter (top left), spring (top right), summer (bottom left), autumn (bottom right).

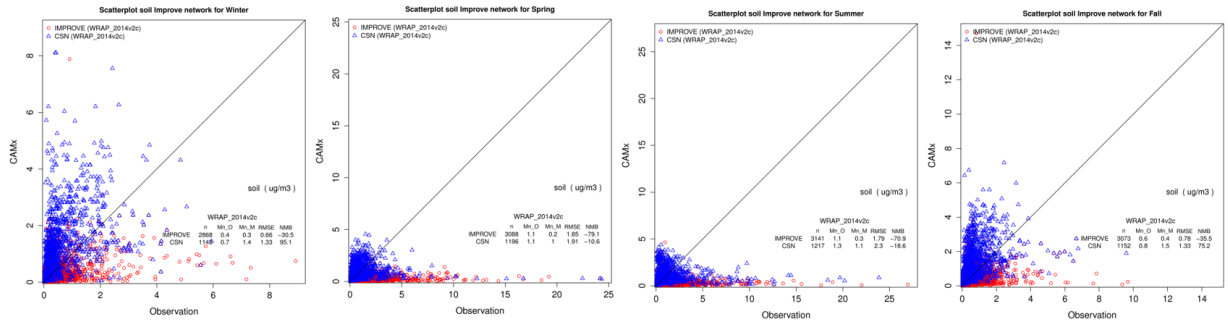

Figure 1-9. Seasonal scatter plots of predicted vs. monitored fine soil concentrations at rural IMPROVE (red) and urban CSN (blue) monitoring sites throughout the 12-km WRAP modeling grid. Left to right: winter, spring, summer, and autumn.

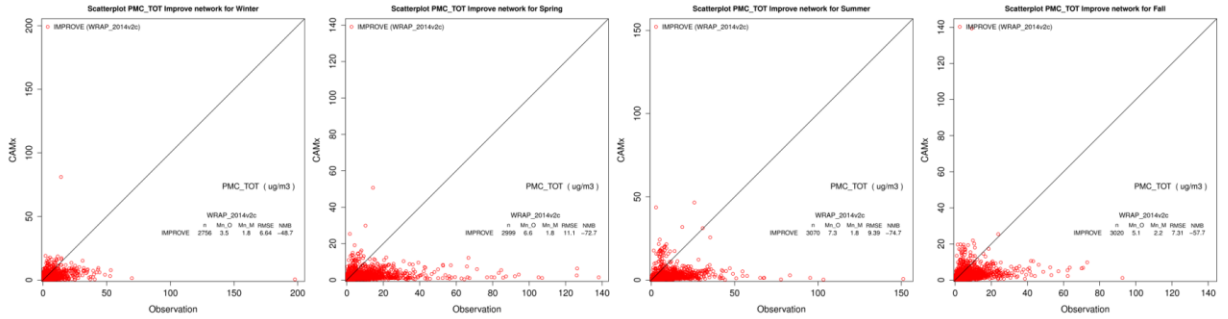

Figure 1-10. Seasonal scatter plots of predicted vs. monitored CM concentrations at rural IMPROVE monitoring sites throughout the 12-km WRAP modeling grid. Left to right: winter, spring, summer, and autumn.

The first modification simply and directly addressed the lack of dust emissions in v1.0. Tests in hemispheric CAMx applications improved dust emission rates over large global desert areas such as the Sahara and across the middle east. The second modification addressed issues for CAMx grid resolutions much greater than the global data resolution. WBDUST v1.0 had simply assigned the 0.1-degree global data to each CAMx grid cell regardless of resolution. While this approach continues in WBDUST v1.1 for CAMx grid resolutions less than 20 km, it was found to be important to average these data for coarser resolutions.

However, the removal of the U* cap resulted in massive over predictions in seasonal WBD emissions and resulting crustal concentrations in the Ramboll 2016 MP. Figure 1-11 compares monthly fine soil concentrations from WBDUST v1.0 and v1.1; Figure 1-12 similarly compares results for CM. Monthly-averaged fine soil concentrations reached 40-90 µg/m^3 in the southwest US during April and July, while monthly-averaged CM concentrations exceeded 300 µg/m^3 in the southwest US during July. The cause for these over predictions was tracked to the manner in which U* is calculated in WBDUST relative to other WBD schemes. Based on these previous analyses, this project revealed several issues that needed to be addressed in WBDUST.

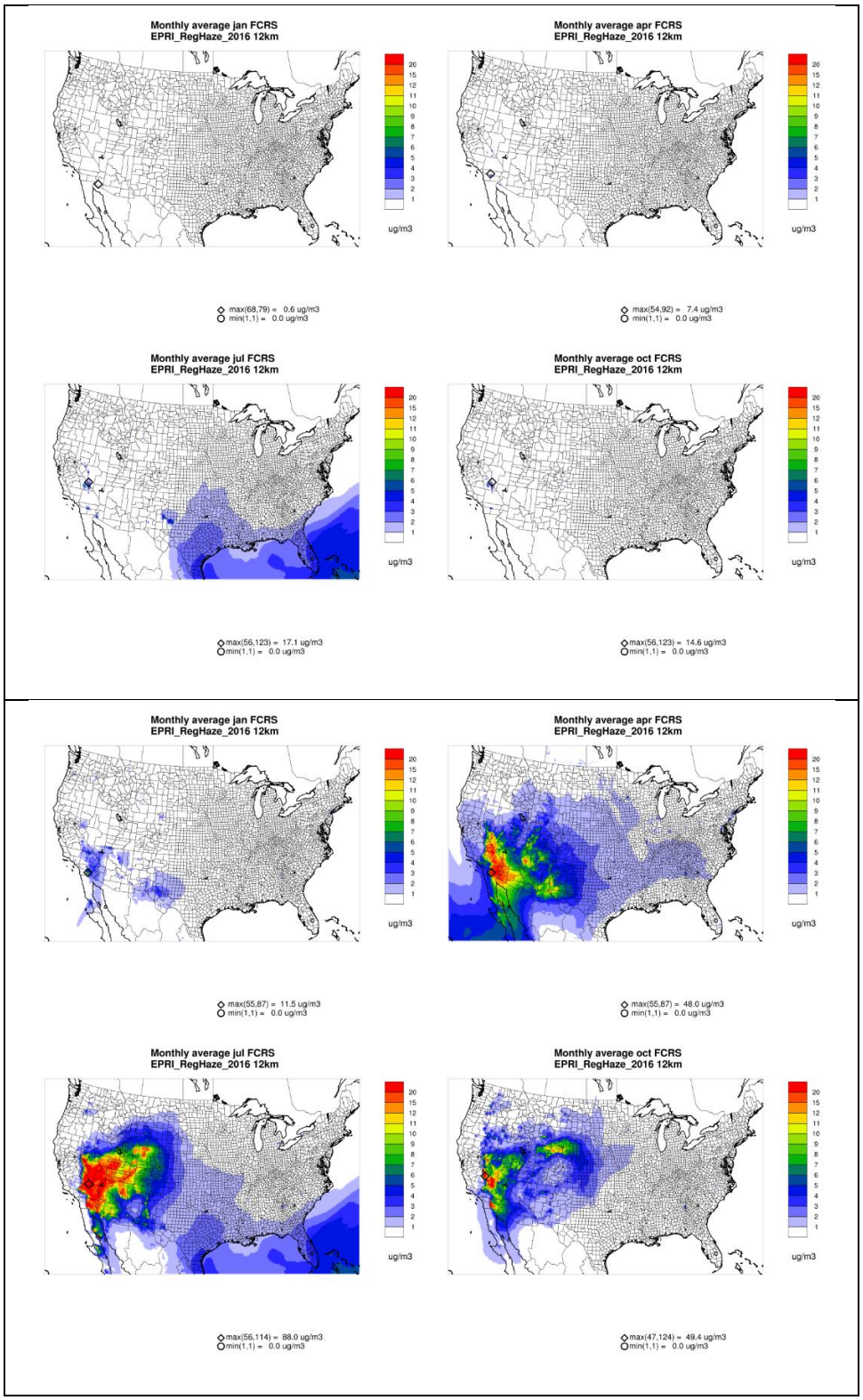

Figure 1-11. Comparison of simulated monthly-averaged fine crustal (FCRS) concentrations for January, April, July, and October from the Ramboll 2016 MP. Results based on WBDUST v1.0 (top panel) and v1.1 (bottom panel).

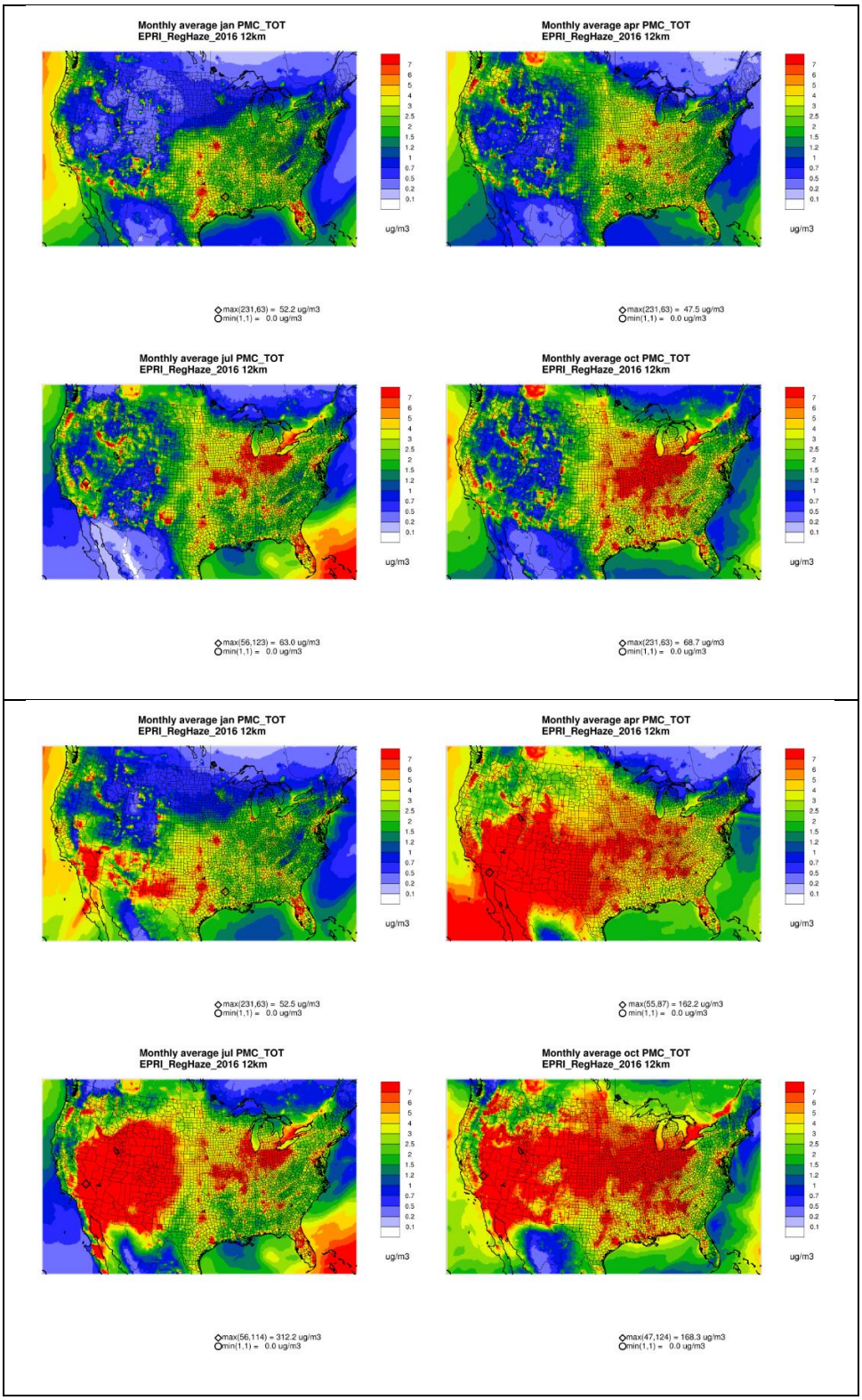

Figure 1-12. Comparison of simulated monthly-averaged CM concentrations for January, April, July, and October from the Ramboll 2016 MP. Results based on WBDUST v1.0 (top panel) and v1.1 (bottom panel).

2.0 ALTERNATIVE WBD METHODS

2.1 The WBDUST v1.0 Algorithm

In 2018, Ramboll developed the WBDUST v1.0 emission model based on an adaptation of the global dust scheme described by Astitha et al. (2012 and references therein, hereafter A12) and Klingmueller et al. (2018, hereafter K18) as employed in the EMAC/MESSY[1] global chemistry-climate model. The design objective of WBDUST was to provide the CAMx user community with a simple dust emission framework that supports multi-scale CAMx applications anywhere in the world. The scheme parallels the techniques of many other models in that it depends on the degree of wind stress (as quantified by "friction velocity") that initiates the saltation process, i.e., lifting large soil particles that bombard or "sand blast" finer-grained particles within the soil thereby generating air emissions of dust. Many specific conditions must align to cause WBD emissions according to numerous internal parameterizations and input data defining meteorology and the state of soil and vegetation.

WBDUST uses the following input datasets:

- CAMx-ready 2-D and 3-D gridded meteorological input files derived from WRF (required): vertical layer heights, pressure, wind speed, temperature, and soil temperature and moisture;
- CAMx-ready 2-D gridded surface characterization input file (required): fractional land use/land cover (LULC) type, optional LAI;
- Global gridded soil clay fraction at 0.1-degree (~10 km) resolution, developed by K18 (required);
- Global gridded soil elemental composition at 0.1-degree (~10 km) resolution, developed by K18 (required): fractions for sodium, magnesium, calcium, and potassium;
- Global gridded monthly-average LAI at 0.1-degree (~10 km) resolution, developed by K18 (optional): derived from Moderate Resolution Imaging Spectroradiometer (MODIS) satellite retrievals from 1998 to 2015;
- Global gridded barren land mask at 0.05-degree (~5 km) resolution, developed by K18 (optional): defined as 1 [emissive] or 0 [not emissive]);

If the global LAI file is provided, WBDUST preferentially used that definition of LAI. WBDUST finds the appropriate month and year of LAI data to use from the date on the CAMx input files. If the year to be processed occurs after 2015, then WBDUST uses the appropriate month from 2015. If global LAI is not provided, WBUST either uses the optional gridded LAI from the CAMx surface input file (if present) or determines LAI based on daily interpolation of default monthly values assigned to each of the 26 CAMx landcover classifications (as is done within CAMx when LAI is not present in the surface input file).

If the global barren land mask is provided, then that definition of emissive land is used as an overlay on top of the landcover distributions defined in the CAMx surface input file. Emissive

[1] The EMAC/MESSy atmospheric chemistry–climate model combines the ECMWF/Hamburg (ECHAM) climate model developed at the Max Planck Institute for Meteorology with the Modular Earth Submodel System (MESSy).

areas in the global file define large, climatologically well-established areas of barren desert lands such as the Sahara, Gobi, and the middle east. In North America, barren lands are limited to relatively small areas of the southwest US and northern Mexico. If the global barren land mask is provided, WBDUST defines potentially emissive areas according to the intersection of barren land and the gridded distribution of barren, grass, shrub, and crop lands from the CAMx surface input file. If the global barren land mask is not provided, WBDUST defines potentially emissive areas solely according to the four CAMx landcover types. This potentially opens more areas for WBD emissions beyond the global barren mask. In both cases (with or without the barren mask), the total fraction among all emissive landcover types within each grid cell is stored and any cells with zero total fraction or with snow cover are ignored for WBD calculations.

2.1.1 Threshold Friction Velocity

The threshold friction velocity over a smooth soil surface (U^*_{t0}) determines the minimum wind stress required to initiate and maintain the saltation process within an emissive grid cell. It depends primarily on saltation particle size (D_p). A12 developed two approaches: a single threshold applicable to the optimal saltation particle size (D_p = 60 µm) at which the threshold is minimum, and a range of thresholds for saltation particle sizes from 0.1 to 1000 µm. WBDUST uses the single threshold approach:

$$U^*_{t0} = \frac{0.129}{\sqrt{1.928\,B^{0.092} - 1}} \sqrt{\frac{\rho_p g D_p}{\rho_\alpha}\left(1 + \frac{0.006}{\rho_p g D_p^{2.5}}\right)}$$

where the friction Reynolds number (B) depends on D_p according to

$$B = 1331\,D_p^{1.56} + 0.38$$

In the equations above, all units are in CGS (U^*_{t0} in cm/s, D_p in cm), ρ_p is particle density (g/cm^3), g is gravitational acceleration (980 cm/s^2), and ρ_α is air density (g/cm^3). A uniform saltation particle density for quartz (2.65 g/cm^3) is assumed for all processes throughout the scheme, which is common in other WBD schemes. Note that the single threshold approach does not account for variations in saltating characteristics (soil composition and size spectra) which conceivably contribute to the lack of WBD emissions.

<u>Adjustment for Soil Moisture</u>

Soil moisture increases resistance to saltation because it affects soil particle cohesion. A factor is applied to U^*_{t0} to raise the threshold for moist soils. Gridded soil moisture is read as an additional diagnostic surface field from the CAMx-ready 2-D meteorological input file. Moisture is taken from WRF's top-most soil layer, which can vary in depth from 1 to 30 cm depending on the chosen land surface model. As discussed later, the moisture content of deep soil layers is not representative of the exposed surface and the related inertia in deep soil drying rates can significantly suppress the saltation process. Soil moisture reported by WRF is expressed as volumetric ratio so it must be converted within WBDUST to gravimetric or mass ratio by

dividing by an assumed typical dry soil density of 1.5 g/cm^3, which again does not account for potentially important variations in soil composition.

The adjustment factor applied to the threshold friction velocity is based on the difference between the gravimetric soil moisture (w) and the residual soil moisture (w', g/g), where w' is dependent on the clay content (in %) of the soil:

$$w' = 0.0014(clay)^2 + 0.17(clay)$$

When w' > w, the adjustment factor F_{mois} is 1. Otherwise, the factor is:

$$F_{mois} = \sqrt{1 + 1.21(w - w')^{0.68}}$$

K18 deactivate the soil moisture factor, stating that this choice results in higher dust loadings in EMAC/MESSy that are closer to satellite-derived aerosol optical depth in the middle east. We elected to maintain this factor in WBDUST.

Adjustment for Surface Roughness

The threshold friction velocity is further adjusted to account for the presence of surface roughness elements that limit momentum flux to the smooth soil surface. Referred to as a drag partitioning scheme, a larger factor should be applied to surfaces with more and larger obstacles (rocks, vegetation, etc.). However, A12 apply a simple constant relationship between the bulk surface roughness length (z_0) and a typical roughness length of soil (z_{0s}):

$$F_{drag} = \frac{1}{1 - \frac{\ln(z_0/z_{0s})}{\ln[0.35(10/z_{0s})^{0.8}]}}$$

where globally uniform values are assigned to z_0 and z_{0s} (0.01 cm and 0.00333 cm, respectively). The lack of cell- or landcover-specific z_0 values may be a limitation in the scheme.

The final adjusted cell-specific threshold friction velocity is thus:

$$U_t^* = F_{mois} \cdot F_{drag} \cdot U_{t0}^*$$

2.1.2 Saltation Flux

For a given grid cell determined to be potentially emissive, WBDUST calculates the actual friction velocity (U*) according to similarity theory (Louis, 1979):

$$U^* = \frac{\varphi k U}{\ln(z/z_0)}$$

where k is the von Karman constant (0.4), U is wind speed (m/s) in the CAMx surface layer, z is height (m) of the wind speed level, φ is a non-dimensional stability parameter calculated by the Louis (1979) scheme, and z_0 is the bulk roughness length (m) for the given grid cell according to the area-weighted fraction of landcover types present (based on monthly default z_0 per

landcover category). Note that z_0 and thus U* and resulting saltation flux are not determined for each individual emissive landcover type present in a grid cell, which is an important oversimplification in WBDUST. K18 cap U* at 0.4 m/s to control the quantity and frequency of dust emissions in the EMAC/MESSy model. We included this cap in WBDUST v1.0 but removed it in v1.1, which led to large WBD over predictions and raised concerns over the veracity of K18's adaptation of the A12 scheme.

If U* exceeds U^*_t, a horizontal saltation flux (H_{salt} in kg/m/s) is calculated for the most optimal saltation particle size (60 µm):

$$H_{salt} = \frac{c\rho_\alpha U^{*3}}{g}\left(1 + \frac{U_t^*}{U^*}\right)\left(1 - \frac{U_t^{*2}}{U^{*2}}\right)$$

where c = 1 in A12, c = 1.5 in K18, and all units are in MKS (U* and U^*_t in m/s, ρ_α in kg/m^3, g is 9.8 m/s^2). WBDUST uses the K18 value of c.

2.1.3 WBD Emission Flux

The vertical flux of dust particles (V_{dust} in kg/m^2/s) from an emissive cell is proportional to the saltation flux, with a sandblasting efficiency (m^{-1}) serving as the proportionality constant that depends on the clay content (in %) of the soil. In A12, the vertical flux is determined from:

$$V_{dust} = H_{salt} \times 1000^{(0.134(clay)-6)} \quad \text{clay} < 20\%$$

$$V_{dust} = H_{salt} \times 10^{-4} \quad 20\% \leq \text{clay} < 45\%$$

$$V_{dust} = H_{salt} \times 10^{-5} \quad \text{clay} \geq 45\%$$

K18 illustrate that the approach above results in a strong discontinuity at 20% clay content, and so they instead apply a Gaussian function for the sandblasting efficiency that provides a smooth profile while maintaining peak efficiency around 20%. Since K18 do not explicitly give the Gaussian function, we approximated the equation to yield a similar shape as K18's Figure 3:

$$V_{dust} = H_{salt} \times 0.013e^{[-(18-clay)^2/50]}$$

where a minimum sandblasting efficiency of 10^{-5} m^{-1} is applied uniformly above 37% clay content.

The amount of dust emitted from an emissive grid cell per time (E_{dust} in kg/s) is calculated by multiplying V_{dust} by the cell area (A in m^2) and scaling by the total fraction of emissive landcover types in the cell (f_{tot}). Following K18, we further scale by the amount of vegetative cover over the entire cell according to input LAI fields:

$$E_{dust} = \left[1 - \frac{\min(LAI, 0.35)}{0.35}\right] f_{tot}\, A\, V_{dust}$$

Note that dust cannot emit from any grid cells where LAI > 0.35, which represents a globally uniform canopy resistance effect. This specific value may be too restrictive for arid brush and grasslands of the western US. K18 also include a topography factor that weights emissions away from mountain tops and toward valleys where sediments accumulate. WBDUST excludes the topography factor.

A12 and K18 assume that vertical dust emissions follow a globally uniform tri-modal distribution with mean diameters (D_V,n) of 0.832, 4.82, and 19.38 µm, geometric standard deviations (σ_n) of 2.1, 1.9 and 1.6, and mass fractions (M_n) of 0.036, 0.957 and 0.007, respectively. We map these distributions directly to the CAMx fine crustal mode (FRCS, 0.04-2.5 µm) and coarse crustal mode (CCRS, 2.5-10 µm) using the standard error function (erf):

$$E_{FCRS} = E_{dust} \sum_{n=1,3} \frac{M_n}{2} \left\{ \text{erf}\left[\frac{\ln\left(2.5/D_{V,n}\right)}{\sqrt{2}\ln\sigma_n} \right] - \text{erf}\left[\frac{\ln\left(0.04/D_{V,n}\right)}{\sqrt{2}\ln\sigma_n} \right] \right\}$$

$$E_{CCRS} = E_{dust} \sum_{n=1,3} \frac{M_n}{2} \left\{ \text{erf}\left[\frac{\ln\left(10/D_{V,n}\right)}{\sqrt{2}\ln\sigma_n} \right] - \text{erf}\left[\frac{\ln\left(2.5/D_{V,n}\right)}{\sqrt{2}\ln\sigma_n} \right] \right\}$$

If elemental speciation is requested, WBDUST splits FCRS among 6 elements and remaining FCRS; no speciation is applied to CCRS. Factors for sodium, magnesium, calcium, and potassium are defined by the input global soil maps developed by K18. Factors for iron and manganese are set according to the same globally uniform values as used within the CAMx aqueous aerosol chemistry module.

2.2 Other WBD Schemes

We conducted a literature review of WBD emission models employed in other modeling systems. These included two methods available in the WRF model coupled to chemistry (WRF-Chem; NOAA, 2021): the Air Force Weather Agency (AFWA) scheme and the University of Cologne (UoC) scheme, both of which are described by LeGrand et al. (2019). We also reviewed the in-line WBD model employed within CMAQ as described by Foroutan et al. (2017; hereafter F17). All three models are parallel to the A12/K18 scheme, as they all depend on the calculation of a threshold friction velocity, adjustments for moisture and drag partitioning, the calculation of a horizontal saltation flux, and the calculation of vertical WBD fluxes. The sections below point out similarities and differences of each scheme.

2.2.1 WRF-Chem AFWA

The AFWA scheme employs the same equation as A12 for the U^*_{t0} calculation. However, AFWA applies this equation to 9 saltation particle sizes ranging from 1.42 to 250 µm, where only the smallest bin is comprised of clay and all other bins are non-clay material. The model assumes that clay particles have a density of 2.5 g/cm^3 while all other particles have a density of 2.65 g/cm^3 (i.e., quartz, like A12). AFWA applies the same soil moisture factor to U^*_{t0} as A12. WRF's volumetric soil moisture in the top 30 cm soil layer is converted to gravimetric moisture as a function of clay content and soil porosity. However, AFWA does not apply a drag partitioning factor.

The same horizontal saltation flux equation is applied as A12 for each of the 9 saltation bins, including the same constant (c = 1 as in A12 vs. c = 1.5 in WBDUST). For each size bin, AFWA applies a weighting factor that accounts for the mass fraction of that bin to the total surface area according to one of three soil categories (sand, silt, and clay) as determined from gridded soil characteristic inputs. The weighted bin-specific fluxes are then integrated over all saltation particle sizes to obtain a total saltation flux.

The vertical dust emission flux is determined from the total saltation flux by multiplying by the same sandblasting efficiency as given by A12 (i.e., without the K18 Gaussian smoothing modification used in WBDUST). However, the units for clay content appear to be in error, as they are given in decimal fraction rather than percent; this results in a nearly constant sandblasting efficiency over the range of clay content. AFWA applies the same topography factor as K18 (which was not applied in WBDUST), and further assumes zero dust flux for any cell-specific roughness lengths exceeding 20 cm to limit dust emission to regions defined by grassland, sparsely vegetated, or barren.

Total vertical dust emission fluxes are distributed into 5 dust emission bins with mean diameters ranging from 1.46 to 12 μm, again where only the finest bin is comprised of fine clay and the other four are non-clay. This distribution depends on size-specific weighting functions using a complex equation that simulates the brittle fragmentation theory of Kok (2011), which assumes impacted soil aggregates will fracture in a manner similar to glass or gypsum material.

The major differences from the WBDUST model are summarized below:

- Threshold friction velocity is determined for 9 saltation particle sizes as opposed to a single optimal saltation size of 60 μm.
- Different particle densities are used depending on whether they are clay or non-clay.
- Soil moisture conversion from volumetric to gravimetric depends on clay content and porosity, rather than a single typical soil density.
- No drag partitioning adjustment is applied to U^*_{t0}.
- Horizontal saltation flux depends on bin-specific weighting factors that account for the mass fractions to total surface area by three soil categories (sand, silt, and clay); these are integrated to total saltation flux.
- The constant used for the horizontal saltation flux is c = 1 (as opposed to c = 1.5 in WBDUST).
- The sandblasting efficiency, while like A12, apparently applies the wrong units for clay content.
- A topographic factor like K18 is applied to vertical dust emission flux, whereas WBDUST does not apply such factor.
- A simple binary surface roughness limitation is applied to the vertical dust emission flux as opposed to the K18 LAI function.
- Total vertical dust flux is distributed into five particle size bins using a complex function of particle composition and fragmentation theory.

2.2.2 WRF-Chem UoC

The UoC scheme employs the equation of Shao and Lu (2000) to calculate the saltation threshold friction velocity for 100 saltation size bins:

$$U_{t0}^{*} = \sqrt{0.0123\left(\frac{\rho_p g D_p}{\rho_\alpha} + \frac{1.65 \times 10^{-4}}{\rho_p D_p}\right)}$$

UoC applies a similar soil moisture factor to U^*_{t0} as AFWA and A12 but maintains soil moisture in volumetric form and varies the empirical constants in the F_{mois} equation as a function of soil texture. UoC also applies a drag partitioning factor as a function of grid cell vegetation fraction:

$$F_{drag} = \sqrt{1 - 0.5\lambda_v} \times \sqrt{1 + 100\lambda_v}$$

$$\lambda_v = -0.35 \ln(1 - A_v)$$

where vegetation fraction (A_v) is determined from monthly climatological MODIS fraction of photosynthetically active radiation (FPAR) absorbed by green vegetation in the default WRF-Chem configuration.

The same horizontal saltation flux equation is applied as AFWA and A12 but using a different constant (c = 2.3 vs. c = 1.0 in AFWA and A12 vs. c = 1.5 in WBDUST) and including an adjustment factor for vegetated fraction of the grid cell (1 - c_f). Additionally, UoC applies the same topography factor as AFWA and K18 to the saltation flux rather than the vertical flux. However, this factor is binary, reset to 1 anywhere the factor is non-zero. As in the AFWA scheme, the saltation flux in each size bin depends on the fraction of soil consisting of that particle size. A particle availability factor includes free soil particles and particles contained in aggregates as separate categories, which is much more complex than the AFWA scheme.

The UoC scheme includes several levels of complexity, and these mostly apply to how the vertical dust flux is calculated. While similar to the simpler AFWA scheme, UoC calculates emission flux in each WBD size bin caused by the saltation flux in each saltation bin, as opposed to a single bulk dust emission mass from all saltating particles, then splitting into dust size bins. The most complex option includes effects of soil particle aggregation, parent soil particle size distribution, saltating particle size distribution, soil plastic pressure, and other soil attributes. A simplifying variation internally sets several variables to constants that are not usually and readily available as inputs to WRF-Chem. Yet another simplifying variation calculates dust emissions based on a single integrated saltation flux as in AFWA, but where the dust particle size distribution is set according to soil type as opposed to assuming a globally uniform set of dust sizes. In all cases, an adjustment factor for vegetated fraction of the grid cell (1 - c_f) is once again applied to the vertical fluxes. LeGrand et al. (2019) note that this repeated application of vegetation factor may be in error. Finally, the UoC scheme applies a very different physical-based continuous function for the sandblasting efficiency (as described for the CMAQ scheme below).

The major differences between the UoC scheme and the WBDUST model are similar to those noted above for the AFWA scheme, but are much more complex given the added detail and data requirements built into the UoC algorithm:

- Threshold friction velocity is determined by a different equation and for 100 saltation particle sizes instead of just one.
- Different particle densities are used depending on whether they are clay or non-clay.
- Soil moisture remains in volumetric units and the moisture factor is modified accordingly.
- A different drag partitioning adjustment is applied that depends on vegetation fraction.
- Horizontal saltation flux depends on bin-specific weighting factors that are more complex than the AFWA approach; a total integrated saltation flux is only calculated for the simplest UoC option.
- The constant used for the horizontal saltation flux is c = 2.3 (as opposed to c = 1.5 in WBDUST)
- A topographic factor like K18, but in a binary form, is applied to the saltation flux (as opposed to the vertical dust flux), and a vegetation coverage factor based on FPAR is also applied as opposed to one based on LAI.
- The vertical dust emission flux is the most complex and variable component of the UoC options, where the most complex option calculates flux in each WBD size bin caused by each saltation bin and relies on many parameters that are unknown and must be assumed.
- A physical-based continuous function is applied for the sandblasting efficiency.
- The vegetative coverage adjustment is again applied to the vertical emission flux (perhaps in error).
- An integration of vertical dust flux is applied to distribute emissions into the same five particle size bins as AFWA using a complex function of particle composition.

2.2.3 CMAQ

The CMAQ scheme uses the same Shao and Lu (2000) equation as UoC to calculate U^*_{t0}. The threshold friction velocity is calculated for four size bins representing coarse and medium sand, silt, and clay. The fractional coverage of each of these 4 saltation types are set according to the gridded distribution of 12 soil types from the US State Soil Geographic (STATSGO) database.

CMAQ also applies the same soil moisture factor as A12 and AFWA with moisture expressed in gravimetric units. CMAQ converts from WRF's volumetric moisture using a parametrization dependent on the fraction of course and medium sand. Soil moisture is taken from the top 1 cm soil layer in the WRF Pleim-Xiu land surface model, which F17 note is most appropriate for WBD generation rather than the top 10 to 30 cm used in the WRF schemes (Darmenova et al., 2009). Darmenova et al. suggest applying a factor of 0.1 to reduce moisture from deep soil layers. Additionally, Myhre et al. (2003) suggest that soil drying times in drylands are shorter than models predict and therefore apply hourly or daily precipitation thresholds for dust suppression.

CMAQ applies a rather complex "double drag partitioning" factor that includes effects from both large solid objects (rocks, etc.) and vegetation:

$$F_{drag} = \sqrt{(1-\sigma_v m_v \lambda_v)(1+\beta_v m_v \lambda_v)\left(1-\sigma_s m_s \frac{\lambda_s}{1-A_v}\right)\left(1+\beta_s m_s \frac{\lambda_s}{1-A_v}\right)}$$

where λ_v has the same definition as the UoC scheme, λ_s depends on landcover type, and the constants are: σ_v = 1.45, m_v = 0.16, β_v = 202, σ_s = 1.0, m_s = 0.5, and βs = 90. Like UoC, gridded MODIS FPAR is used as a surrogate for vegetation cover fraction A_v.

When calculating actual friction velocity U*, CMAQ uses a surface roughness length applicable for dust generation over relatively smooth soil surfaces. F17 argue that surface roughness elements can both impede saltation (which are addressed by schemes described previously) but can also enhance saltation by increasing turbulent momentum flux to the soil surface up to a critical point beyond which impedance effects dominate. To account for this, the CMAQ scheme employs the following z_0 relationships based on analysis of previous field and laboratory data:

$$z_0 = 0.96\, h\, \lambda^{1.07} \qquad \lambda < 0.2$$

$$z_0 = 0.083\, h\, \lambda^{-0.46} \qquad \lambda \geq 0.2$$

where $\lambda = \lambda_s + \lambda_v$ from the F_{drag} equation above, and h is given by:

$$h = \frac{h_v \lambda_v + h_s \lambda_s}{\lambda_v + \lambda_s}$$

The value of h_s depends only on landcover type while h_v depends on landcover type and month.

CMAQ uses the same horizontal saltation flux equation as applied by UoC, AFWA and A12, but for the 4 saltation size bins (where c = 1.0 as in AFWA and A12 vs. c = 1.5 in WBDUST). Like AFWA and A12, a total saltation flux is calculated by summing contributions over all 4 bins and weighting each bin's contribution by the product of its coverage and erodibility fractions as a function of soil type.

The vertical dust emission flux is determined from the total saltation flux by multiplying by a sandblasting efficiency that is similar in form to the UoC scheme:

$$V_{dust} = H_{salt} \frac{C_\alpha g f \rho_b}{2p}\left(0.24 + C_\beta U^* \sqrt{\frac{\rho_p}{p}}\right)$$

where f is the fraction of fine particles in the soil, p is the soil plastic pressure, ρ_b is the bulk soil density, and C_α and C_β are constants. All parameters are functions of 4 soil sub-types mapped from the 12 STATGO soil types upon which the scheme is based. No topography factor is applied (in contrast to K18, AFWA and UoC, but like WBDUST).

As in A12 and K18, the amount of total dust emitted from an emissive grid cell is the sum of V_{dust} from each emissive landcover type (shrubland, shrub/grass, cropland, and sparse/barren)

multiplied by its fractional coverage, and scaled by the amount of total vegetative cover in the cell ($1 – A_v$). Total dust emissions are then distributed to four size bins (0.1–1.0, 1.0–2.5, 2.5–5.0, and 5.0–10.0 µm) where the first two bins are mapped to the CMAQ fine accumulation mode with geometric mean diameter of 1.39 µm and standard deviation of 2.0, and the second two bins are mapped to the coarse mode with the geometric mean diameter of 5.26 µm and standard deviation of 2.0.

The major differences between the CMAQ scheme and the WBDUST model are similar to those noted above for the AFWA and UoC schemes:

- Threshold friction velocity is determined by a different equation and for 4 saltation particle sizes according to 12 soil types.
- Soil moisture is converted to volumetric units using a parameterization based on sand content by soil type; moisture is taken from the top 1 cm soil layer in the Pleim-Xiu land surface model, while for other soil models using deeper layers it is suggested to scale moisture by 0.1.
- A more complex drag partitioning adjustment is applied that depends on solid roughness elements as a function of landcover type, and vegetation roughness that depends on landcover and month.
- Actual friction velocity is determined using a surface roughness that varies according to the density of solid and vegetative elements that may enhance or impede saltation. Note that WBDUST uses bulk z_0 for the entire grid cell, which overestimated U* for saltation.
- Horizontal saltation flux depends on bin-specific weighting factors that account for the mass fractions to total surface area and erodibility of 4 soil types/sizes by 12 soil categories; these are integrated to total saltation flux.
- The constant used for the horizontal saltation flux is c = 1 (as opposed to c = 1.5 in WBDUST)
- The vertical dust emission flux equation is similar in form to the UoC scheme using a physical-based parametrization for sandblasting efficiency but uses only the single integrated saltation flux instead of size-resolved fluxes.
- A vegetative coverage adjustment is applied to the vertical emission flux based on FPAR rather than LAI.
- A split of total vertical dust flux is applied to distribute emissions into four particle size bins, which are then mapped to fine and coarse modes for transport within CMAQ.

2.3 Selected Modifications to WBDUST

Based on the in-depth review summarized in Section 2.2 and from initial process-level testing, we selected specific updates for the WBDUST parameterization that: (1) improve upon several simple methods and assumptions; (2) provide additional detail for important processes without the burden of requiring additional input data; and (3) result in higher, more spatially widespread and temporally variable emission rates without ad hoc modifications such as the removal of certain limitations in the A12/K18 scheme. Specifically, several formulation features of the CMAQ scheme (F17) were adopted as they provide a reasonable balance between technical rigor and detail supported by available data. The updated WBDUST model (v2.0) continues to use CAMx-ready input files for meteorology and landcover and continues to allow

for global inputs of soil type and elemental speciation so that the model can be used globally. Additional updates that allow for more specific agricultural landcover information within the US are described in Section 3. The specific formulation updates are listed below:

1. Remove the global barren land mask from K18 as this was identified to be a major factor in limiting potential WBD emissive areas in the US;
2. To support the updates below, map 7 individual CAMx landcover classes to 4 general emissive landcover types (shrub, grass, crops, barren/desert), and use existing input global clay fraction to assign each grid cell to one of 12 soil types, which is possible because each soil type is defined by a unique clay fraction;
3. Change to the Shao and Lu (2000) equation for threshold friction velocity for each of 4 saltation particle types/size bins (coarse and medium sand, silt, and clay) instead of the single A12 equation for optimal saltation size;
4. Change to the F17 parameterization to convert from volumetric to gravimetric soil moisture as a function of soil type, instead of assuming a uniform soil density;
5. Change to the F17 double drag partitioning factor that includes effects from both large solid objects and vegetation as a function of landcover type, instead of the simple globally uniform roughness assumptions in A12 (details of this approach were later changed in the final WBDUST formulation, as described in Section 4 and Appendix A);
6. Use the existing saltation flux equation (equivalent among all models), but apply it individually for each emissive landcover type and each of 4 saltation particle bins, summing over all saltation bins and weighting by each bin's coverage and erodibility fractions; also change from c = 1.5 to c = 1.0 (details of this approach were later changed in the final WBDUST formulation, as described in Section 4 and Appendix A);
7. Calculate vertical dust emission flux for each emissive landcover type using the F17 sandblasting efficiency parameterization as a function of soil type, instead of the artificial Gaussian profile assumed by K18 (retain the 3 dust emission size modes from A12/K18);
8. Sum vertical dust emissions over all emissive landcover types, scaling by each landcover's fractional area and vegetative cover following F17, as well as by a topography factor to zero dust emissions from high altitudes above treeline.
9. Redefine 100% vegetative cover at LAI = 1.00 instead of LAI = 0.35 to open up more areas for emissions (this was tested extensively in initial test-bed simulations);
10. Include a user-supplied factor that scales down soil moisture from WRF's top-most soil layers ≥10 cm deep;
11. Add an additional criterion that suppresses dust emissions for grid cells with surface precipitation rate exceeding 0.01 in/hour;
12. Expand chemical speciation from 4 elemental species (Na, Mg, Ca, K via global soil composition input) to 9 elemental species, adding Al, Fe, and Si based on regional measurement data reported by Wang (2015) from Southwest US, Sahara, Middle East, Asia, South America, and Australia, and adding Ti and Mn as set in the CMAQ in-line WBD scheme.

The specific modifications listed above were selected based on sensitivity testing using a simulation testbed developed for process-level quality assurance/quality control (QA/QC)

assessments of the updated Fortran code (Ramboll, 2020b). The single-day testing was conducted for a few documented high-wind dust episodes that occurred during 2014 in the southwest and south-central US (e.g., NWS, 2014). Meteorological inputs were taken from the WRAP 2014 MP (IWDW, 2021). Figure 2-1 shows examples of WBD emission estimates during a particularly heavy dust event on April 28 from three versions of WBDUST: v1.0, v1.1 in which the wind stress cap was removed, and WBDUST v2.0 with most of the updates listed above. Whereas WBDUST v1.0 generated hardly any emissions and v1.1 resulted in widespread emissions across the western US, the improvements listed above resulted in reasonable emission rates and patterns between the extremes of v1.0 and v1.1. Note that these qualitative examples are shown to simply demonstrate differences resulting from the formulation updates. Section 4 presents in-depth quantitative testing with CAMx by evaluating simulated crustal PM concentrations against IMPROVE crustal PM measurements throughout the south-central US.

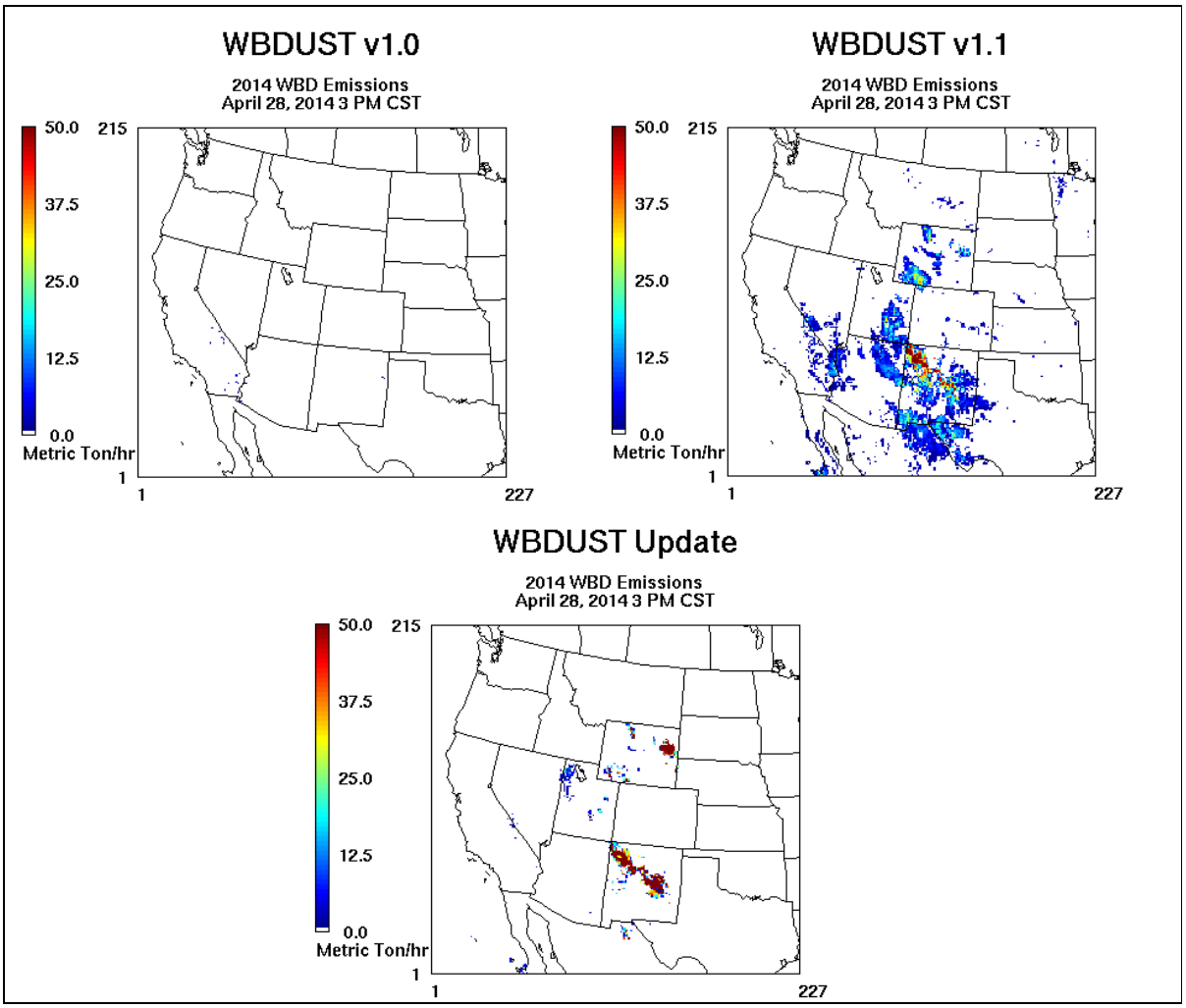

Figure 2-1. Comparison of WBD emission estimates (metric tons per hour) from three versions of the WBDUST model on April 28, 2014, 3 PM CST: (top left) v1.0; (top right) v1.1; (bottom) most updates developed in this project for v2.0.

3.0 ALTERNATIVE LANDCOVER AND AGRICULTURAL DATASETS

As described in Section 2, WBDUST uses the CAMx-ready surface characterization input file and (optionally) a global monthly LAI file to define the spatial characterization of vegetation, or more precisely, where vegetation is sufficiently lacking to establish emissive lands. The total fraction among all emissive landcover types (barren, shrubland, grassland, cropland) within each grid cell is stored and any cells with zero total fraction or with snow cover are ignored for WBD calculations. LAI is used as a surrogate for the total amount of vegetation cover present in each grid cell.

A key disadvantage of WBDUST v1.0 was the restriction of dust emissive areas to large permanent natural barren lands such as deserts, with limited regard to seasonal and spatial variations in smaller-scale erodible lands such as exposed agricultural fields associated with cultivation cycles. Correctly representing the spatial and temporal variations in surface vegetation is important due to its multiple effects on dust generation, including drag partitioning, local wind acceleration, and near-source removal. Agricultural cultivation via tilling exposes land tracts to seasonal wind erosion, but besides the extent to which LAI can characterize activity, this type of WBD source was not well resolved temporally or spatially. This aspect of WBD is critically important to areas within and around Texas, and so we conducted an extensive review of available datasets from which to enhance the set of WBDUST inputs for US applications.

3.1 Review of Supplemental Vegetation Datasets

3.1.1 2016 NLCD

The US Geological Survey (USGS) National Landcover Database (NLCD; USGS, 2021) provides a modern, nation-wide dataset (48 conterminous states) at 30-meter resolution. It contains spatial reference and descriptive data for characteristics of the land surface such as thematic class (e.g., urban, agriculture, and forest), percent impervious surface, and percent tree canopy cover. NLCD is updated every five years and is considered the definitive US land cover database; the latest version represents the year 2016. NLCD coverage does not extend outside the US into Mexico or Canada and does not provide yearly information on crop vegetative type or season-specific activity.

Representing a modern US landcover distribution, 2016 NLCD is likely an improvement over older datasets used in WRF and translated to CAMx via the “WRFCAMx” interface. In many, if not most CAMx applications, modelers tend to use the landcover inputs directly produced by WRFCAMx and thus implicitly rely on whichever dataset was applied in WRF. However, TCEQ expends considerable effort to combine several landcover datasets (Texas-specific data, NLCD, USDA, MODIS, and BELD) to develop the best possible spatial characterization for their applications. It is assumed, therefore, that TCEQ will include the 2016 NLCD in their new CAMx modeling datasets and so we did not consider the 2016 NLCD further in this project.

3.1.2 CropScape

The National Agricultural Statistics Service (NASS) "CropScape" mapping tool (NASS, 2012, 2021a) provides annual landcover data including very detailed crop type over the conterminous US at 30-meter resolution (Figures 3-1 and 3-2). The Cropland Data Layer (CDL) includes a geo-referenced raster dataset that is available annually for 1997–2020. The CDL was created to provide acreage estimates to the Agricultural Statistics Board and to produce a digital, crop-specific, categorized geo-referenced output product. The CDL is based on moderate resolution satellite imagery and extensive agricultural ground truthing to increase precision and accuracy as discussed in detail by NASS (2021b). Different satellite data products were utilized for different years depending on availability.

NASS notes that the emphasis of the CDL is on characterizing agricultural landcover categories in detail, while it relies on the 2001 NLCD for non-agricultural land cover classes. Therefore, NASS recommends that users consider modern NLCD datasets for non-agricultural landcover categories. The CropScape website also offers additional products such as a Crop Frequency Layer for four major crops: corn, cotton, soybeans, and wheat, which provides the number of years since 2008 that a particular crop was planted at a particular location. This highlights the importance of using year-specific crop data for agricultural dust emissions.

The CDL raster pixels are each assigned a value ranging from 0 to 255, and each value defines a particular crop or other LULC type. For example, 1 corresponds to corn and 2 corresponds to cotton. Other codes are assigned to non-crop types such as water bodies, urban/developed areas, forests, shrublands, etc. Not all 256 values are assigned to a specific crop or landcover type: for example, in the 2016 CDL dataset approximately 120 of the 256 values are assigned to a crop or LULC type, and all other values are blank. This section later describes how the CDL data were mapped to CAMx landcover categories and paired with crop calendar cycles, from which to characterize spatial and temporal variations in potentially emissive croplands.

3.1.3 CMAQ Crop Calendar

We anticipated employing a "crop calendar" dataset associated with CropScape. However, only the Crop Frequency Layer described above was found, which does not contain data on annual planting/harvesting schedules by crop type. We also investigated Texas-specific agricultural datasets, but those also did not include needed information. Furthermore, Texas datasets present limited applicability for regional modeling.

The CMAQ in-line WBD algorithm (Section 2.2.3) also provides the ability to optionally define erodible agricultural lands and specifically utilizes a state-level, crop-specific planting/harvesting schedule. The CMAQ crop calendar data are contained in a text file called "CPCALED.txt" that is not year specific but lists monthly activity schedules for 18 specific crop types (Table 3-1). Documentation on the source of these data could not be found but they generally align with schedules published by the US Department of Agriculture (https://ipad.fas.usda.gov/countrysummary/Default.aspx?id=US). We adapted WBDUST to use the CPCALED.txt file directly.

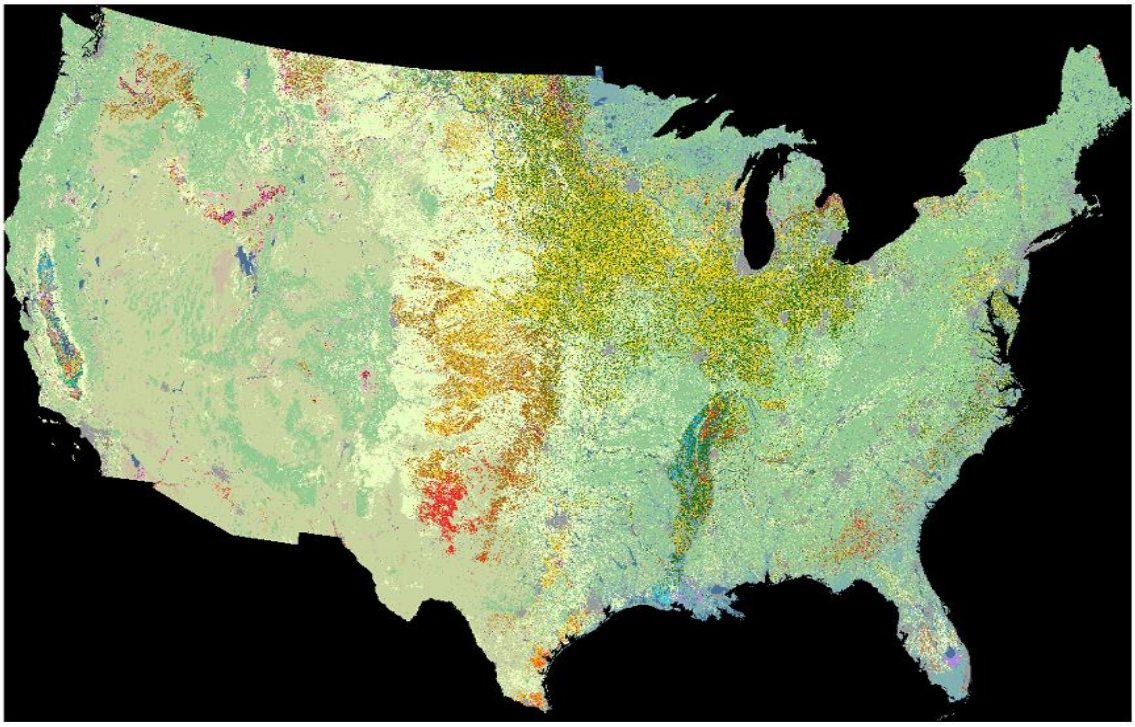

Figure 3-1. Coverage of the 2016 CropScape 30-m dataset (NASS, 2021b) with colors representing 256 landcover categories mostly as specific crop types.

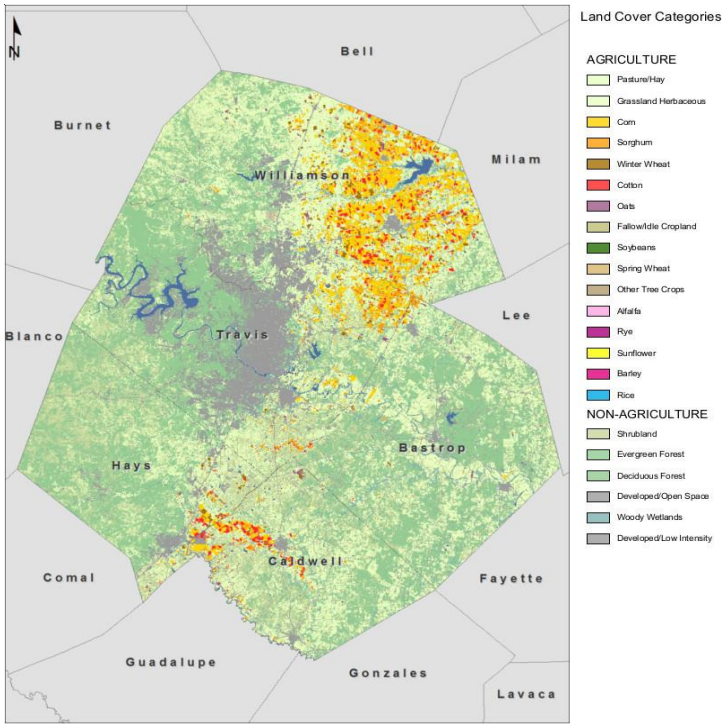

Figure 3-2. An example of 2016 CropScape 30-m data (NASS, 2021b) for Austin MSA showing the subset of landcover categories for the region.

Table 3-1. Specific crops listed in the CMAQ crop calendar file "CPCALED.txt".

1 Alfalfa	10 Potatoes
2 Spring Barley	11 Rice
3 Fall Barley	12 Rye
4 Corn	13 Sorghum
5 Cotton	15 Soybeans
6 Hay	15 Sugar beets
7 Spring Oats	16 Tobacco
8 Fall Oats	17 Spring Wheat
9 Peanuts	18 Winter Wheat

The format of the crop calendar is rather simple and therefore easy to incorporate into programs of any language. For each of the 18 crop types the file lists the planting/seeding and harvesting schedules in each of 47 conterminous states (excluding Rhode Island). CMAQ code documentation provides an example for Kansas:

```
Barley-Spring
KS 3 1 3 5 4 1 5 1 6 10 6 25 7 1 7 10
Barley-Fall
KS 9 15 10 1 10 15 11 1 6 20 6 15 7 1 7 5
```

The start date for planting is given by the first 2 values and the end date is given by the 7th and 8th values (highlighted yellow). The harvesting end date is given by the 15th and 16th values (highlighted green). For example, spring barley planting begins March 1 and ends May 1, while harvesting ends July 10. Fall barely planting begins September 15 and ends November 1, while harvesting ends July 5 of the following year.

3.2 Processing of Datasets and Use in WBDUST

3.2.1 CropScape

A single year of raw US CropScape data is massive and burdensome to use. To be efficiently useful in WBDUST, we developed a set of Python scripts to recast the 256 CropScape classifications to a smaller sub-set that aligns with the CAMx landcover categories, and to reproject and translate the 30-m raster data to gridded area fractions on the CAMx grid.

First, the script "`raster_reclassify.py`" reclassifies CropScape's list of 256 pixel values to the 26 CAMx LULC categories plus an additional 15 unique crop categories that align with the crop calendar (3 crop calendar categories – cotton, corn, and rice – directly align with CAMx landcover types for a total of 18 crop types). Additionally, CropScape includes a pixel classification called "Developed/Open Space". Based on our graphical analysis, this category is ubiquitous throughout rural and agricultural areas and clearly represents roads and open lots, particularly access roads between individual fields. Since in rural areas such roads and lots are most likely unpaved and thus potentially emissive, we maintain this as a separate category in our reclassified landcover list, resulting in 42 total categories. Appendix A lists the mapping of

116 categories with non-zero counts in the 2016 CropScape dataset to the 42 WBDUST categories. This script can take up to several hours to run. Figure 3-3 shows the resulting US-wide map of reclassified 30-m data used for QA/QC review.

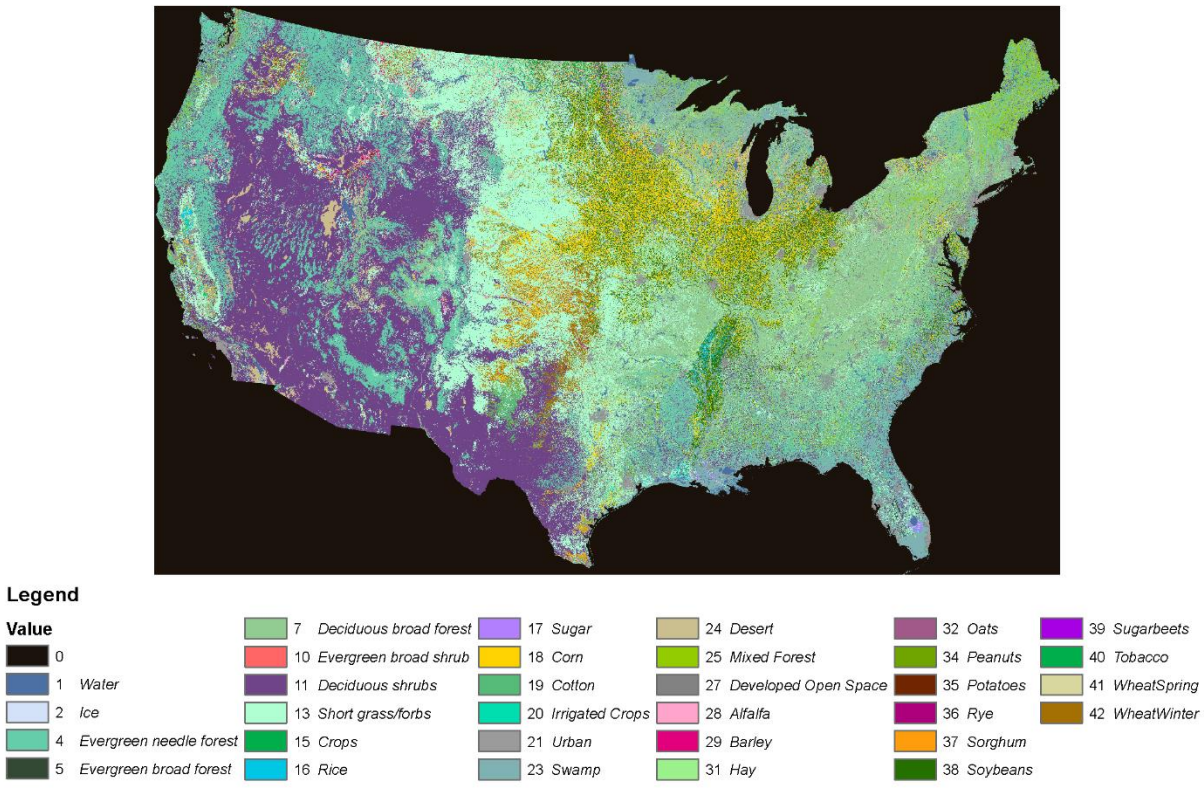

Figure 3-3. 2016 CropScape 30-m dataset reclassified to the 42 CAMx/WBDUST categories.

Next, the script "`raster_camx_grids_count.py`" casts the reclassified 30-m raster data to the map projection of the target CAMx modeling grid. It then aggregates the pixel data to the CAMx grid using a "fishnet" Python function and counts the number of pixels in each grid cell for each of the 42 landcover categories. This script can also take up to several hours to run.

A third script "`raster_camx_grids_count2nc.py`" derives the fractional area per grid cell for each of the 42 landcover categories, ensuring that the sum over all categories in each grid cell sum to 1. It then overlays a shapefile defining the boundaries of the 48 conterminous US states onto the CAMx grid and identifies which state each cell occupies (to facilitate the use of the state-level crop calendar in WBDUST). The script then writes the processed CropScape dataset and the resulting gridded state identification array to a netCDF data file that is directly read by WBDUST. This script takes only a few minutes to run. Figure 3-4 displays fractional grid cell coverages of 3 WBDUST landcover categories and the total sum over all categories in the 2016 EPA 12-km modeling grid used for QA/QC review.

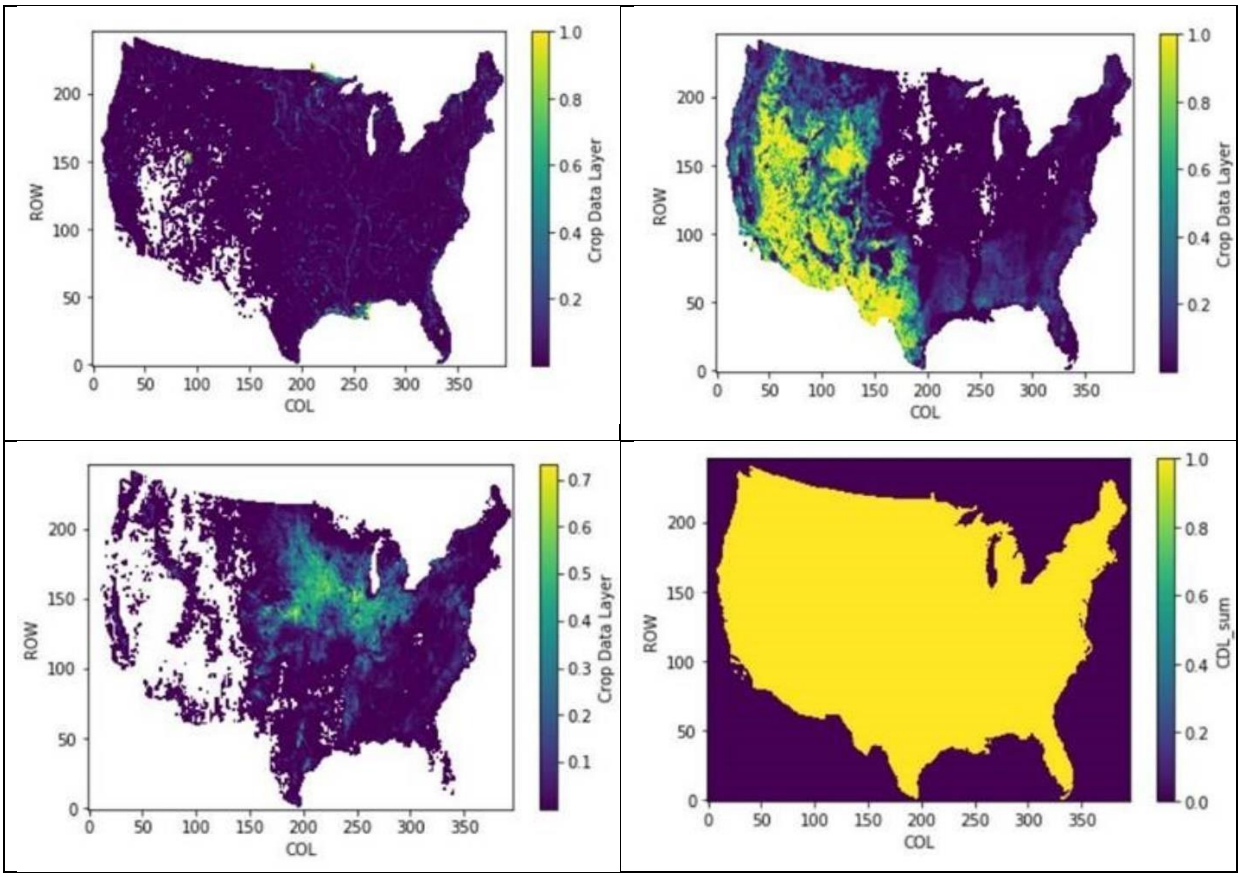

Figure 3-4. Fractional coverages of 3 WBDUST landcover categories (lakes and rivers, top left; shrubland, top right, corn, bottom left) and the total sum over all categories (bottom right) in the 2016 EPA 12-km modeling grid. White areas represent undefined or zero fraction. The sum over all fractions in each grid cell must be 1.0.

3.2.2 Updates to WBDUST

We implemented additional updates in WBDUST to utilize the CMAQ crop calendar and processed/gridded CropScape datasets. These data provide the basis for modifying input CAMx landcover distributions to reflect locations and extents of tilled croplands that are barren and thus potentially emissive.

WBUST optionally reads the processed CropScape data and the crop calendar data file (the latter will be distributed with the WBDUST code, similarly to the global soil composition and clay content datasets). For CAMx grids extending beyond US borders, no cropland adjustments to the input CAMx landcover fields can be made. Since CAMx landcover files are developed via many different approaches, there are potentially very large differences between CAMx and CropScape gridded landcover coverages that present significant complications in reconciling and blending CropScape and CAMx landcover datasets. The most obvious example is that CAMx LULC files may comprise only a single dominant category per grid cell as processed by the WRFCAMx interface program (because WRF only output such information). Since crop types and coverages in CropScape are year-specific and very detailed, we consider that dataset to be

definitive. To alleviate the need for a complex reconciliation of the two datasets when processed CropScape data are optionally provided, WBDUST preferentially uses the CropScape data for the 26 standard CAMx land cover fractions and the 15 additional crop-specific fractions for each US grid cell (superseding the 26 standard landcover fractions from the CAMx landuse input file).

Then, WBDUST cross-references the 18 specific crop calendar types to the CropScape categories and saves each of their fractional areas. These crop types are then checked against the state-level crop calendar input file. According to the date being processed, the fractional coverage of each of these crop types may be converted to the CAMx "barren" landcover classification to designate them as potentially emissive. This conversion is assigned only for crops for which the planting season is active for the given date. We assume that tilling/cultivation occurs only during planting period, and that crop residue after the previous harvest are not tilled under until the planting season to avoid erosion during the interim period. However, rice crops are ignored because they are not considered potentially emissive given their water-borne cultivation. We originally assumed that 100% of all tillable croplands are emissive over the entire planting season, which led to over predictions of WBD in crop-intensive states. As described in Section 4 and Appendix A, we changed this to arbitrarily assume that 25% of tillable croplands had been cultivated and are emissive within a recent period around any given date during the planting season (this is a more reasonable assumption that improved model performance as detailed in Section 4 but should be further evaluated).

Finally, WBDUST considers the spatial coverage of the "developed open space" category that was separately tracked in the CropScape data processing step. For each US grid cell, WBDUST saves the open space fraction with an adjustment to account for the fraction associated with urban landcover (which is assumed to be paved). The rural unpaved fraction is determined from scaling open space by the non-urban cell fraction minus an additional 10% to account for some paved areas (highways, etc.). This means that up to 90% of the open space fraction in fully rural grid cells are assumed to be unpaved and potentially emissive. The resulting rural open space fraction is added to the CAMx "barren" landcover classification. The remaining urban open space fraction is assigned to the CAMx "urban" landcover classification and thus never emissive.

4.0 EVALUATION OF THE UPDATED WBDUST MODEL

Ramboll conducted numerous seasonal inert test runs using CAMx to evaluate simulated dust concentrations from the original and updated WBDUST formulation, and to test sensitivity to algorithm adjustments to further improve the temporal and spatial characterization of dust patterns and magnitudes. Upon settling on a final WBDUST configuration, we conducted a final full-year CAMx chemistry run with elemental dust speciation and performed a comprehensive evaluation against speciated measurements at IMPROVE sites throughout the south-central US.

4.1 Test Runs

An initial set of inert test cases involved running CAMx v7.1 over the March-April 2016 period using the Ramboll 2016 MP. Particulate monitoring of fine soil and coarse mass at IMPROVE sites throughout the southwest US indicated high concentrations of dust during the windy and dry March-April period. All model inputs except WBD emissions were taken from EPA's national 2016 modeling platform at 12 km grid resolution covering the continental US (see also Section 1). We ran CAMx with only WBD emissions and simulated the inert dispersion of un-speciated fine crustal (FCRS) and coarse crustal (CCRS) PM, including removal by dry and wet deposition. Density for both FCRS and CCRS was set to the CAMx default value of 3.0 g/cm^3. This model configuration allowed us to run and analyze many WBD sensitivity runs quickly. Table 4-1 lists the ten individual test runs, their configuration, and their purpose. Simulated concentrations of CCRS were compared to IMPROVE total coarse mass measurements at six regional sites selected to represent various geographies surrounding Texas (Figure 4-1): Big Bend (BIBE), Guadalupe Mountains (GUMO), Salt Creek (SACR), Bandelier (BAND), Wichita Mountains (WIMO), and Caney Creek (CACR).

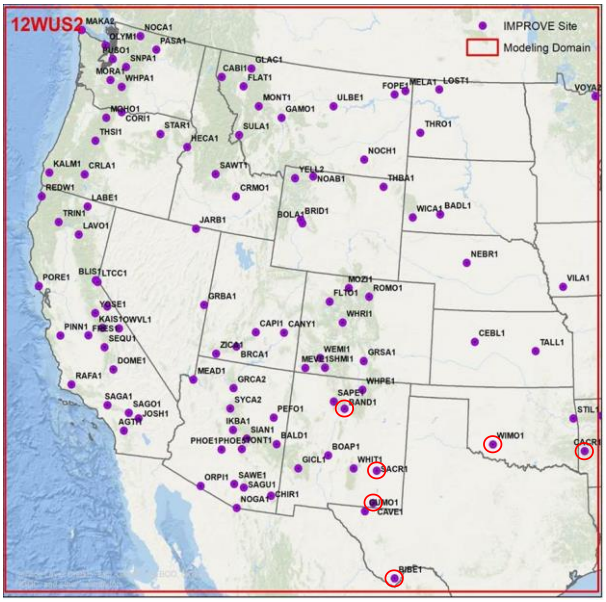

Figure 4-1. Map of all IMPROVE sites over the western US. While results from most sites were reviewed for each run during QA/QC review, red circled sites were used to critically evaluate and demonstrate crustal PM performance from the inert CAMx test runs described here.

Table 4-1. List of inert test runs conducted with CAMx to evaluate WBDUST and sensitivity to algorithm and input modifications.

Run	WBDUST Configuration	Purpose	Result
0	Original WBDUST algorithm	Reference simulation	Negligible dust estimates
1	WBDUST formulation update without cropland updates (Section 2.3) - Global LAI inputs	Test/evaluate against Reference	Practically identical to Run 0
2	As in Run 1, but - No global LAI inputs; cell composite from LULC defaults	Test/evaluate against Reference, sensitivity to LAI inputs	Practically identical to Run 0
3	WBDUST formulation update with cropland updates (Section 3.2) - Global LAI inputs	Test/evaluate cropland updates	Similar to Runs 0-2, consistently more dust in area and magnitude
4	As in Run 3, but - No global LAI inputs; cell composite from LULC defaults	Test/evaluate cropland updates, sensitivity to LAI inputs	Similar to Runs 0-2, consistently more dust in area and magnitude
5	Remove drag partitioning (lower threshold friction velocity) and vegetative factor (raise emission flux) - Global LAI inputs	Test vegetation limits on WBD by removing their effects	Large and widespread overpredictions
6	Remove only drag partitioning (lower threshold friction velocity) - Global LAI inputs	Verify that vegetative effects on drag partitioning are the main squelching influence on WBD	Reduced over predictions but dust remained too high
7	As in Run 3, but - Define vegetative cover for each of 4 emissive LULC types from LULC-specific LAI, instead of cell-total LAI from either global inputs or default cell-composite LAI. - Replace F17 roughness equations with default minimum surface roughness for 4 emissive LULC types	Test LULC-specific LAI to lower drag partitioning and thus threshold friction velocity for each emissive LULC; and test use of default minimum roughness to raise friction velocity and WBD emission rates. This configuration removes the option for global LAI inputs and requires LAI to be determined from the CAMx gridded LULC inputs.	Improved dust results greatly with good agreement against measurements; WBD events from croplands in the central plain states remained over predicted
8	As in Run 7, but - Increase λ_S (Section 2.2.3) and thus drag partitioning for barren land (tilled crops)	Test increase to barren threshold friction velocity to reduce WBD over predictions from croplands.	Widespread under predictions
9	As in Run 7, but - Reduce amount of tilled cropland to 25% instead of applying 100% for entire planting season	Test reduction in tilled cropland to reduce WBD over predictions from croplands. This represents the final WBDUST configuration.	Improved agreement in crop-heavy states while not impacting otherwise good performance achieved in Run 7
10	As in Run 9, but - Fix a minor coding error in applying the saltation erodibility fraction	Check effect of code update.	Modest changes to WBD emissions, improved bias at the expense of some increase in over predictions in the central plain states

CAMx Run 0 simulated the dispersion of WBD emissions generated from the original WBDUST v1.0 program. Runs 1 and 2 used WBD estimates from the updated WBDUST algorithm described in Section 2.3; Run 1 employed monthly global LAI inputs while Run 2 used default LAI assigned by CAMx landcover classification. Runs 3 and 4 used WBD estimates from the updated WBDUST code plus the CropScape and crop calendar data described in Section 3.3.2;

Run 3 used global LAI while Run 4 used default LAI. As described below, all tests up through Run 4 continued to exhibit large WBD under predictions. Run 5 entailed a sensitivity run that removed key limitations on dust generation (drag partitioning and vegetative scaling) to test if WBDUST was at all capable of emitting sufficient dust routinely and over broad areas of the western US. Run 5 led to large PM overpredictions at all IMPROVE sites.

The remaining 4 runs adjusted key parameters and/or formulations to find a medium between under predictions from Runs 3/4 and over predictions from Run 5. Run 6 reinstated vegetative scaling that was removed in Run 5 but continued to ignore drag partitioning to maximize WBD emissions; this run verified that drag partitioning was the key influence in limiting WBD emissions. Run 7 reinstated drag partitioning but made it dependent on LULC-specific LAI rather than cell-aggregate LAI, and used LULC-specific minimum default surface roughness for wind stress over the complex roughness approach of F17. This resulted in the removal of the global LAI input option because it requires the setting of LAI from gridded fractional LULC inputs. Run 8 increased the drag partitioning parameter for barren soil (tilled croplands) to reduce an over prediction tendency from croplands. Run 9 instead reduced the area of tilled cropland from 100% to 25% to account for the fact that not all croplands are instantly cultivated on any given day nor remain barren for the entirety of the 2-3 month planting seasons.

4.1.1 Initial Tests

As described in Section 1, Run 0 led to negligible dust estimates (Figures 4-2 and 4-3, Table 4-2). Results from Runs 1 and 2 continued to exhibit similarly large under predictions of dust concentrations that were practically identical to Run 0, despite generating somewhat more dust both in area and magnitude on a few days. We attribute these under predictions to the fact that dust plumes in Runs 0 through 2 were very limited in spatial extent and thus continued to miss many of the IMPROVE monitoring sites resulting in near zero concentrations. Results from Runs 3 and 4 were again very similar to Runs 0 through 2, despite generating consistently more dust both in area and magnitude with the introduction of CropScape inputs. Simulated dust concentrations from Runs 3 and 4 reached some IMPROVE sites in the southwest US (southern Arizona) with better model-measurement agreement for some dust event days, but as shown in Figure 4-3, the model continued to miss most sites and events throughout the south-central plains (Kansas through west Texas) and southern Rockies (Colorado, New Mexico).

4.1.2 Intermediate Tests to Adjust the Formulation

Several intermediate tests involved identifying and adjusting key parameters and/or formulations in WBDUST to increase the area and magnitude of emissions. Run 5 was conducted to test if WBDUST was at all capable of emitting sufficient dust routinely and over broad areas of the western US when two key limitations were removed. We verified that

Table 4-2. Seasonal normalized mean bias (%) for simulated coarse crustal (CCRS) PM from each CAMx WBD run described in Table 4-1. Bias values are calculated over all days with valid IMPROVE data at each of six sites during March-April 2016 (BAND=Bandelier; BIBE=Big Bend; CACR=Caney Creek; GUMO=Guadalupe Mountains; SACR=Salt Creek; WIMO=Wichita Mountains). The column labelled "All" is the bias over all six sites and all valid days. Model biases within a factor of 2 (-50% to +100%) of observations are noted in green.

Run	BAND	BIBE	CACR	GUMO	SACR	WIMO	All
0	-96	-99	-97	-98	-99	-98	-98
1	-95	-99	-96	-98	-99	-97	-98
2	-95	-98	-96	-98	-99	-97	-98
3	-95	-98	-96	-98	-99	-97	-98
4	-94	-98	-93	-98	-98	-95	-97
5	1249	1945	2934	1456	1419	2759	1840
6	1080	1395	2095	1098	986	1980	1388
7	**-16**	-55	120	**-22**	-56	**56**	**-13**
8	-68	-88	**-43**	-83	-88	-64	-78
9	**-19**	-70	**10**	**-36**	-68	**-14**	**-42**
10	**18**	-54	**80**	**-5**	-51	**44**	**-10**

removal of drag partitioning and vegetation scaling led to large PM overpredictions at all IMPROVE sites throughout the March-April modeling period (Figure 4-4). Therefore, the remaining WBDUST tests involved more refined adjustments to find a medium between the large under predictions from Runs 3/4 and massive over predictions from Run 5.

Reinstating vegetative scaling in Run 6 reduced WBD over predictions somewhat relative to Run 5 but coarse PM remained far too high, indicating that drag partitioning was the key factor controlling WBD emissions. Changes to drag partitioning and surface roughness in Run 7 improved WBD results greatly with good agreement against measured coarse PM concentrations throughout the desert southwest US (Arizona, New Mexico, Utah, and Colorado). However, WBD events from croplands in the central plain states (Texas, Oklahoma, Kansas) remained over predicted (Figure 4-5, Table 4-2).

4.1.3 Final Tests

Runs 8 and 9 attempted to adjust WBD from tilled croplands downward. Run 8 increased drag partitioning and thus threshold friction velocity only for barren lands, but again resulted in widespread PM under predictions (Figure 4-6, Table 4-2). Run 9 did not change drag partitioning but rather imposed the assumption that 25% of tilled croplands are barren on any given day during the planting season instead of 100%. Run 9 improved WBD agreement in crop-heavy states while not impacting good performance achieved in Run 7 in desert southwest states (Figures 4-6 and 4-7, Table 4-2). Therefore, the WBDUST configuration tested in Run 9 represents the final formulation as described in Appendix A.

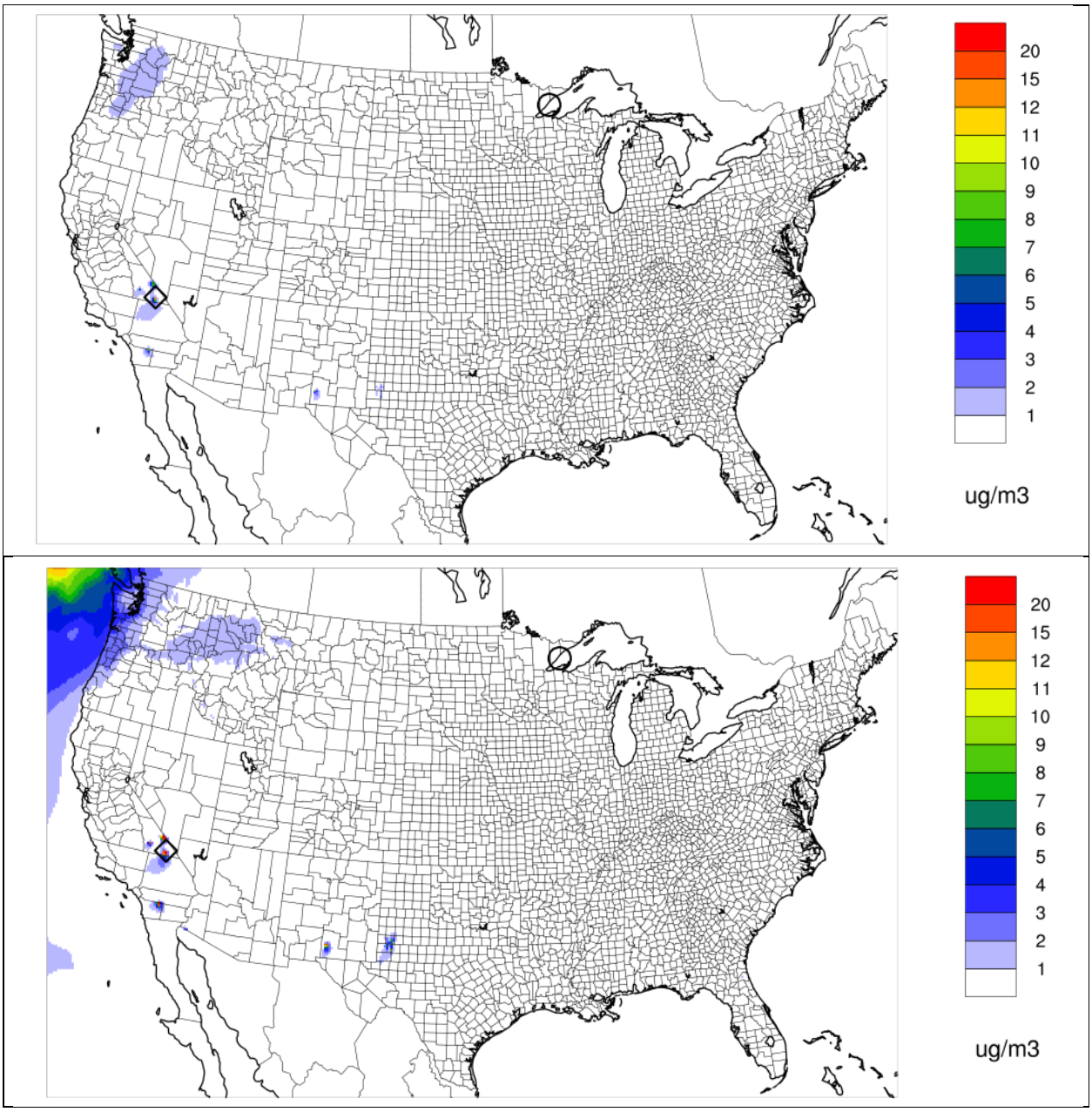

Figure 4-2. Simulated 24-hour fine crustal (FCRS; top) and coarse crustal (CCRS; bottom) concentrations on April 6, 2016 from CAMx WBD Run 0. The largest concentrations in the Pacific northwest are contributed by boundary conditions of these species.

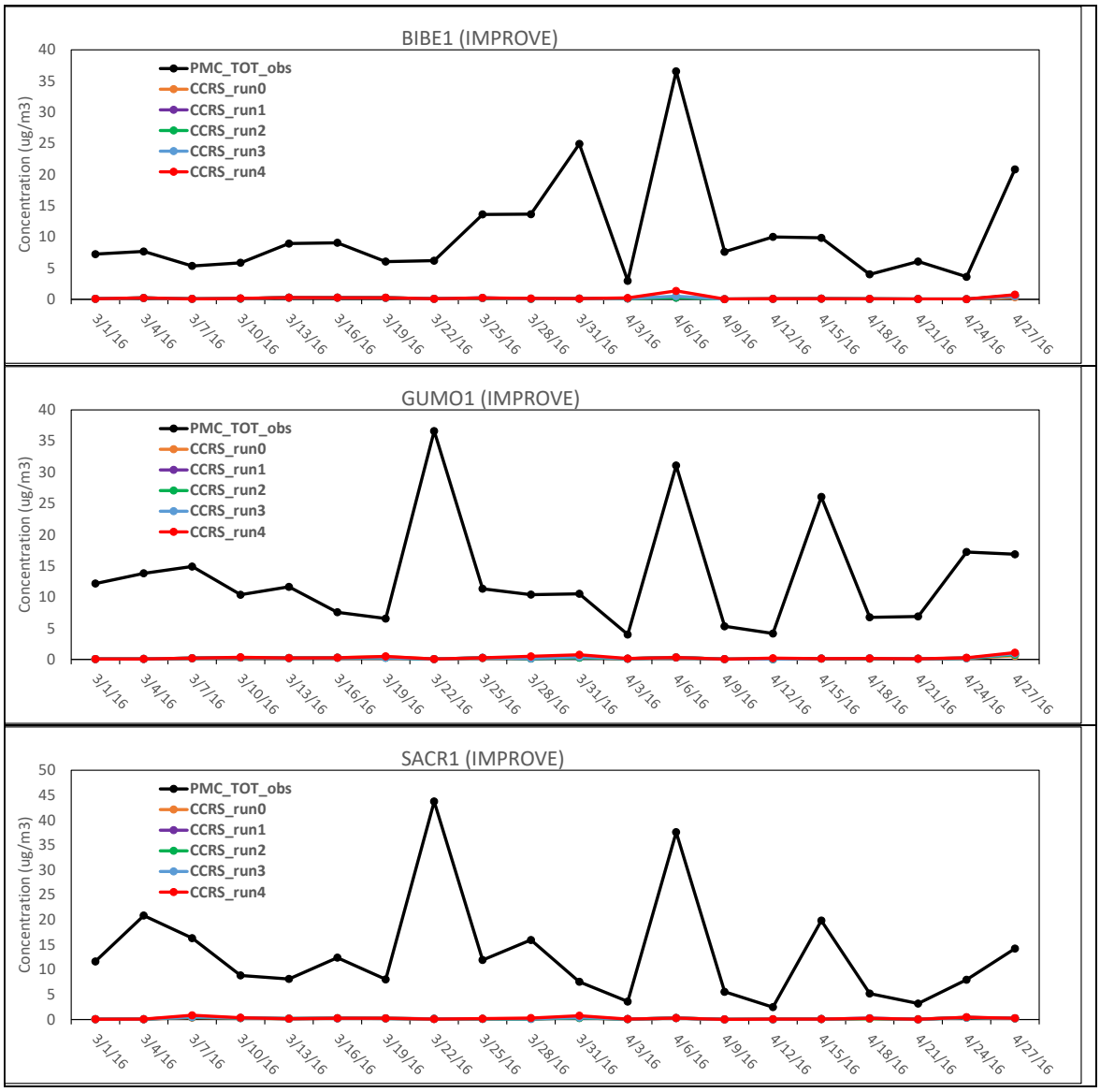

Figure 4-3. Time series of 24-hour coarse PM concentrations over March-April 2016. CAMx simulated coarse crustal (CCRS) concentrations are paired with IMPROVE coarse mass (PMC) measurements taken every 3 days. See Table 4-1 for a description of CAMx Runs 0 through 4.

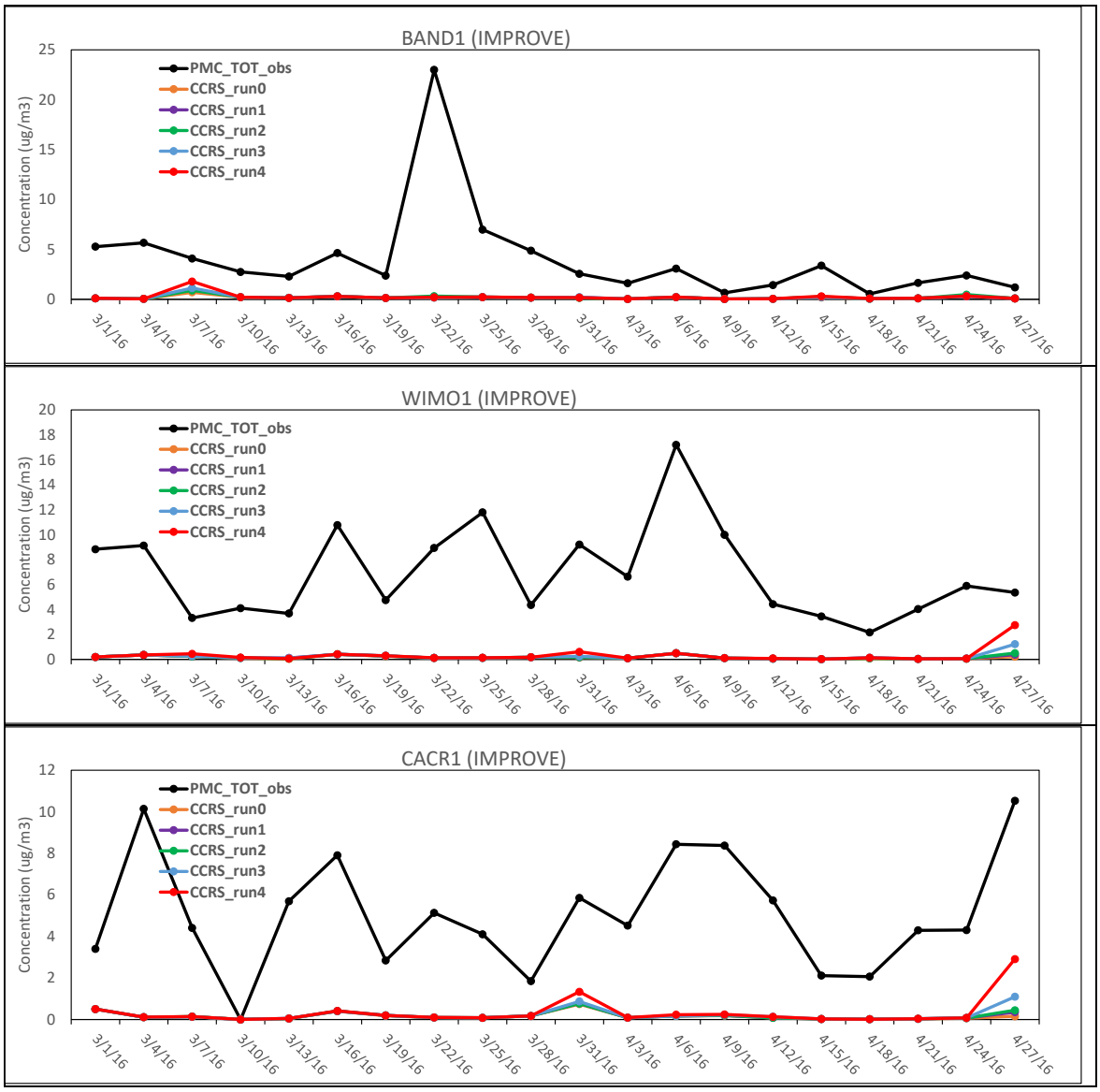

Figure 4-3 (concluded).

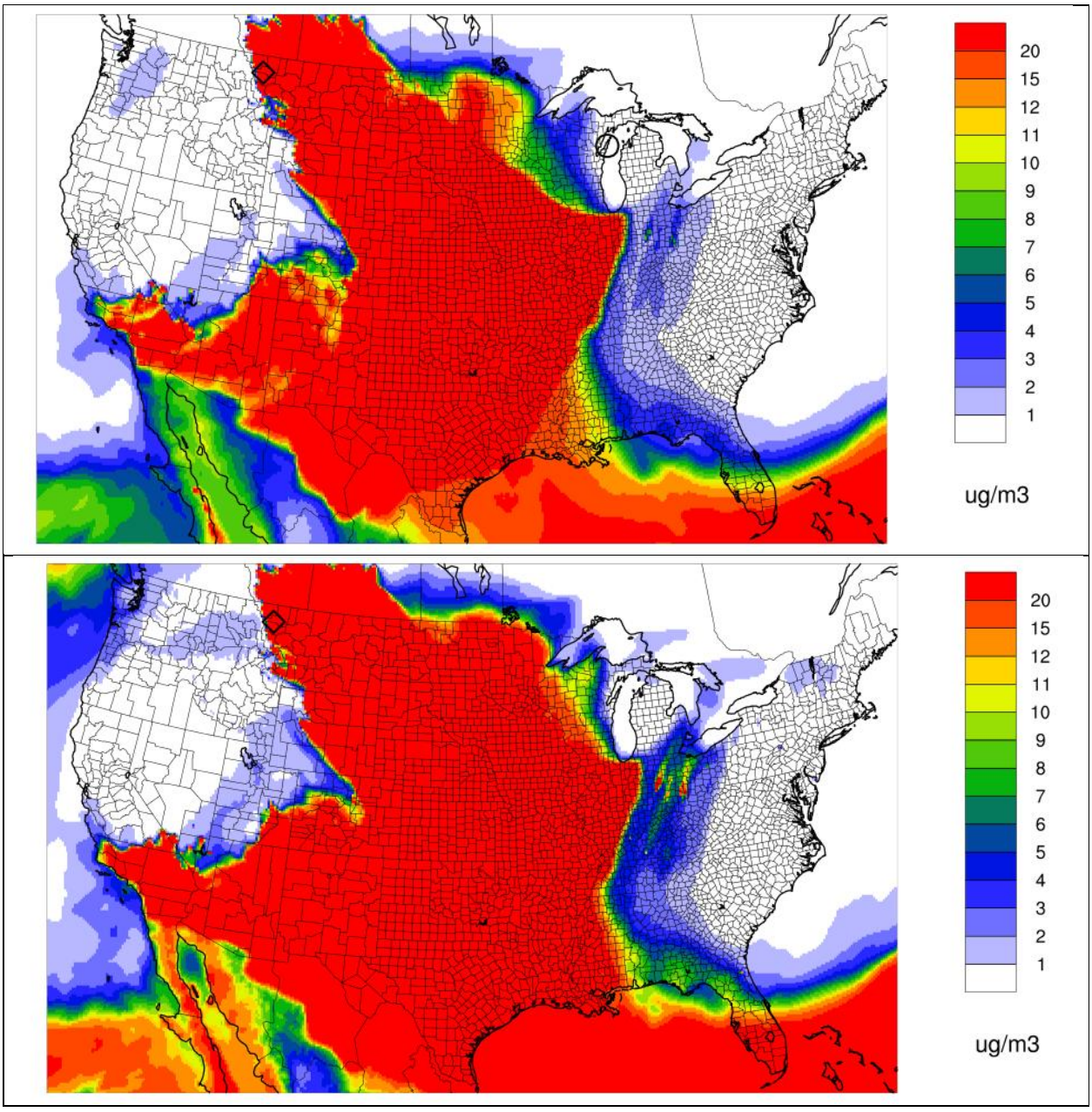

Figure 4-4. Simulated 24-hour fine crustal (FCRS; top) and coarse crustal (CCRS; bottom) concentrations on April 6, 2016 from CAMx WBD Run 5.

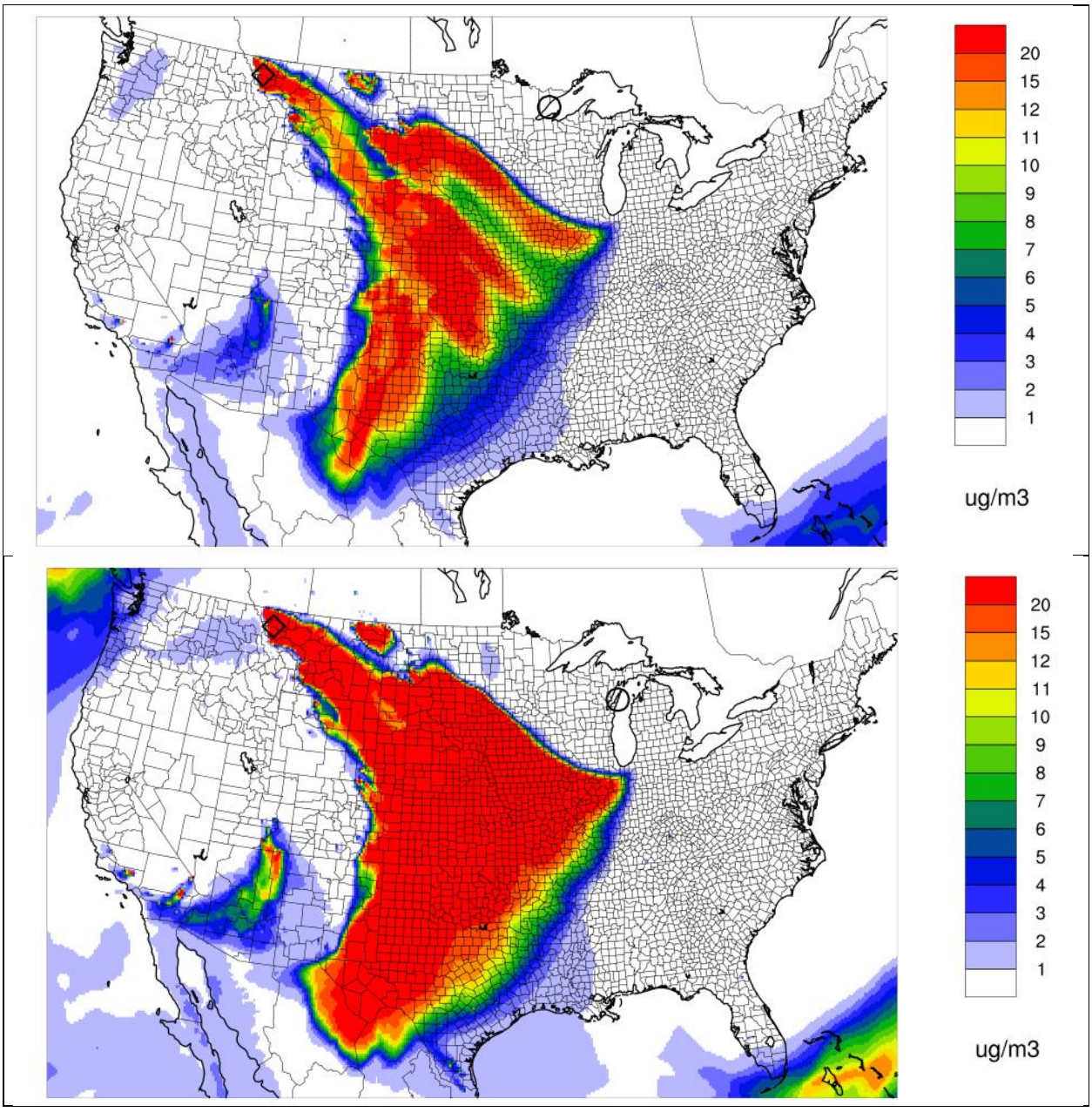

Figure 4-5. Simulated 24-hour fine crustal (FCRS; top) and coarse crustal (CCRS; bottom) concentrations on April 6, 2016 from CAMx WBD Run 7.

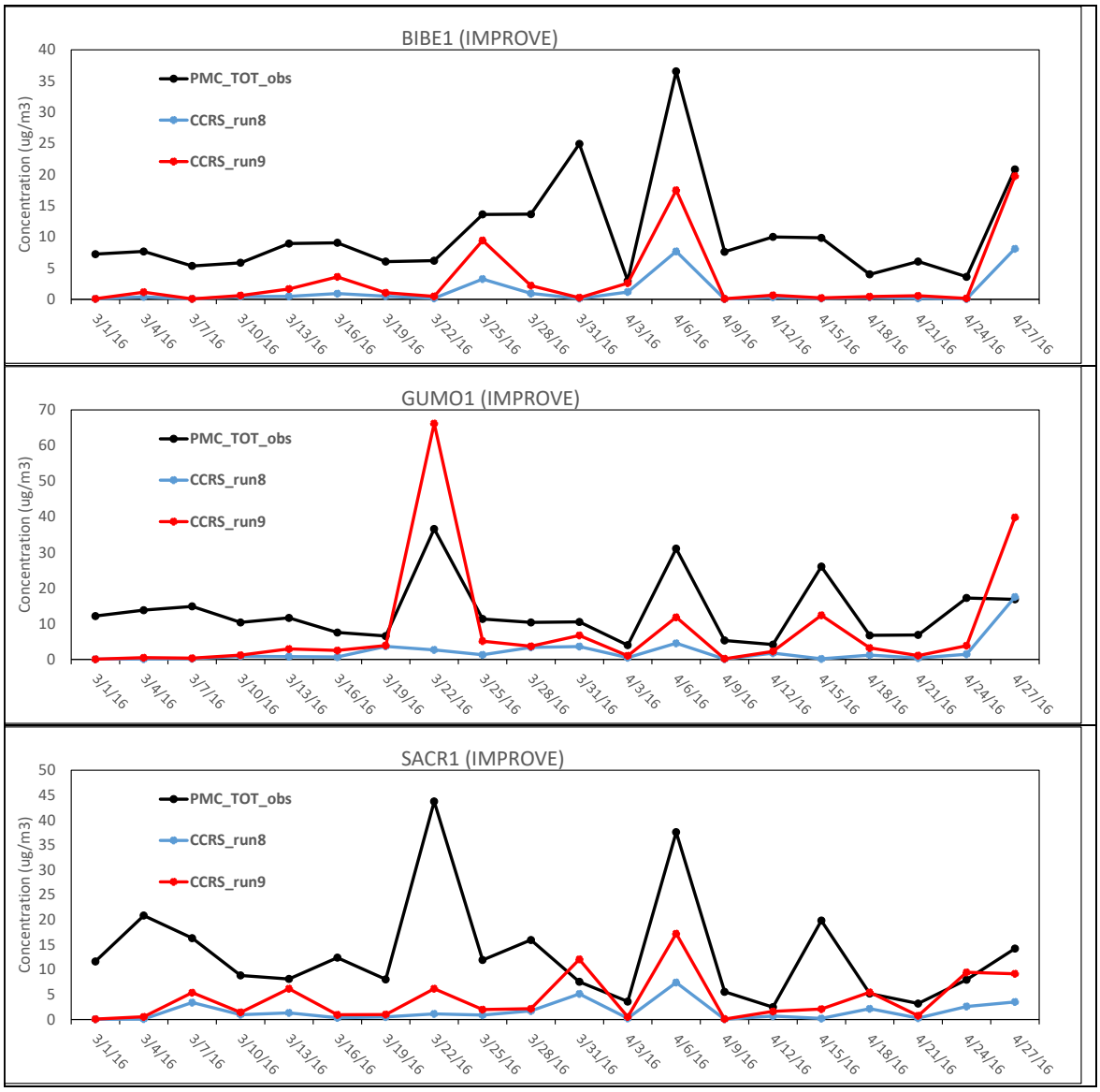

Figure 4-6. Time series of 24-hour coarse PM concentrations over March-April 2016. CAMx simulated coarse crustal (CCRS) concentrations are paired with IMPROVE coarse mass (PMC) measurements taken every 3 days. See Table 4-1 for a description of CAMx Runs 8 and 9.

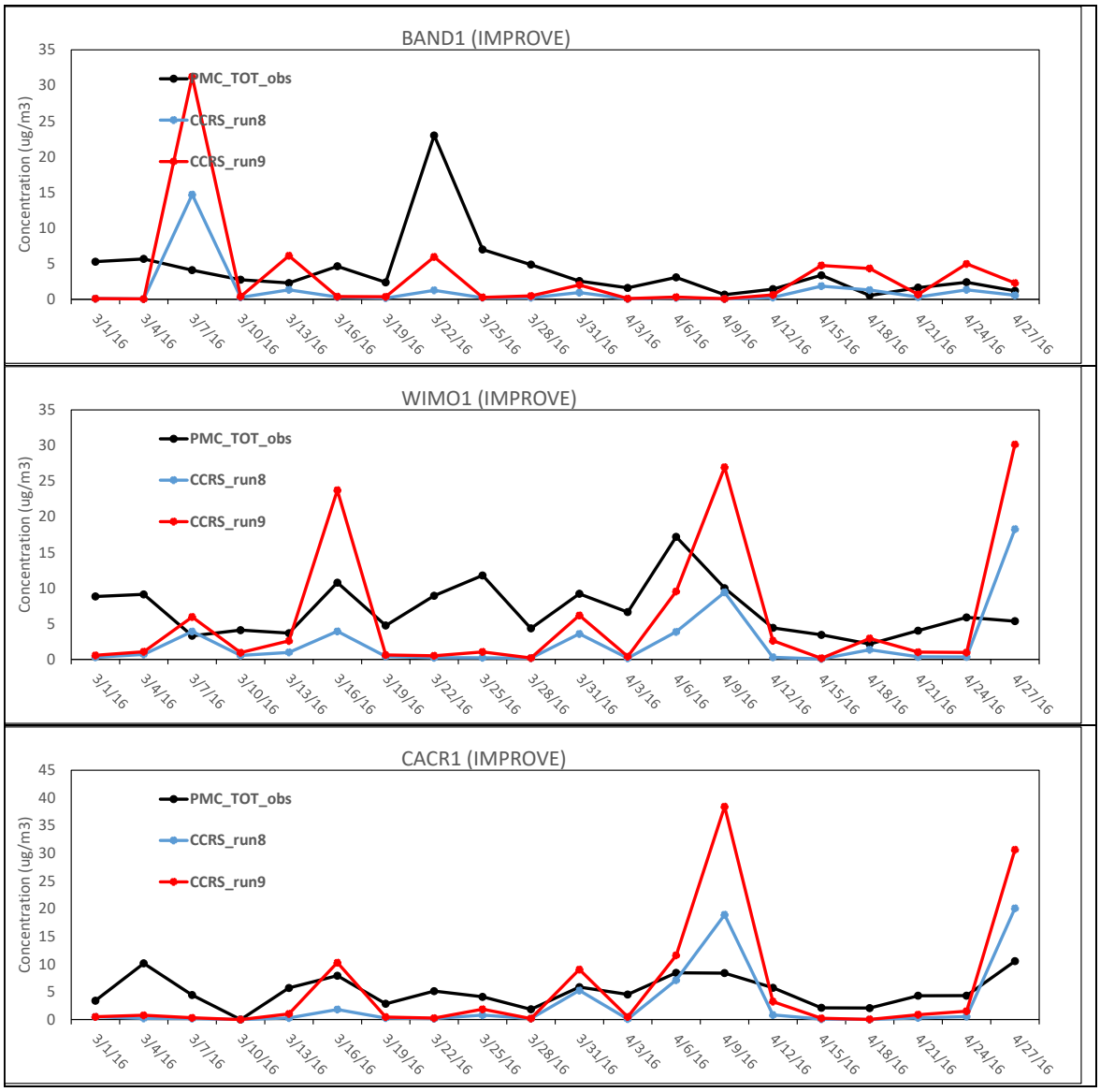

Figure 4-6 (concluded).

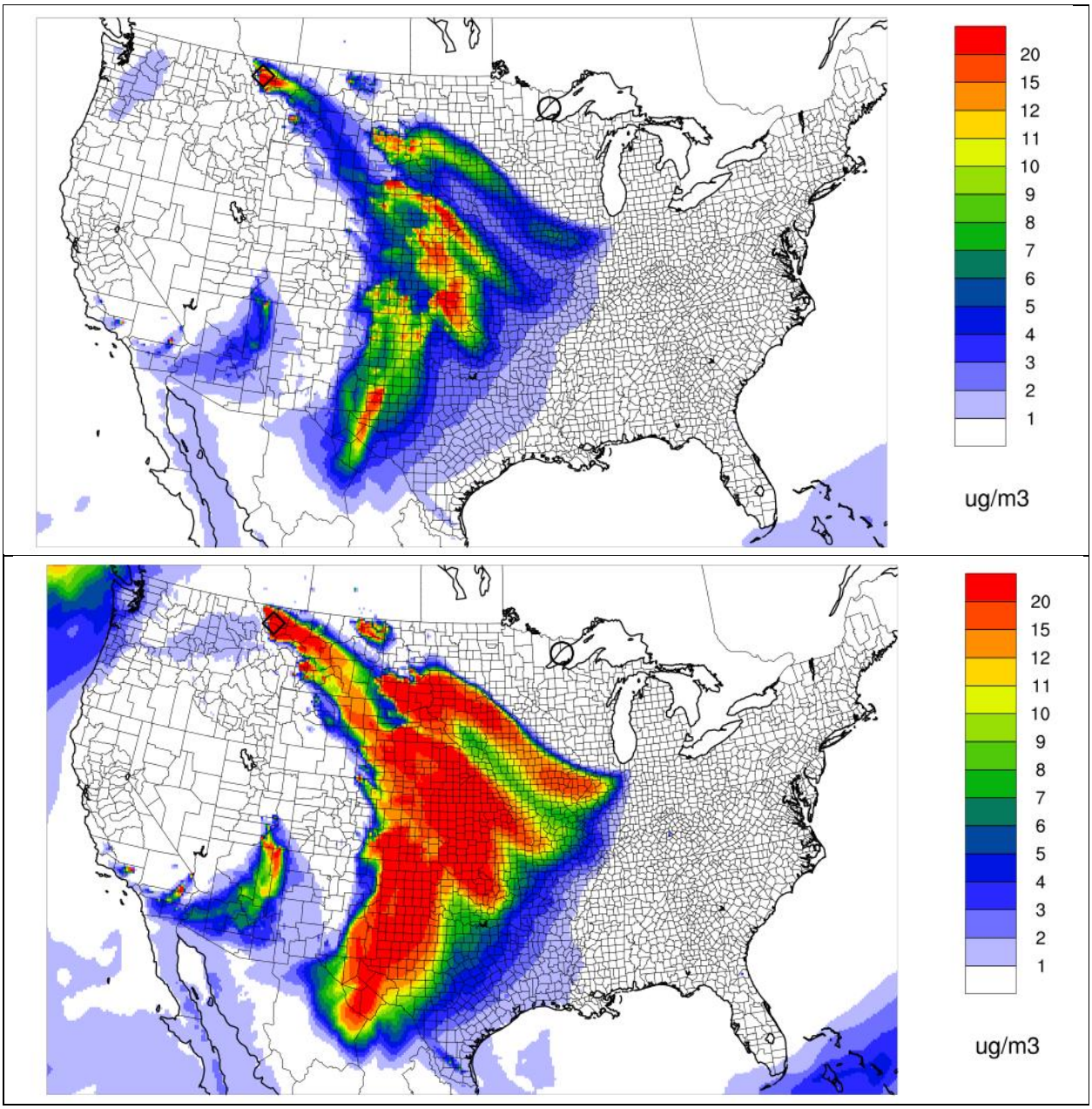

Figure 4-7. Simulated 24-hour fine crustal (FCRS; top) and coarse crustal (CCRS; bottom) concentrations on April 6, 2016 from CAMx WBD Run 9.

4.2 Full Chemistry Test with Dust Speciation

We conducted a final full-year CAMx chemistry simulation involving the entire natural and anthropogenic emission inventory from the 2016 MP, with elemental WBD speciation for areas in the US (see Appendix A, Table A-1), and performed a comprehensive evaluation against speciated measurements at IMPROVE sites throughout the south-central US.

4.2.1 Configuration

The WDUST configuration followed from Run 9. However, it included a subsequent update to fix a minor coding error in applying the saltation erodibility fraction (Section 2.3), which was revealed during final QA/QC review of the WBDUST code. This update led to modest changes to WBD emissions in space and magnitude, but fortuitously, it generally improved WBD bias over Run 9 at the expense of some increase in over predictions in the central plain states (see Run 10 in Tables 4-1 and 4-2). Appendix A details the final WBDUST formulation.

We ran CAMx v7.1 using the Ramboll 2016 MP with a standard model configuration, as follows:

Advection Solver	Piecewise Parabolic Method (PPM)
Chemistry	Carbon Bond 6 revision 4 (CB6r4) gas photochemical mechanism; CF2/SOAP inorganic and organic PM chemistry mechanism, including; 8 explicit elements (Fe, Al, Si, Ca, Ti, K, Mg, Mn), other un-speciated fine and coarse crustal (FCRS, CCRS), and other non-crustal, un-speciated fine and coarse primary PM (FPRM, CPRM);
Chemistry Solver	Euler-Backward Iterative
PiG Submodel	Off
Probing Tools	None
Dry Deposition	Zhang
Wet Deposition	On
Bi-directional NH_3	On
Inline Oceanic Iodine Emissions	On
ACM2 Diffusion	Off
Timestep Super Stepping	On
Gridded Emissions	On (full emission inventory, including WBD)
Point Emissions	On (full emission inventory)

4.2.2 Model Performance Evaluation for Dust Species

Figures 4-8 through 4-13 display monthly-averaged concentrations of dust components at the same 6 IMPROVE sites as presented in Section 4.1 (BAND, BIBE, CACR, GUMO, SACR, WIMO). Concentrations are presented as bar charts of individual species, which IMPROVE defines as soil-derived PM, for each month of 2016 to give a sense of seasonal variation. For the fine PM mode, IMPROVE "reconstructs" fine soil concentrations from the composite of 5 measured elemental concentrations: Si, Fe, Ca, Al, and Ti. Therefore, we directly compare monthly modeled and measured concentrations of these 5 elemental species as stacked bar charts. For the coarse PM mode, IMPROVE only reports total coarse mass, and so we compare modeled total coarse mass (CCRS + CPRM) to measured coarse mass. Although IMPROVE measures

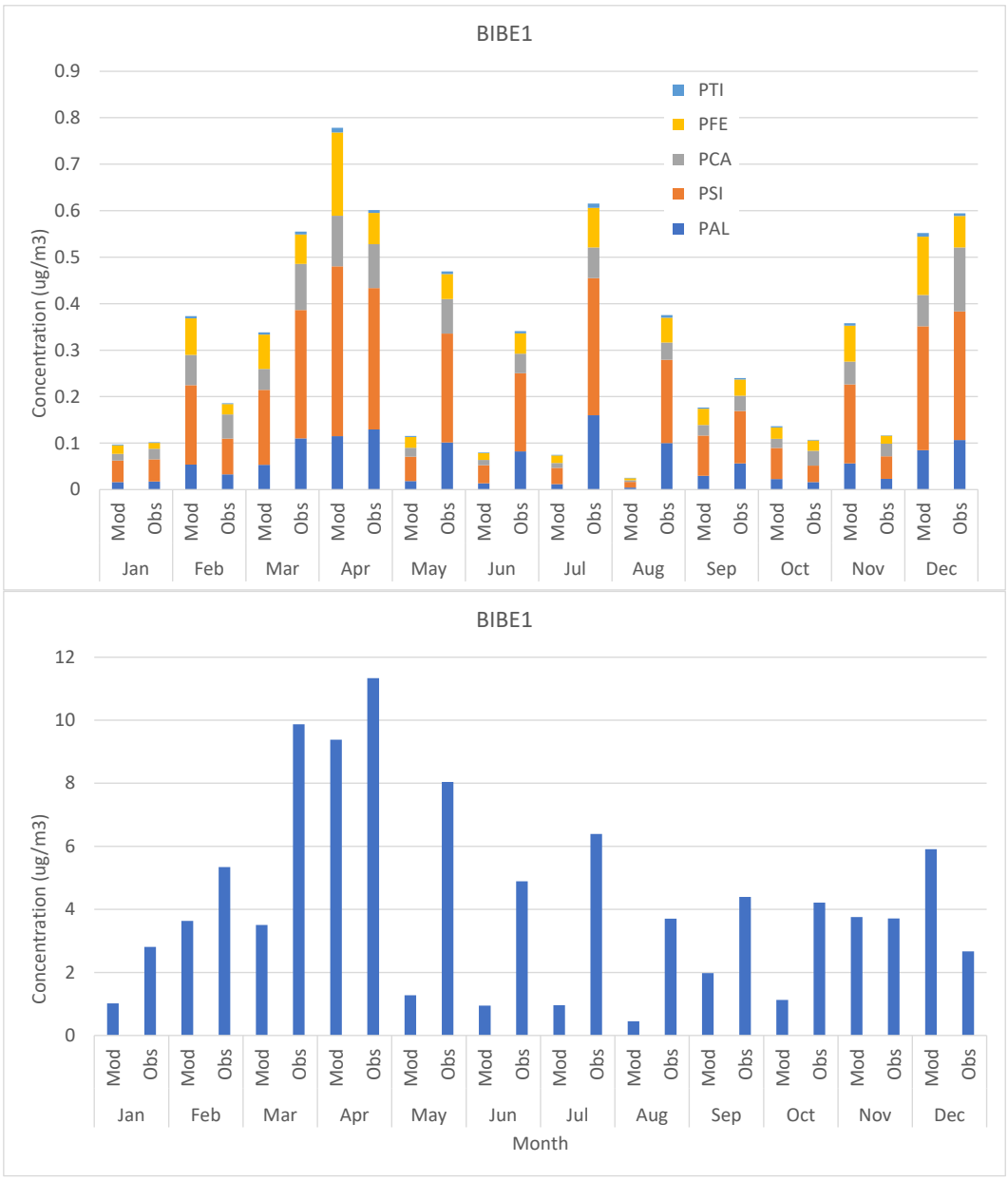

Figure 4-8. Comparisons of 2016 monthly averaged modeled and measured fine dust elemental concentrations (top) and total coarse mass concentrations (bottom) at the Big Bend IMPROVE monitoring site.

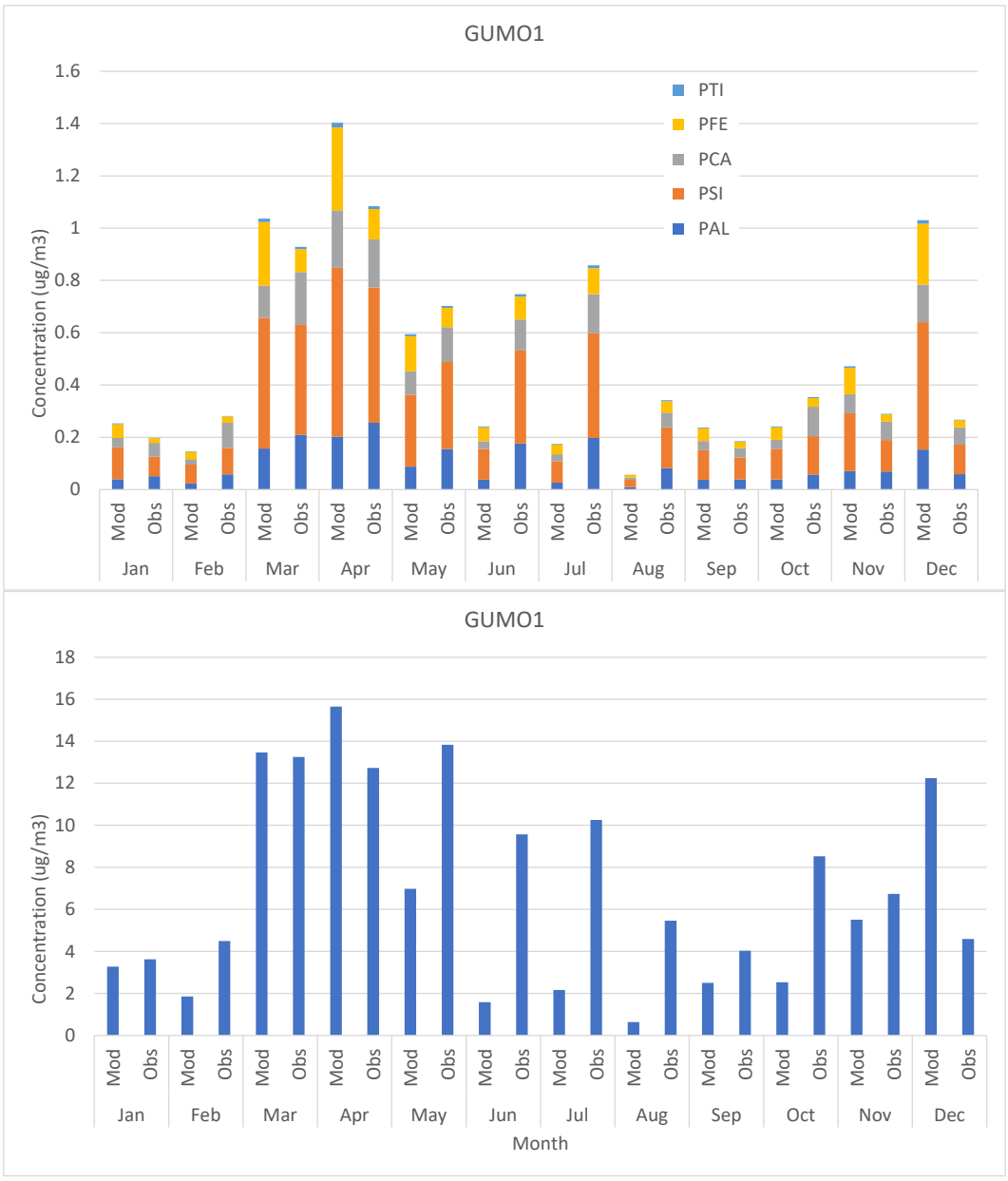

Figure 4-9. Comparisons of 2016 monthly averaged modeled and measured fine dust elemental concentrations (top) and total coarse mass concentrations (bottom) at the Guadalupe Mountains IMPROVE monitoring site.

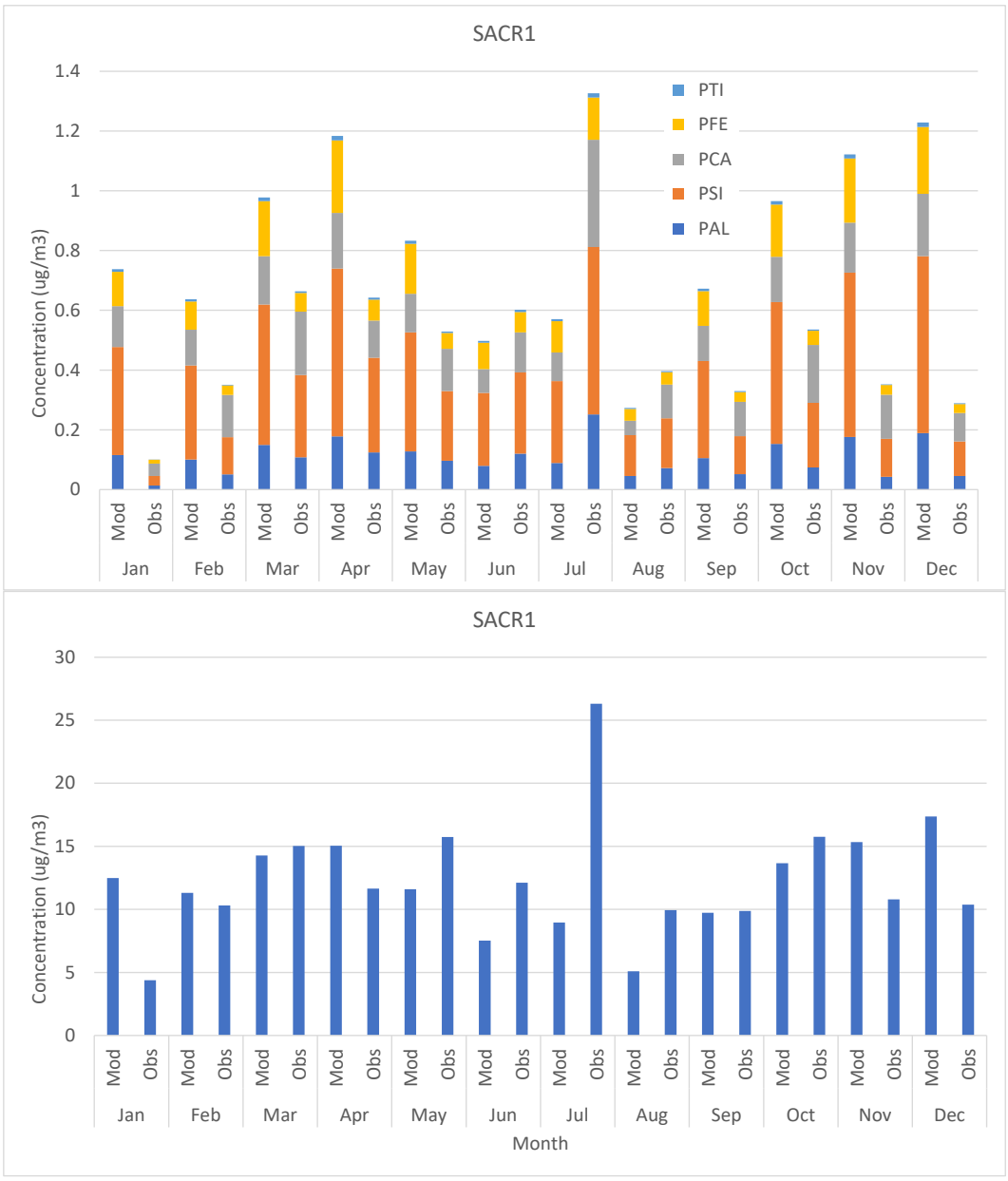

Figure 4-10. Comparisons of 2016 monthly averaged modeled and measured fine dust elemental concentrations (top) and total coarse mass concentrations (bottom) at the Salt Creek IMPROVE monitoring site.

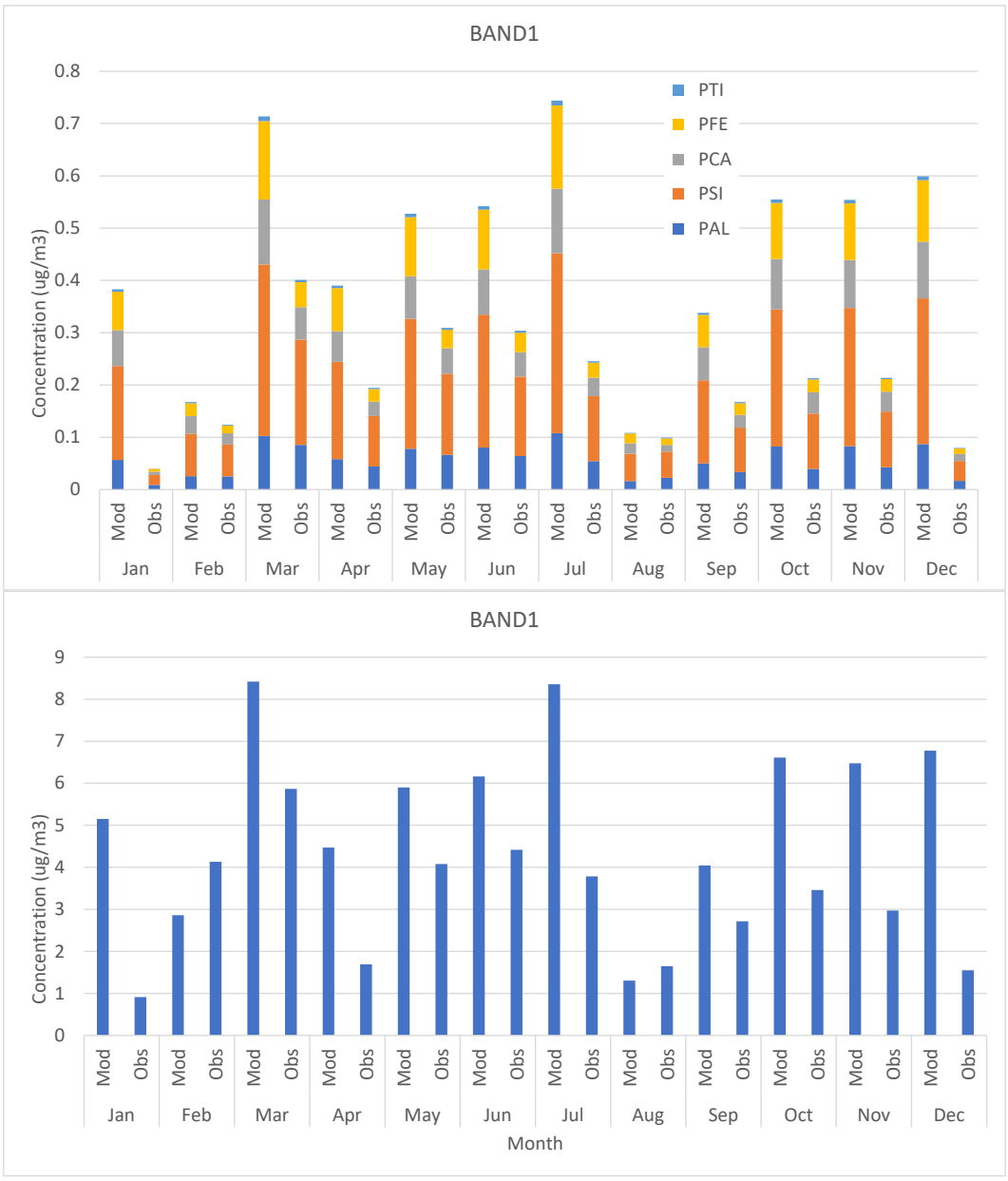

Figure 4-11. Comparisons of 2016 monthly averaged modeled and measured fine dust elemental concentrations (top) and total coarse mass concentrations (bottom) at the Bandelier IMPROVE monitoring site.

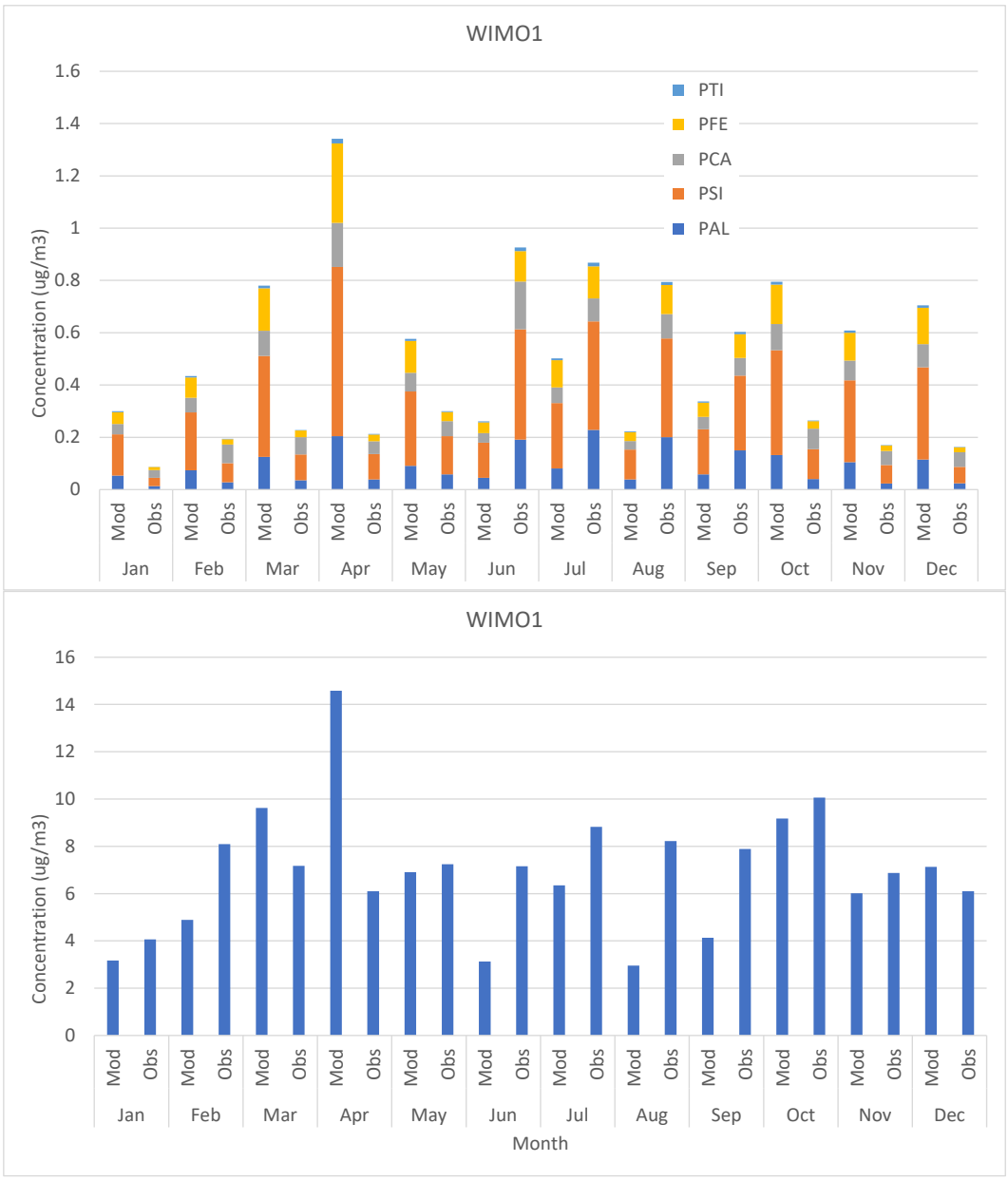

Figure 4-12. Comparisons of 2016 monthly averaged modeled and measured fine dust elemental concentrations (top) and total coarse mass concentrations (bottom) at the Wichita Mountains IMPROVE monitoring site.

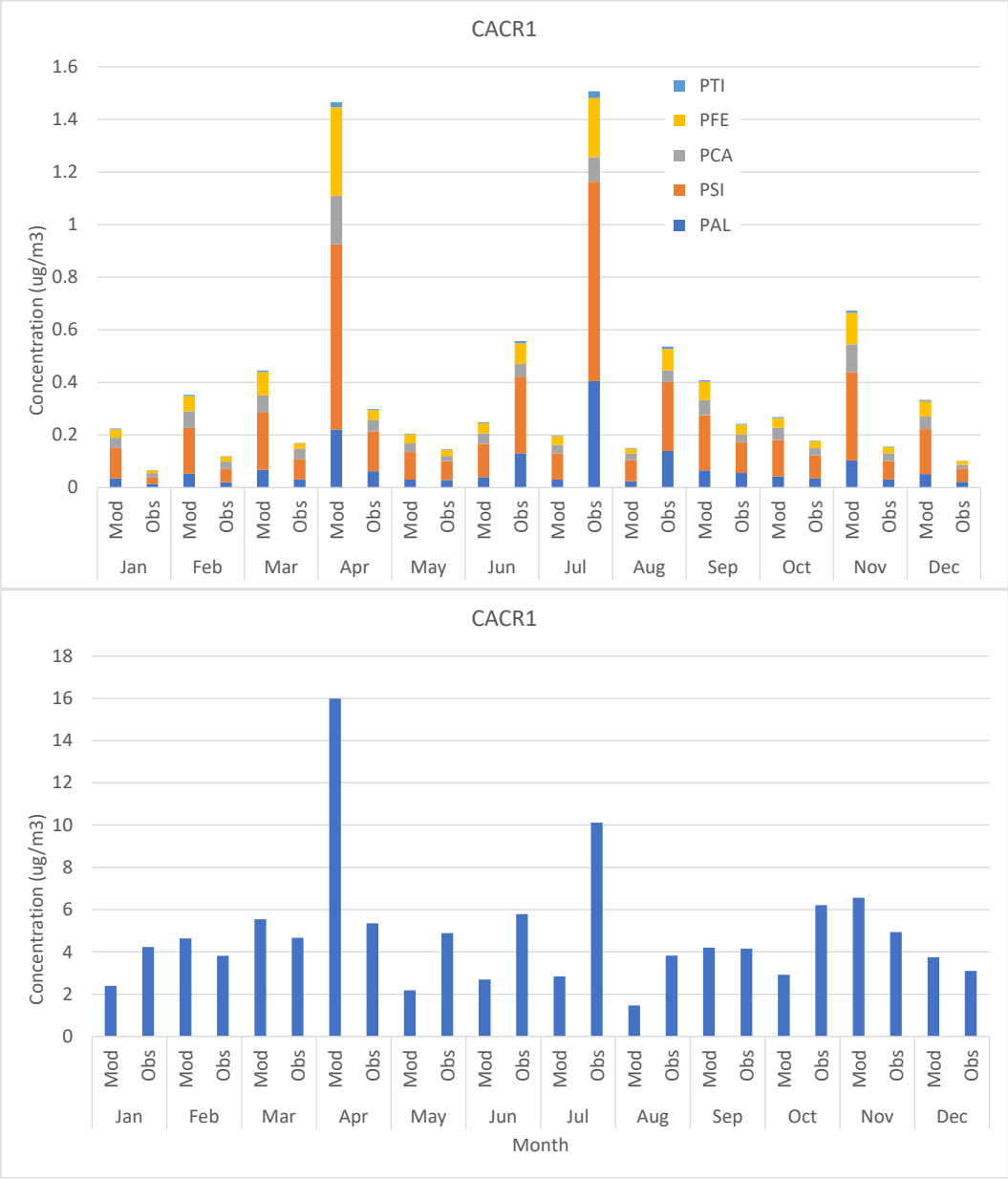

Figure 4-13. Comparisons of 2016 monthly averaged modeled and measured fine dust elemental concentrations (top) and total coarse mass concentrations (bottom) at the Caney Creek IMPROVE monitoring site.

other elemental concentrations, those derive more from other major sources such as fires (potassium), sea salt (sodium), and industry (magnesium and manganese) and are thus not the best markers for dust. Beyond the elemental species, IMPROVE does not measure any "other" remaining fine soil mass that would map to the modeled FCRS species, so we were unable to assess FCRS.

Model-observation agreement for fine soil and coarse mass has improved substantially with the use of the updated WBDUST model over older results described in Section 1 using the original

version. Whereas previously the original WBDUST model resulted in practically zero dust everywhere and at all times, the new model is capable of generating sufficient dust that agrees fairly well with measured concentrations all year round. However, model performance varies substantially across months and sites. Generally, the model over predicts fine dust components and total coarse mass in the spring and autumn, but under predicts during the summer when measured levels increase. Model performance for coarse mass tends to be better than for individual fine mass components or their sums. There are no clear performance tendencies for fine elemental concentrations across the sites, but overall, the charts in Figures 4-8 through 4-13 indicate that the relative elemental compositions are appropriately characterized with the majority of mass contained in silicon, aluminum, and iron. This suggests that the various sources of dust speciation applied in WBDUST are generally characterizing regional US soil composition adequately.

Table 4-3 lists annual normalized mean bias for simulated fine elemental and total fine dust concentrations, and for total coarse mass at each IMPROVE site. Across the entirety of 2016, the model reproduces component concentration within a factor of two of measurements. Again, there is no discernable central tendency in model-observation agreement across species and sites, except that iron tends to be consistently over predicted and that total coarse mass is better simulated than the fine mass components. However, many more sources beyond WBD contribute to the total coarse mass budget, and so superior agreement may be more of a corroboration of the overall coarse PM emission inventory.

Table 4-3. Annual normalized mean bias (%) for simulated fine elemental and total fine dust concentrations, and total coarse mass, at six IMPROVE sites and the average over all sites from the full emissions/chemistry CAMx run using the final WBDUST configuration (BAND=Bandelier; BIBE=Big Bend; CACR=Caney Creek; GUMO=Guadalupe Mountains; SACR=Salt Creek; WIMO=Wichita Mountains). Model biases within a factor of 2 (-50% to +100%) of observations are noted in green.

Dust Component	BAND	BIBE	CACR	GUMO	SACR	WIMO	Average
Si	121	-28	23	-2	83	56	42
Fe	293	24	55	98	183	114	128
Ca	154	-39	69	-34	-12	-2	22
Al	64	-49	-22	-37	44	9	2
Ti	148	-14	10	16	106	48	52
Total Fine Dust	135	-28	22	-6	59	43	38
Total Coarse Mass	79	-50	-10	-30	-6	-11	-5

4.2.3 Dust Impacts on Inorganic PM Chemistry

In CAMx, ambient dust concentrations impact the rate of heterogeneous sulfate formation and the partitioning of several inorganic compounds (sulfate, nitrate, ammonia, sodium, chloride) among gas and particle phases (Ramboll, 2021). Five crustal elements (Fe, Mn, Ca, Mg and K) are used in aqueous chemistry; Fe and Mn catalytically contribute to the oxidation of SO_2 to sulfate, while Ca, Mg and K impact cloud pH and thus the solubility of SO_2 in cloud water. Up to five elements (Na, Cl, Ca, Mg, K) influence inorganic aerosol partitioning depending on the

chosen chemical scheme. All elements are used along with FPRM and FCRS to determine aerosol surface area for heterogenous reactions of SO_2 and N_2O_5. Nitric acid (HNO_3) reacts with calcium in soil dust particles to form calcium nitrate.

Given their influence on the chemistry of other inorganic species, it was important to evaluate the impacts from substantially higher elemental concentrations resulting from the updated WBDUST model. For each month of the 2016 simulation, we compared 24-hour concentrations of sulfate, nitrate, and ammonium between CAMx runs using the original WBDUST v1.0 and the new v2.0. We plotted spatial distributions of monthly maximum differences (*max[v2.0 – v1.0]*) and monthly minimum differences (*min[v2.0 – v1.0]*) of these three species. Figures 4-14 and 4-15 show examples for selected months that contain the annual peak maxima and minima (i.e., the largest differences in 24-hour sulfate, nitrate, and ammonia over the entirety of 2016). Note that maximum differences in some areas can be negative, and vice versa, especially for the most sensitive and non-linear compounds like nitrate. Results for other months are consistent with those shown in the figures but exhibit smaller domain-wide peak impacts.

Enhanced WBD emissions result in both increases and decreases in all of the secondary inorganic particulate species. Monthly and annual peak differences are usually constrained to one or two grid cells where there is a strong source of WBD and/or a large source of secondary PM precursors (SO_2, NOx, or NH_3). For sulfate, monthly maximum and minimum differences range mostly between 0.1 $\mu g/m^3$ with perhaps a slight tendency toward concentration increases than decreases in any month. However, larger sulfate differences (both positive and negative) tend to occur in the eastern US with higher sulfur emissions. Nitrate concentrations tend to be higher in all months with much smaller decreases. We attribute this to increased abundance of neutralizing cations (e.g., calcium) that convert gaseous nitric acid to particulate nitrate. There is no obvious seasonal effect for nitrate, but larger nitrate differences tend to occur in the western US with higher WBD emissions. Differences in ammonium are opposite from nitrate, with generally larger concentration decreases than increases in all months, although the differences are smaller than for sulfate and nitrate. This suggests that WBD cations tend to displace ammonia as neutralizing agents for sulfate and nitrate. Like nitrate, the largest ammonia differences (reductions) occur in the western US.

4.3 Summary

Test runs revealed that key parameters controlling dust are drag partitioning and, to a lesser extent, vegetation fraction. Specifically, it was very important to specify vegetation cover for each individual emissive LULC type rather than relying on grid-composite LAI. That adjustment, affecting both partitioning and vegetative scaling, greatly improved WBD emission estimates and resulting simulated FCRS and CCRS concentrations throughout the western US.

Model-observation agreement for fine soil and coarse mass has improved substantially with the updated WBDUST model over the original version. The new model is capable of generating sufficient dust that agrees fairly well with measured concentrations in all seasons. Across the entirety of 2016, the model reproduces component concentration within a factor of two of measurements.

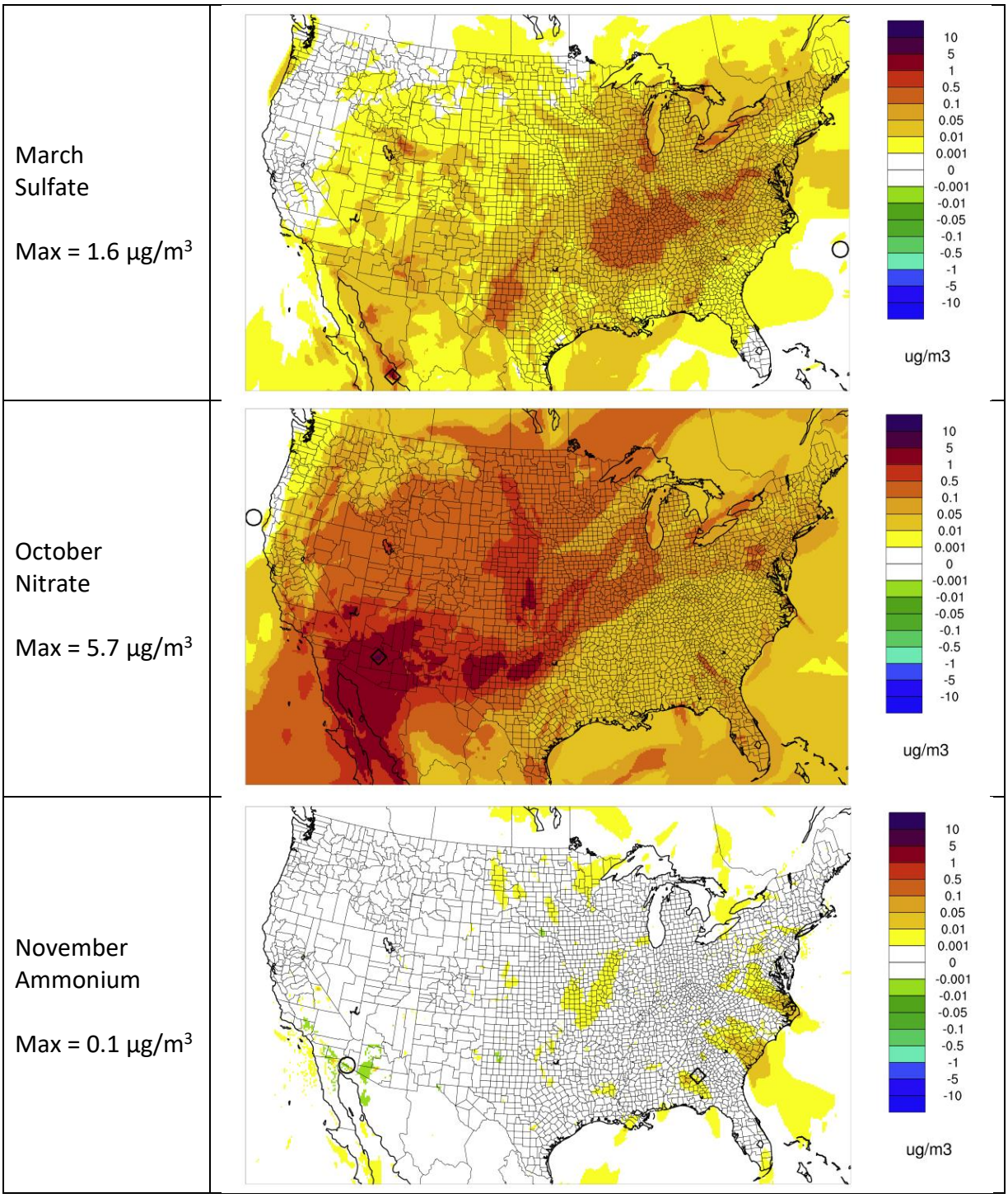

Figure 4-14. Spatial distributions of selected monthly maximum differences in 24-hour sulfate (top), nitrate (middle) and ammonium (bottom) concentrations from CAMx simulations using WBDUST v2.0 and v1.0 (*max[v2.0 – v1.0]*). The selected months contain the annual peak maximum difference for each species.

June
Sulfate

Max = -0.2 µg/m^3

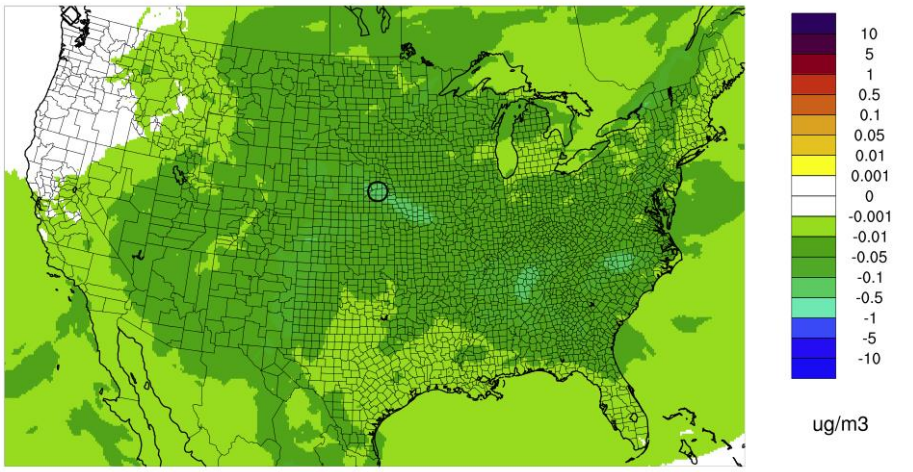

October
Nitrate

Max = -0.5 µg/m^3

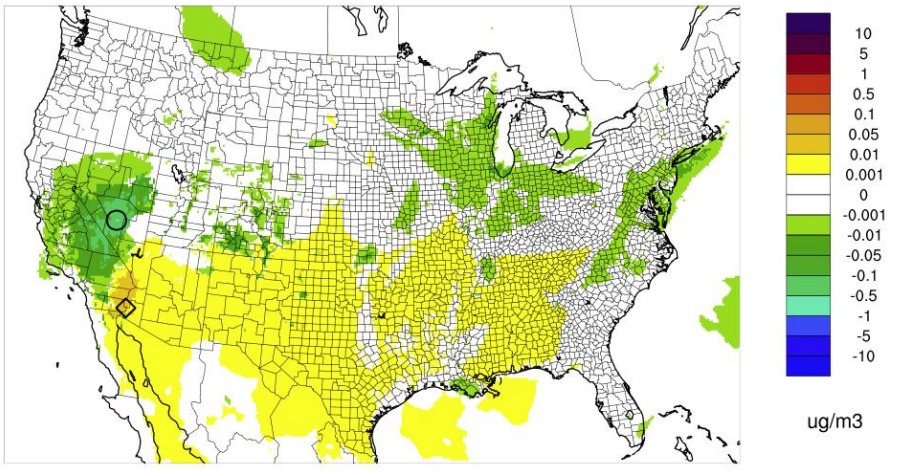

October
Ammonium

Max = -0.7 µg/m^3

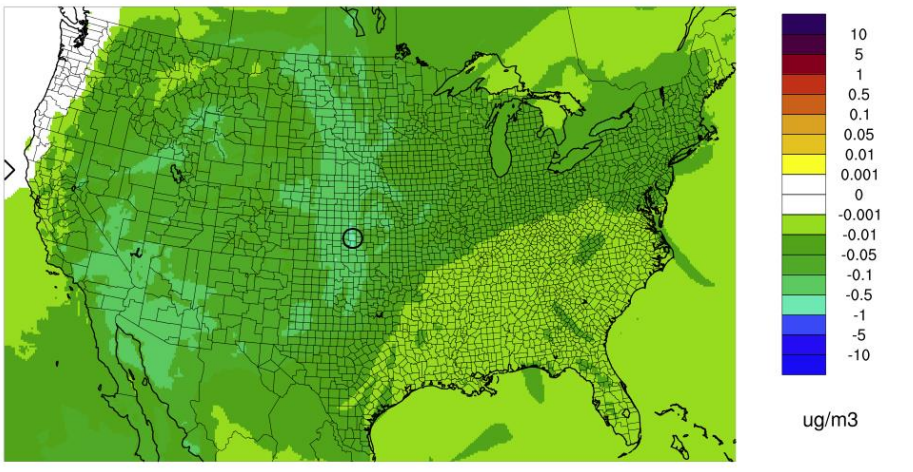

Figure 4-15. Spatial distributions of selected monthly minimum differences in 24-hour sulfate (top), nitrate (middle) and ammonium (bottom) concentrations from CAMx simulations using WBDUST v2.0 and v1.0 (*min[v2.0 – v1.0]*). The selected months contain the annual peak minimum difference for each species.

Model performance varies substantially across months and sites. Generally, the model over predicts fine dust components and total coarse mass in the spring and autumn, but under predicts during the summer when measured levels increase. Model performance for coarse mass tends to be better than for individual fine dust elemental components or their sums. There are no clear performance tendencies for fine elemental concentrations across the sites, but overall, the relative elemental compositions are appropriately characterized with the majority of mass contained in silicon, aluminum, and iron. This suggests that the various sources of dust speciation applied in WBDUST generally characterize regional US soil composition adequately.

Enhanced WBD emissions result in both increases and decreases in all of the secondary inorganic particulate species. For sulfate, impacts are generally small with perhaps some tendency toward concentration increases than decreases, especially in the eastern US with higher sulfur emissions. Nitrate concentrations tend to be higher in all months, especially in the western US, with much smaller decreases due to increased abundance of neutralizing cations that convert gaseous nitric acid to particulate nitrate. Effects on ammonium are opposite and smaller, with generally more concentration decreases than increases in the western US for all months. This suggests that WBD cations tend to displace ammonia as neutralizing agents for sulfate and nitrate.

While simple scaling adjustments can be easily applied to minimize WBD bias over wider spatial and time scales, larger gross errors and poor correlation against measurements at specific times and locations indicate the distinctly stochastic nature of WBD emissions and local contributions that cannot be resolved. Numerous modeled phenomena, all with their own inherent errors, must align in the modeling system to generate dust, disperse it, and deposit it, including:

- Meteorology (surface wind speeds, stability/wind stress);
- Soil conditions (type/content, moisture level, saltation particle size distributions/coverages, soil roughness by land cover type, elemental speciation fractions);
- Vegetation conditions (type/mix, coverage/density, roughness by land cover type);
- Deposition rates (dust size/density).

Additional improvements in the details of source mechanisms and soil types and distributions would likely result in diminished returns, while supporting datasets would be exceedingly difficult to find, utilize and extend to regional and continental scales. However, we recognize some lingering issues:

- Overstated springtime dust emissions from expansive cropland areas indicate continued over-simplification of how they are treated in the WBDUST model, e.g., whether they are irrigated or not (the latter being implicitly assumed). Improved information on irrigation and tilling activity is needed.
- Proper land use and vegetative characterization in modeling WBD are critical and have a direct influence on WBD emissions in space and time.

5.0 CONCLUSIONS AND RECOMMENDATIONS

Ramboll has identified specific shortcomings in the original WBDUST emission model and implemented updated parameterizations and more locally specific and temporally resolved activity data for croplands. A key disadvantage of the original formulation was the restriction of emissive areas to large permanent natural barren lands such as deserts, with limited regard to seasonal and spatial variations in smaller-scale erodible lands such as exposed agricultural fields associated with cultivation cycles. Correctly representing the spatial and temporal variations in surface vegetation is important due to its multiple effects on dust generation and suppression. In particular, dust emissions from tilled croplands are critically important to areas within and around Texas.

The project began with a detailed evaluation of other widely used WBD models and a comparison against the WBDUST modeling framework. From this review, we identified and implemented specific improvements based on the work of Foroutan et al. (2017) that provide a reasonable balance between technical rigor and detail supported by available data. We confirmed that these updates: (1) improve upon several simple methods and assumptions; (2) provide additional detail for important processes without the burden of requiring additional input data; and (3) result in higher, more spatially widespread and temporally variable emission rates without the need for ad hoc modifications. The updated WBDUST model continues to use CAMx-ready input files for meteorology and landcover and continues to allow for global inputs of soil type and elemental speciation so that the model can be used globally. Test runs revealed that key parameters controlling dust emissions are drag partitioning and, to a lesser extent, the amount of vegetative dust suppression. Specifically, we found that it is very important for both processes to specify vegetation cover for each individual emissive LULC type rather than relying on grid-composite LAI. This additional refinement greatly improved resulting crustal PM concentrations throughout the western US.

We then identified and adapted US-specific alternative landcover (the NASS CropScape) and year/season-specific cropland activity datasets (CMAQ Crop Calendar) to further improve the characterization of WBD from agricultural lands. We implemented additional updates in WBDUST to optionally utilize these data as the basis for modifying input CAMx landcover distributions to reflect locations and extents of tilled croplands that are barren and thus potentially emissive. In the process we developed several Python scripts to process raw annual CropScape data to the target grid structure and to the CAMx LULC categories.

Finally, we assessed the cumulative effects of these updates using a US-wide CAMx photochemical model simulation for the entire year of 2016. Modeling results were compared against measurements from IMPROVE monitoring sites throughout the western US and specifically surrounding Texas. Model-observation agreement for fine and coarse WBD has improved substantially with the updated WBDUST model over the original version. The new model is capable of generating sufficient dust on par with measured concentrations in all seasons. Across the entirety of 2016, the model reproduces component concentration within a factor of two of measurements. Model performance varied substantially across months and sites. Generally, the model systematically over predicted fine dust components and total

coarse mass in the spring and autumn, but under predicted during the summer when measured levels increase. Model performance for coarse mass tended to be better than for individual fine dust elemental components or their sums. There were no clear performance tendencies for fine elemental concentrations across the sites analyzed here, but overall, the relative elemental compositions are appropriately characterized with the majority of mass contained in silicon, aluminum, and iron. This suggests that the various sources of dust speciation applied within WBDUST generally characterize US regional soil composition adequately.

Crustal elements in WBD impact the chemistry of secondary inorganic and potentially organic compounds. Improved WBD emissions result in both increases and decreases in all of the secondary inorganic particulate species. For sulfate, impacts are generally small with perhaps some tendency toward concentration increases more than decreases, especially in the eastern US with higher sulfur emissions. Nitrate concentrations tend to be higher in all months, especially in the western US, due to increased abundance of neutralizing cations that convert gaseous nitric acid to particulate nitrate. Effects on ammonium are opposite and smaller, with generally more concentration decreases than increases in the western US for all months. WBD cations tend to displace ammonia as neutralizing agents for sulfate and nitrate.

We offer the following recommendations for future consideration:

- Land use characterization is critically important to WBD from both natural and crop landscapes, and so we encourage the use of the most detailed land type coverages available.
- Temporal variations in vegetative patterns are equally important as their spatial distribution. Overstated springtime dust emissions from expansive cropland areas indicate continued over-simplification of how they are treated in the WBDUST model, e.g., what fraction is cultivated/emissive at any given time during the planting seasons, and what fraction is consistently irrigated or not (the latter being implicitly assumed). Improved information on tilling activity and irrigation is needed.
- Certain elemental species exhibit consistent high bias relative to IMPROVE measurements, particularly iron, which is an important catalyst for aqueous sulfate production from SO_2. Speciation profiles should be reviewed and updated as new information becomes available.
- Related to the point above, proper modeling of surface conditions is essential to the WBD process. Updates to WBDUST may be necessary as WRF performance in simulating several surface variables improves, particularly soil moisture.
- An inter-model comparison among WBDUST and the other models and schemes reviewed herein (e.g., WRF-Chem/AFWA and CMAQ) should be conducted in the most consistent manner possible.

6.0 REFERENCES

Astitha, M., J. Lelieveld, M.A. Kader, A. Pozzer, A. de Meij, 2012. Parameterization of dust emissions in the global atmospheric chemistry-climate model EMAC: impact of nudging and soil properties. *Atmos. Chem. Phys*., 12(22):11057-11083, 2012. doi:10.5194/acp-12-11057-2012.

Darmenova, K., I.N. Sokolik, Y. Shao, B. Marticorena, G. Bergametti, 2009. Development of a physically based dust emission module within the Weather Research and Forecasting (WRF) model: Assessment of dust emission parameterizations and input parameters for source regions in Central and East Asia. *J. Geophys. Res. Atmos.*, 114, D14201, doi:10.1029/2008JD011236.

EPA, 2019. Technical Support Document (TSD) for EPA's Updated 2028 Regional Haze Modeling. Prepared by the United States Environmental Protection Agency, Office of Air Quality Planning and Standards (September 2019). https://www.epa.gov/sites/production/files/2019-10/documents/updated_2028_regional_haze_modeling-tsd-2019_0.pdf.

EPA, 2021a. Regional Haze Program website: https://www.epa.gov/visibility/regional-haze-program.

EPA, 2021b. Air Emissions Inventories, 2014 National Emissions Inventory (NEI) Data website: https://www.epa.gov/air-emissions-inventories/2014-national-emissions-inventory-nei-data.

EPA, 2021c. Community Multiscale Air Quality (CMAQ) model website: https://www.epa.gov/cmaq.

EPA, 2021d. Ambient Monitoring Technology Information Center (AMTIC), Chemical Speciation Network (CSN) website: https://www.epa.gov/amtic/chemical-speciation-network-csn.

Foroutan, H., J. Young, S. Napelenok, L. Ran, K.W. Appel, R.C. Gilliam, J.E. Pleim, 2017. Development and evaluation of a physics-based windblown dust emission scheme implemented in the CMAQ modeling system. *J. Adv. Model. Earth Syst*., 9, 585–608, doi:10.1002/2016MS000823.

IMPROVE, 2021. Monitoring data website: http://vista.cira.colostate.edu/Improve/data-page/.

IWDW, 2020. Intermountain Data Warehouse Modeling Platforms website. https://views.cira.colostate.edu/iwdw/Modeling/Platforms.aspx.

Klingmueller K., S. Metzger, M. Abdelkader, V.A. Karydis, G.L. Stenchikov, A. Pozzer, J. Lelieveld, 2018. Revised mineral dust emissions in the atmospheric chemistry-climate model EMAC (MESSy 2.52 DU_Astitha1 KKDU2017 patch). *Geosci. Model Dev*., 11, 989–1008, https://doi.org/10.5194/gmd-11-989-2018.

Kok, J. F., 2011. A scaling theory for the size distribution of emitted dust aerosols suggests climate models underestimate the size of the global dust cycle. *Proc. Natl. Acad. Sci*. USA, 108, 1016–1021, https://doi.org/10.1073/pnas.1014798108.

LeGrand, S.L., C. Polashenski, T.W. Letcher, G.A. Creighton, S.E. Peckham, J.D. Cetola, 2019. The AFWA dust emission scheme for the GOCART aerosol model in WRF-Chem v3.8.1. *Geosci. Model Dev.*, 12, 131–166, https://doi.org/10.5194/gmd-12-131-2019.

Louis, J.F. 1979. A Parametric Model of Vertical Eddy Fluxes in the Atmosphere. *Bound. Lay. Meteor.*, 17, 187-202.

Myhre, G., A. Grini, J.M. Haywood, F. Stordal, B. Chatenet, D. Tanre, J.K. Sundet, I.S.A. Isaksen, 2003. Modeling the radiative impact of mineral dust during the Saharan Dust Experiment (SHADE) campaign. *J. Geophys. Res*., 108(D18), 8579, doi:10.1029/2002JD002566.

NASS, 2012. "CropScape-cropland data layer." USDA National Agricultural Statistics Service: Washington, DC.

NASS, 2021a. CropScape webpage: https://nassgeodata.gmu.edu/CropScape/.

NASS, 2021b. Research and Science, CropScape and Cropland Data Layers website: https://www.nass.usda.gov/Research_and_Science/Cropland/sarsfaqs2.php.

NCAR, 2021. Weather Research and Forecasting (WRF) meteorological model website: http://www2.mmm.ucar.edu/wrf/users/.

NEIC, 2021. National Emissions Inventory Collaborative, 2016v1 Emissions Modeling Platform website. http://views.cira.colostate.edu/wiki/wiki/10202.

NOAA, 2021. Weather Research and Forecasting model coupled to Chemistry (WRF-Chem) web page: https://ruc.noaa.gov/wrf/wrf-chem/.

NWS, 2014. National Weather Service events website: NWS Lubbock, TX, Wind and Blowing Dust, April 27-29,2014. https://www.weather.gov/lub/events-2014-20140428-wind.

Ramboll, 2019. Western Regional Modeling and Analysis Platform Modeling Plan -- Phase I: 2014 Platform Development and Shake-Out. Prepared by Ramboll, Novato, CA; submitted to the Western Regional Air Partnership (March 2019). http://views.cira.colostate.edu/wiki/Attachments/Attachments/WRAP_2014/WRAP_2014_Shake-Out_Plan_Phase-I_v4_2019-03-09.pdf.

Ramboll, 2020a. Regional haze modeling to evaluate progress in visibility in and near Texas. Final Report prepared by Ramboll, Novato, CA; submitted to the Texas Commission on Environmental Quality, Austin, TX (June 2020). https://www.tceq.texas.gov/assets/public/implementation/air/am/contracts/reports/pm/5822010567009-20200625-ramboll-RegionalHazeModelingEvaluateProgressVisibility.pdf.

Ramboll, 2020b. Quality Assurance Project Plan: Project 20 – 011, Improving Estimates of Wind-Blown Dust from Natural and Agricultural Sources. Prepared for the Texas Air Quality Research Program (AQRP), the University of Texas at Austin (July 17, 2020).

Ramboll, 2021. User's Guide: Comprehensive Air quality Model with extensions, Version 7.10 (January 2021). http://www.camx.com/files/camxusersguide_v7.10.pdf.

Shao, Y., and H. Lu, 2000. A simple expression for wind erosion threshold friction velocity. *J. Geophys. Res*., 105(D17), 22,437–22,443, doi:10.1029/2000JD900304.

USGS, 2021. Multi-Resolution Land Characteristics Consortium Project: https://www.mrlc.gov/national-land-cover-database-nlcd-2016.

Wang, J.X.L., 2015. Mapping the Global Dust Storm Records: Review of Dust Data Sources in Supporting Modeling/Climate Study. *Curr. Pollution Rep*., 1, 82–94 (2015). https://doi.org/10.1007/s40726-015-0008-y.

APPENDIX A: FINAL WBDUST V2.0 FORMULATION

WBDUST v2.0 is based on an adaptation of the windblown dust (WBD) emission scheme described by Foroutan et al. (2017; hereafter F17). The design objective of WBDUST continues to provide the CAMx user community with a dust emission framework that supports multi-scale CAMx applications anywhere in the world. Version 2.0 includes an update specific to US applications that refines the seasonal emissive properties of croplands based on year-specific, high-resolution data for 18 crop types in combination with a state-level crop calendar.

Like other models, WBDUST relies on wind stress (via "friction velocity") to initiate the saltation process; i.e., lifting large soil particles that bombard or "sand blast" finer-grained particles thereby generating air emissions of dust. Many specific conditions must align to cause WBD emissions according to numerous internal parameterizations and input data defining meteorology and the state of soil and vegetation.

WBDUST uses the following input datasets:

- CAMx-ready 2-D and 3-D gridded meteorological input files derived from WRF: vertical layer heights, pressure, wind speed, temperature, and soil temperature and moisture;
- CAMx-ready 2-D gridded surface characterization input file: fractional coverage of 26 landcover types;
- Global gridded soil clay fraction at 0.1-degree (~10 km) resolution, developed by Klingmueller et al. (2018);
- Global gridded soil elemental composition at 0.1-degree (~10 km) resolution, developed by Klingmueller et al. (2018): fractions for sodium, magnesium, calcium, and potassium.

WBDUST assigns monthly leaf area index (LAI) values to each of the 26 landcover categories. LAI values were updated in v2.0 based on an analysis of monthly MODIS-derived LAI fields at 0.1-degree resolution over the conterminous US spanning the 72 months of 2010-2015, as developed by Klingmueller et al. (2018).

WBDUST maps 7 individual CAMx landcover classes (shrub, grass, crops+sugar+maize+cotton, desert) to 4 general emissive landcover types (shrub, grass, crops, barren) used in the F17 scheme. WBDUST uses input global clay fraction to assign each grid cell to one of 12 soil types used in the F17 scheme, which is possible because each soil type is defined by a unique clay fraction. Each of the 12 soil types is assigned unique fractions of 4 saltation particle types/size bins representing coarse and medium sand, silt, and clay.

To summarize the process, WBDUST first identifies potentially emissive grid cells and then proceeds to calculate a threshold friction velocity for each, above which the saltation process is activated. Individual threshold friction velocities and horizontal saltation fluxes are determined for a matrix of 4 emissive landcover types by 4 saltation particle types and related size bins. A total saltation flux is determined by summing contributions from each landcover and saltating particle type with scaling to account for the available coverage and erodibility fraction of saltating particles. A total vertical dust flux is then calculated from the product of the total

saltation flux, a sandblasting efficiency dependent on soil type, fraction of total emissive landcover in the cell, fraction of vegetation in the cell, and a factor for topographic altitude. The final dust flux is split into fine and coarse modes according to 3 overlapping dust emission size modes. A final speciation step is optionally applied to split fine mode dust into as many as 8 elements and remaining mass.

A.1 Threshold Friction Velocity

The threshold friction velocity over a smooth soil surface (U^*_{t0}) determines the minimum wind stress required to initiate and maintain the saltation process within an emissive grid cell. The Shao and Lu (2000) relationship depends primarily on saltation particle size (D_p):

$$U^*_{t0} = \sqrt{0.0123\left(\frac{\rho_p g D_p}{\rho_\alpha} + \frac{1.65 \times 10^{-4}}{\rho_p D_p}\right)}$$

where ρ_p is particle density, g is gravitational acceleration, and ρ_α is air density, and all units are MKS. A uniform saltation particle density for quartz (2650 kg/m^3) is assumed for all processes throughout the scheme, which is common in other WBD schemes. The threshold friction velocity is calculated for each of 4 saltation particle sizes: coarse sand (690 µm), medium sand (210 µm), silt (125 µm), and clay (2 µm).

Adjustment for Soil Moisture

Soil moisture increases resistance to saltation because it affects soil particle cohesion. A factor is applied to U^*_{t0} to raise the threshold for moist soils. Gridded soil moisture is read as an additional diagnostic surface field from the CAMx-ready 2-D meteorological input file. Soil moisture is taken from WRF's top-most soil layer, which can vary in depth from 1 to 30 cm depending on the WRF land surface model that was run. Soil moisture reported by WRF is expressed as volumetric ratio so it must be converted within WBDUST to gravimetric or mass ratio by dividing by soil density (ρ_s in g/cm^3) using a parametrization involving the soil fraction of course (F_{cs}) and medium (F_{ms}) sand (F17):

$$\rho_s = \frac{\rho_p}{1000}[0.511 + 0.125(F_{cs} + F_{ms})]$$

The soil moisture adjustment factor is based on the difference between the gravimetric soil moisture (w) and the residual soil moisture (w', g/g), where w' is dependent on the clay content (in %) of the soil:

$$w' = 0.0014(clay)^2 + 0.17(clay)$$

When w' > w, the adjustment factor F_{mois} is 1. Otherwise, the factor is:

$$F_{mois} = \sqrt{1 + 1.21(w - w')^{0.68}}$$

F17 note that it is most appropriate to use soil moisture from the top few centimeters for WBD generation, such as in the WRF Pleim-Xiu land surface model, rather than the top 10 to 30 cm

used in other WRF schemes (Darmenova et al., 2009). The moisture content of deep soil layers is not representative of the exposed surface and the related inertia in deep soil drying rates can significantly suppress the saltation process. Darmenova et al. suggest applying a factor of 0.1 to reduce moisture from deep soil layers. Therefore, WBDUST includes a user-defined scaling factor for soil moisture: we suggest setting the factor to 1.0 when soil moisture is taken from the Pleim-Xiu scheme and to 0.1 when taken from other schemes.

Adjustment for Surface Roughness

The threshold friction velocity is further adjusted to account for the presence of surface roughness elements that limit momentum flux to the smooth soil surface. Referred to as a drag partitioning scheme, a larger factor should be applied to surfaces with more and larger obstacles (rocks, vegetation, etc.). WBDUST has adopted the "double drag partitioning" factor of F17:

$$F_{drag} = \sqrt{\left(1 - \sigma_v m_v \lambda_{v,i}\right)\left(1 + \beta_v m_v \lambda_{v,i}\right)\left(1 - \sigma_s m_s \frac{\lambda_{s,j}}{1 - A_{v,i}}\right)\left(1 + \beta_s m_s \frac{\lambda_{s,j}}{1 - A_{v,i}}\right)}$$

where the constants are: σ_v = 1.45, m_v = 0.16, β_v = 202, σ_s = 1.0, m_s = 0.5, and βs = 90. The parameter $\lambda_{s,j}$ is assigned a unique value for each of the 4 saltation particle types (j), while $\lambda_{v,i}$ is defined from

$$\lambda_{v,i} = -0.35\ \ln\left(1 - A_{v,i}\right)$$

where $A_{v,i}$ is the vegetative fractional coverage according to LAI assigned to each of the 4 emissive landcover types (i):

$$A_{v,i} = \min(LAI_i, 1.0)$$

The final adjusted cell-specific threshold friction velocity is thus:

$$U_t^* = F_{mois} \cdot F_{drag} \cdot U_{t0}^*$$

A.2 Saltation Flux

For a given grid cell determined to be potentially emissive, WBDUST calculates the actual friction velocity (U*) for each of 4 emissive landcover types from surface wind speed according to similarity theory (Louis, 1979):

$$U^* = \frac{\varphi k U}{\ln(z/z_0)}$$

where k is the von Karman constant (0.4), U is wind speed in the CAMx surface layer, z is height of the wind speed level, φ is a non-dimensional stability parameter calculated by the Louis (1979) scheme, and z_0 is the surface roughness length assigned to each of the 4 emissive land cover types. All units are MKS.

Then a horizontal saltation flux (H_{salt} in kg/m/s) is calculated if U* exceeds U^*_t:

$$H_{salt} = \frac{c\rho_\alpha U^{*3}}{g}\left(1+\frac{U_t^*}{U^*}\right)\left(1-\frac{U_t^{*2}}{U^{*2}}\right)$$

where c = 1 following F17. A total saltation flux for each emissive land cover type is calculated by summing contributions over all 4 saltation particle types, and weighting each saltation contribution by the product of its coverage and erodibility fraction as a function of soil type.

A.3 WBD Emission Flux

The vertical flux of dust particles (V_{dust} in kg/m^2/s) is proportional to the total saltation flux, with a sandblasting efficiency (m^{-1}) serving as the proportionality constant:

$$V_{dust} = H_{salt}\frac{C_\alpha g f \rho_s}{2p}\left(0.24 + C_\beta U^* \sqrt{\frac{\rho_p}{p}}\right)$$

where f is the fraction of emissive dust particles in the soil, p is the soil plastic pressure, ρ_s is the soil density, and C_α and C_β are constants. The parameters f, p, C_α and C_β are set according to F17.

The amount of dust emitted from an emissive grid cell per time (E_{dust} in kg/s) is calculated by summing V_{dust} over all 4 emissive landcover types, scaling by the area of each emissive landcover type in the cell (A_i), the amount of that type's unvegetated area, and by a topographic factor (F_{topo}):

$$E_{dust} = \sum_{i=1}^{4} F_{topo}\, A_i \left(1 - A_{v,i}\right) V_{dust}$$

A simple topographic adjustment is applied to the final emission estimate to reduce the potential for dust emissions with altitude: from full potential at or below 1000 m to zero potential at a typical treeline altitude of 2500 m.

WBDUST continues to assume that vertical dust emissions follow a globally uniform tri-modal distribution with mean diameters (D_V,n) of 0.832, 4.82, and 19.38 µm, geometric standard deviations (σ_n) of 2.1, 1.9 and 1.6, and mass fractions (M_n) of 0.036, 0.957 and 0.007, respectively. WBDUST maps these distributions directly to the CAMx fine crustal mode (FRCS, 0.04-2.5 µm) and coarse crustal mode (CCRS, 2.5-10 µm) using the standard error function (erf):

$$E_{FCRS} = E_{dust}\sum_{n=1,3}\frac{M_n}{2}\left\{\mathrm{erf}\left[\frac{\ln\left(2.5/D_{V,n}\right)}{\sqrt{2}\ln\sigma_n}\right] - \mathrm{erf}\left[\frac{\ln\left(0.04/D_{V,n}\right)}{\sqrt{2}\ln\sigma_n}\right]\right\}$$

$$E_{CCRS} = E_{dust}\sum_{n=1,3}\frac{M_n}{2}\left\{\mathrm{erf}\left[\frac{\ln\left(10/D_{V,n}\right)}{\sqrt{2}\ln\sigma_n}\right] - \mathrm{erf}\left[\frac{\ln\left(2.5/D_{V,n}\right)}{\sqrt{2}\ln\sigma_n}\right]\right\}$$

Speciation

If elemental speciation is requested, WBDUST splits FCRS into as many as 9 elements and remaining FCRS; no speciation is applied to CCRS. Factors for sodium, magnesium, calcium, and potassium are defined by the input global soil maps developed by Klingmueller et al. (2018). Globally uniform factors for titanium and manganese are set according values used in the CMAQ in-line dust algorithm. Factors for iron, aluminum, and silicon are set according to continental measurement data reported by Wang (2015) from the Southwest US, Sahara, Middle East, Asia, South America, and Australia. Table A-1 lists the speciation factors used in WBDUST v2.0.

Table A-1. Elemental speciation factors used in WBDUST v2.0.

Element	Sahara	Arabia	Asia	Australia	Patagonia	US
Fe[1]	0.045	0.020	0.027	0.041	0.043	0.056
Al[1]	0.071	0.010	0.058	0.050	0.082	0.035
Si[1]	0.189	0.189[2]	0.232	0.185	0.288	0.122
Na[3]	Global input	Global input	Global input	Global input	Global input	Global input
Mg[3]	Global input	Global input	Global input	Global input	Global input	Global input
Ca[3]	Global input	Global input	Global input	Global input	Global input	Global input
K[3]	Global input	Global input	Global input	Global input	Global input	Global input
Ti[4]	0.003	0.003	0.003	0.003	0.003	0.003
Mn[4]	0.001	0.001	0.001	0.001	0.001	0.001

[1] From Wang (2015)
[2] Not reported by Wang (2015); set to value for Africa/Sahara
[3] From Klingmueller et al. (2018)
[4] From CMAQ in-line dust algorithm

A.4 CropScape and Crop Calendar

WBDUST v2.0 includes the option to utilize processed/gridded CropScape datasets in combination with the CMAQ crop calendar. These data provide the basis for modifying input CAMx landcover distributions to reflect locations and extents of tilled croplands that are barren and thus potentially emissive.

A single year of raw US CropScape data is massive and burdensome to use. To be efficiently useful in WBDUST, we developed a set of Python scripts to recast the 256 CropScape classifications to a smaller sub-set that aligns with the CAMx landcover categories, and to reproject and translate the 30-m raster data to gridded area fractions on the CAMx grid.

First, the script "`raster_reclassify.py`" reclassifies CropScape's list of 256 pixel values to the 26 CAMx LULC categories plus an additional 15 unique crop categories that align with the crop calendar (3 crop calendar categories – cotton, corn, and rice – directly align with CAMx landcover types for a total of 18 crop types). Additionally, CropScape includes a pixel classification called "Developed/Open Space". Based on our graphical analysis, this category is ubiquitous throughout rural and agricultural areas and clearly represents roads and open lots, particularly access roads between individual fields. Since in rural areas such roads and lots are most likely unpaved and thus potentially emissive, we maintain this as a separate category in our reclassified landcover list, resulting in 42 total categories. Table A-2 lists the mapping of

116 categories with non-zero counts in the 2016 CropScape dataset to the 42 WBDUST categories. This script can take up to several hours to run.

Next, the script "`raster_camx_grids_count.py`" casts the reclassified 30-m raster data to the map projection of the target CAMx modeling grid. It then aggregates the pixel data to the CAMx grid using a "fishnet" Python function and counts the number of pixels in each grid cell for each of the 42 landcover categories. This script can also take up to several hours to run.

A third script "`raster_camx_grids_count2nc.py`" derives the fractional area per grid cell for each of the 42 landcover categories, ensuring that the sum over all categories in each grid cell sum to 1. It then overlays a shapefile defining the boundaries of the 48 conterminous US states onto the CAMx grid and identifies which state each cell occupies (to facilitate the use of the state-level crop calendar in WBDUST). The script then writes the processed CropScape dataset and the resulting gridded state identification array to a netCDF data file that is directly read by WBDUST. This script takes only a few minutes to run.

The crop calendar lists, for each of the 18 crop types, the planting/seeding and harvesting schedules in each of 47 conterminous states (excluding Rhode Island). Below is an example for Kansas:

```
Barley-Spring
KS 3 1 3 5 4 1 5 1 6 10 6 25 7 1 7 10
Barley-Fall
KS 9 15 10 1 10 15 11 1 6 20 6 15 7 1 7 5
```

The start date for planting is given by the first 2 values and the end date is given by the 7th and 8th values (highlighted yellow). The harvesting end date is given by the 15th and 16th values (highlighted green). For example, spring barley planting begins March 1 and ends May 1, while harvesting ends July 10. Fall barely planting begins September 15 and ends November 1, while harvesting ends July 5 of the following year.

CropScape in WBDUST

WBUST optionally reads the processed CropScape data and the crop calendar file. For CAMx grids extending beyond US borders, no cropland adjustments to the input CAMx landcover fields can be made. Since CAMx landcover files are developed via many different approaches, there are potentially very large differences between CAMx and CropScape gridded landcover coverages that present significant complications in reconciling and blending CropScape and CAMx landcover datasets. The most obvious example is that CAMx LULC files may comprise only a single dominant category per grid cell as processed by the WRFCAMx interface program (because WRF only output such information). Since crop types and coverages in CropScape are year-specific and very detailed, we consider that dataset to be definitive. To alleviate the need for a complex reconciliation of the two datasets when processed CropScape data are optionally provided, WBDUST preferentially uses the CropScape data for the 26 standard CAMx land cover

fractions and the 15 additional crop-specific fractions for each US grid cell (superseding the 26 standard landcover fractions from the CAMx landuse input file).

Then, WBDUST cross-references the 18 specific crop calendar types to the CropScape categories and saves each of their fractional areas. These crop types are then checked against the state-level crop calendar input file. According to the date being processed, the fractional coverage of each of these crop types may be converted to the CAMx "barren" landcover classification to designate them as potentially emissive. This conversion is assigned only for crops for which the planting season is active for the given date. We assume that tilling/cultivation occurs only during planting period, and that crop residue after the previous harvest are not tilled under until the planting season to avoid erosion during the interim period. However, rice crops are ignored because they are not considered potentially emissive given their water-borne cultivation. We arbitrarily assume that 25% of tillable croplands had been cultivated and are emissive within a recent period around any given date during the planting season, as opposed to assuming that 100% of all tillable croplands are emissive over the entire planting season.

Finally, WBDUST considers the spatial coverage of the "developed open space" category that was separately tracked in the CropScape data processing step. For each US grid cell, WBDUST saves the open space fraction with an adjustment to account for the fraction associated with urban landcover (which is assumed to be paved). The rural unpaved fraction is determined from scaling open space by the non-urban cell fraction minus an additional 10% to account for some paved areas (highways, etc.). This means that up to 90% of the open space fraction in fully rural grid cells are assumed to be unpaved and potentially emissive. The resulting rural open space fraction is added to the CAMx "barren" landcover classification. The remaining urban open space fraction is assigned to the CAMx "urban" landcover classification and thus never emissive.

Table A-2. Mapping of 116 CropScape categories with non-zero pixel counts throughout the US to the 42 intermediate categories to be used in WBDUST. Data are ranked in order of 2016 pixel counts.

Count	CropScape ID	Name	CAMx/ WBDUST ID	Mapped Name
2,092,704,769	152	Shrubland	11	Deciduous shrubs
1,468,881,161	176	Grassland/Pasture	13	Short grass/forbs
1,100,960,404	141	Deciduous Forest	7	Deciduous broad forest
1,088,166,195	142	Evergreen Forest	4	Evergreen needle forest
421,565,199	1	Corn	18	Corn
367,186,823	5	Soybeans	38	Soybeans
351,485,013	190	Woody Wetlands	23	Swamp
286,196,156	121	Developed/Open Space	27	Developed open space
155,930,199	111	Open Water	1	Water
148,419,661	24	Winter Wheat	42	WheatWinter
129,988,342	143	Mixed Forest	25	Mixed forest
129,415,822	122	Developed/Low Intensity	21	Urban
121,301,667	61	Fallow/Idle Cropland	13	Short grass/forbs
114,369,177	37	Other Hay/Non-Alfalfa	31	Hay
102,548,874	195	Herbaceous Wetlands	23	Swamp
98,104,023	131	Barren	24	Desert
87,423,519	36	Alfalfa	28	Alfalfa
60,399,324	123	Developed/Med Intensity	21	Urban
55,521,671	23	Spring Wheat	41	WheatSpring
48,747,688	2	Cotton	19	Cotton
32,283,304	4	Sorghum	37	Sorghum
20,456,058	124	Developed/High Intensity	21	Urban
16,568,648	26	Dbl Crop WinWht/Soybeans	38	Soybeans
14,241,290	3	Rice	16	Rice
12,083,632	21	Barley	29	Barley
9,363,450	22	Durum Wheat	41	WheatSpring
8,301,653	42	Dry Beans	20	Irrigated crops
7,340,416	28	Oats	32	Oats
7,118,944	31	Canola	15	Crops
6,984,288	53	Peas	20	Irrigated crops
6,754,265	75	Almonds	7	Deciduous broad forest
6,334,670	6	Sunflower	15	Crops
6,033,608	10	Peanuts	34	Peanuts
5,510,707	69	Grapes	11	Deciduous shrubs
5,102,414	41	Sugarbeets	39	Sugarbeets
5,037,794	59	Sod/Grass Seed	13	Short grass/forbs
4,833,282	45	Sugarcane	17	Sugar
4,351,417	212	Oranges	5	Evergreen broad forest
4,287,874	43	Potatoes	35	Potatoes
4,048,330	52	Lentils	20	Irrigated crops
3,045,309	27	Rye	36	Rye
2,868,737	29	Millet	15	Crops
2,179,770	68	Apples	7	Deciduous broad forest
1,934,931	76	Walnuts	7	Deciduous broad forest
1,802,361	74	Pecans	7	Deciduous broad forest

Count	CropScape ID	Name	CAMx/ WBDUST ID	Mapped Name
1,595,725	205	Triticale	36	Rye
1,588,053	112	Perennial Ice/Snow	2	Ice
1,535,272	54	Tomatoes	20	Irrigated crops
1,444,924	225	Dbl Crop WinWht/Corn	18	Corn
1,419,401	32	Flaxseed	15	Crops
1,370,315	12	Sweet Corn	18	Corn
1,344,475	204	Pistachios	7	Deciduous broad forest
1,101,574	92	Aquaculture	1	water
942,522	13	Pop or Orn Corn	18	Corn
878,923	66	Cherries	7	Deciduous broad forest
876,408	58	Clover/Wildflowers	15	Crops
866,511	242	Blueberries	11	Deciduous shrubs
790,846	236	Dbl Crop WinWht/Sorghum	37	Sorghum
761,157	33	Safflower	15	Crops
641,847	49	Onions	20	Irrigated crops
606,723	72	Citrus	5	Evergreen broad forest
602,594	71	Other Tree Crops	7	Deciduous broad forest
573,898	57	Herbs	20	Irrigated crops
569,878	11	Tobacco	40	Tobacco
547,669	70	Christmas Trees	4	Evergreen needle forest
498,853	238	Dbl Crop WinWht/Cotton	19	Cotton
487,307	46	Sweet Potatoes	35	Potatoes
356,087	226	Dbl Crop Oats/Corn	18	Corn
339,467	35	Mustard	15	Crops
306,094	254	Dbl Crop Barley/Soybeans	38	Soybeans
267,374	50	Cucumbers	20	Irrigated crops
262,779	206	Carrots	20	Irrigated crops
261,133	44	Other Crops	15	Crops
260,798	56	Hops	11	Deciduous shrubs
253,268	227	Lettuce	20	Irrigated crops
216,457	48	Watermelons	20	Irrigated crops
207,501	47	Misc Vegs & Fruits	20	Irrigated crops
197,873	77	Pears	7	Deciduous broad forest
192,169	67	Peaches	7	Deciduous broad forest
174,837	221	Strawberries	20	Irrigated crops
167,070	237	Dbl Crop Barley/Corn	18	Corn
155,062	220	Plums	7	Deciduous broad forest
154,353	229	Pumpkins	20	Irrigated crops
136,036	219	Greens	20	Irrigated crops
135,828	222	Squash	20	Irrigated crops
127,746	211	Olives	5	Evergreen broad forest
123,804	209	Cantaloupes	20	Irrigated crops
122,305	243	Cabbage	20	Irrigated crops
111,677	217	Pomegranates	7	Deciduous broad forest
105,069	208	Garlic	20	Irrigated crops
104,602	216	Peppers	20	Irrigated crops
92,024	214	Broccoli	20	Irrigated crops
89,702	240	Dbl Crop Soybeans/Oats	32	Oats
88,387	55	Caneberries	11	Deciduous shrubs

Count	CropScape ID	Name	CAMx/ WBDUST ID	Mapped Name
81,765	25	Other Small Grains	15	Crops
78,628	39	Buckwheat	15	Crops
62,436	60	Switchgrass	15	Crops
52,935	250	Cranberries	10	Evergreen broad shrub
41,866	30	Speltz	41	WheatSpring
35,180	14	Mint	15	Crops
33,468	246	Radishes	20	Irrigated crops
27,274	213	Honeydew Melons	20	Irrigated crops
18,152	244	Cauliflower	20	Irrigated crops
16,904	207	Asparagus	20	Irrigated crops
16,267	224	Vetch	15	Crops
12,881	34	Rape Seed	15	Crops
10,444	241	Dbl Crop Corn/Soybeans	38	Soybeans
9,624	247	Turnips	35	Potatoes
8,566	245	Celery	20	Irrigated crops
6,100	218	Nectarines	7	Deciduous broad forest
3,131	38	Camelina	15	Crops
2,405	248	Eggplants	20	Irrigated crops
1,228	249	Gourds	20	Irrigated crops
903	51	Chickpeas	20	Irrigated crops
856	223	Apricots	7	Deciduous broad forest
71	232	Dbl Crop Lettuce/Cotton	19	Cotton